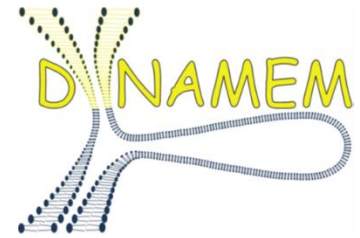




JOHANNES GUTENBERG  
UNIVERSITÄT MAINZ



# Membrane Modulation and Cardiolipin Interaction of Small Molecules and Proteins

Dissertation

zur Erlangung des Grades

„Doktor der Naturwissenschaften“

im Promotionsfach Chemie

am Fachbereich Chemie, Pharmazie, Geografie und Geowissenschaften

der Johannes-Gutenberg-Universität Mainz

Isabel Kleinwächter

geboren. in Hanau (Hessen)

Mainz, 2022



Die vorliegende Dissertation wurde im Zeitraum von April 2018 bis Dezember 2021 am Department für Chemie der Johannes Gutenberg-Universität Mainz unter der Betreuung von [REDACTED] durchgeführt. Ich versichere, dass ich diese Arbeit selbständig verfasst habe und keine anderen als die angegebenen Quellen und Hilfsmittel benutzt habe.

Dekanin: [REDACTED]

1. Berichterstatter: [REDACTED]

2. Berichterstatter: [REDACTED]



Für meine Familie



# Table of content

<b>I. Summary</b> .....	11
<b>II. Zusammenfassung</b> .....	13
<b>1. Introduction</b> .....	15
<b>1.1. Membranes</b> .....	<b>15</b>
<b>1.1.1. Structure and Properties of Biological Membranes</b> .....	15
<b>1.2. Mitochondria</b> .....	<b>19</b>
<b>1.2.1. Structure and Membrane Properties of Mitochondria</b> .....	20
<b>1.3. Cardiolipin</b> .....	<b>21</b>
<b>1.4. Membrane Targeting and Modulation</b> .....	<b>23</b>
<b>1.5. Model Membranes</b> .....	<b>23</b>
<b>1.6. Objectives of This Thesis</b> .....	<b>25</b>
<b>2. Materials</b> .....	27
<b>2.1. Chemicals and Expendable Material</b> .....	27
<b>2.2. Buffers and Solutions</b> .....	27
<b>2.3. Kits and Standard Marker</b> .....	30
<b>2.4. Media and Bacterial Strains</b> .....	31
<b>2.5. Plasmids</b> .....	32
<b>2.6. Instruments</b> .....	33
<b>2.7. Software</b> .....	34
<b>3. Methods</b> .....	35
<b>3.1. Molecular Biological Methods</b> .....	<b>35</b>
<b>3.1.1. Polymerase Chain Reaction and Site Directed Mutagenesis</b> .....	35
<b>3.1.2. Agarose Gel Electrophoresis</b> .....	36
<b>3.1.3. Plasmid Preparation</b> .....	37
<b>3.1.4. Restriction Digest of DNA</b> .....	37
<b>3.1.5. Ligation</b> .....	37
<b>3.1.6. Construct Design of DRP1 constructs (Chapter 6)</b> .....	38
<b>3.1.7. Tafazzin Construct Design (Chapter 7)</b> .....	39
<b>3.2. Microbiological Methods</b> .....	<b>39</b>
<b>3.2.1. Transformation of Competent Bacteria</b> .....	39
<b>3.2.2. Plasmid Transformation</b> .....	40
<b>3.2.3. Heterologous Expression of Proteins</b> .....	40
<b>3.2.4. Growth Assay and Determination of Minimal Inhibitory Concentrations 50 (MIC50) (Chapter 4)</b> .....	41
<b>3.2.5. Oxygen Consumption of <i>E. coli</i> (Chapter 5)</b> .....	41
<b>3.2.6. Fluorescence Microscopy of <i>E. coli</i> (Chapter 6)</b> .....	42

---

<b>3.3. Biochemical Methods</b> .....	<b>42</b>
<b>3.3.1. Purification of Proteins</b> .....	42
<b>3.3.2. SDS-PAGE</b> .....	43
<b>3.3.3. Western Blot Analysis</b> .....	44
<b>3.3.4. Membrane Association Assay (Chapter 7)</b> .....	44
<b>3.3.5. Liposome Preparation</b> .....	45
<b>3.3.6. Sedimentation Assay (Chapter 6)</b> .....	46
<b>3.4. Biophysical Methods</b> .....	<b>46</b>
<b>3.4.1. Laurdan Fluorescence Spectroscopy and Generalized Polarization Values</b> .....	46
<b>3.4.2. Fluorescence Measurements Using the Emission of SM19 (Chapter 5)</b> .....	47
<b>3.4.3. Fluorescence Measurements of SM19 in Presence of <i>E.coli</i> (Chapter 5)</b> .....	48
<b>3.4.4. LogP Correlation (Chapter 4)</b> .....	48
<b>4. The Bacteriostatic Activity of 2-Phenylethanol Derivatives Correlates with Membrane Binding Affinity</b> .....	<b>49</b>
<b>4.1. Author Contributions</b> .....	<b>49</b>
<b>4.2. Abstract</b> .....	<b>50</b>
<b>4.3. Introduction</b> .....	<b>51</b>
<b>4.4. Results and Discussion</b> .....	<b>53</b>
<b>4.4.1. Membrane Partitioning and the Impact of 2-PEtOH Derivatives on the Membrane Structure</b> .....	54
<b>4.4.2. 2-PEtOH and Derivatives are Bacteriostatic</b> .....	58
<b>4.4.3. Hydrophobicity, Membrane Fluidity, and Bacterial Growth Correlate</b> .....	59
<b>5. CLiB - a Novel Cardiolipin-Binder Isolated via Data-Driven and <i>In Vitro</i> Screening</b> .....	<b>61</b>
<b>5.1. Author Contributions</b> .....	<b>61</b>
<b>5.2. Summary</b> .....	<b>62</b>
<b>5.3. Introduction</b> .....	<b>63</b>
<b>5.4. Results and Discussion</b> .....	<b>67</b>
<b>5.4.1. Rational Identification of 22 Candidate Molecules with a Putative Cardiolipin-Binding Propensity</b> .....	68
<b>5.4.2. Membrane Binding Properties of SM<sub>1-22</sub></b> .....	75
<b>5.4.3. Impact of SM<sub>19</sub> on Cardiolipin-Containing Cellular Membranes</b> .....	80
<b>6. A Cardiolipin Detector Based on an eYFP-Coupled Dynamin Related Protein 1 Fragment</b> .....	<b>85</b>
<b>6.1. Summary</b> .....	<b>85</b>
<b>6.2. Introduction</b> .....	<b>85</b>



<b>6.3. Results and Discussion</b> .....	<b>87</b>
<b>6.3.1. Expression of eYFP-Stalk in <i>E. coli</i></b> .....	89
<b>6.3.2. The eYFP-Stalk Construct Binds to Cardiolipin-Containing LUVs</b> .....	90
<b>6.3.3. The eYFP-Stalk Construct Binds to GUVs and Changes Their Structure</b> .....	91
<b>7. Human Tafazzin is a Membrane-Attached, but not a Transmembrane Protein</b> .....	95
<b>7.1. Summary</b> .....	<b>95</b>
<b>7.2. Introduction</b> .....	<b>95</b>
<b>7.3. Results and Discussion</b> .....	<b>97</b>
<b>7.3.1. The Predicted Membrane Anchor Presumably Lies in an Inaccessible         Region</b> .....	98
<b>7.3.2. The N-terminal Helix is not Alone Responsible for Membrane         Association of Tafazzin</b> .....	99
<b>8. References</b> .....	103
<b>9. List of Abbreviations</b> .....	123
<b>10. List of Figures</b> .....	127
<b>11. List of Tables</b> .....	129
<b>12. Author Affiliations</b> .....	131
<b>13. Appendix</b> .....	133
<b>13.1. Methods</b> .....	<b>133</b>
<b>13.1.1. Addition Chapter 4:</b> [REDACTED] .....	133
<b>13.1.2. Addition Chapter 5:</b> [REDACTED] .....	133
<b>13.1.3. Addition Chapter 5:</b> [REDACTED] .....	138
<b>13.2. Full Article of Chapter 4</b> .....	<b>140</b>



## I. Summary

In the first part of this work, the relationship between the bacteriostatic effect and the effect on the membrane structure of 2-phenyl ethanol (2-PEtOH) and derivatives has been investigated. Here, on the one hand, the influence on the fluidity of model membranes was investigated by spectral fluorometric methods, and on the other hand, the bacteriostatic effect was studied via following *Escherichia coli* (*E. coli*) growth in presence of the respective substances. Our results show a clear correlation between the hydrophobicity, of the molecules analyzed here and their bacteriostatic activity. Thus, the biological activity of the molecules can be linked to the cell membrane. In the future, this correlation may help to predict how likely or if a molecule influences the membrane and/or an organism.

The second project focused on finding one or more molecules that specifically interact with the lipid cardiolipin. Using *in silico* methods, we identified the necessary physical and chemical cardiolipin binding properties of a molecule and screened a database for promising candidates. The 22 identified molecules were then studied for their cardiolipin specificity, using model membranes. We were able to identify one molecule showing a clear preference towards cardiolipin. In the future, this molecule, we named it CliB (Cardiolipin Binder), will allow to systematically analyze the role of cardiolipin in biological membranes and membrane-bound processes. Furthermore, our workflow can be applied to other databases and enable to screen for more promising cardiolipin binders.

In the third project, we developed and established an enhanced yellow fluorescence protein (eYFP)-coupled protein construct as a cardiolipin marker. Using genetic engineering methods, the construct was produced and its specificity towards cardiolipin was investigated using model membranes. We found a clear preference of the construct towards cardiolipin compared to another negatively charged lipids. Interestingly, the construct induces structural changes in model membranes. This would have been expected for the full-length protein, but not for the truncated construct. In order to use the construct as a specific cardiolipin marker, it should be clarified where these changes come from and if they can be eliminated.

In the last project, membrane association of tafazzin was investigated in more detail. We were able to show that the predicted N-terminal helix of the protein is involved in

membrane binding. However, our results also clearly show that it is not the only part of the protein that attaches it to the membrane. Further studies are urgently needed to definitively clarify what holds tafazzin at the membrane.

## II. Zusammenfassung

Im ersten Teil dieser Arbeit wurde der Zusammenhang zwischen der bakteriostatischen Wirkung und der Wirkung von 2-PEtOH und einiger seiner Derivate auf die Membranstruktur von biologischen Membranen untersucht. Dabei wurde zum einen mittels fluorimetrischer Methoden der Einfluss auf die Fluidität von Modellmembranen und zum anderen mittels des Wachstums von *E. coli* die bakteriostatische Wirkung, untersucht. Unsere Ergebnisse zeigen eine klare Korrelation zwischen der Hydrophobizität der hier analysierten Moleküle und ihrer bakteriostatischen Aktivität. Die biologische Aktivität der Moleküle lässt sich somit mit der Zellmembran in Verbindung bringen. In Zukunft kann dieser Zusammenhang helfen, vorherzusagen, wie wahrscheinlich es ist, ob ein Molekül einen Einfluss auf eine Membran und/oder einen Organismus hat.

Das zweite Projekt konzentrierte sich auf die Suche nach einem oder mehreren Molekülen, die spezifisch mit dem Lipid Cardiolipin interagieren. Mithilfe von *in silico* Methoden haben wir die erforderlichen physikalischen und chemischen Cardiolipin-Bindungseigenschaften ermittelt und eine Datenbank nach vielversprechenden Kandidaten durchsucht. Die 22 identifizierten Moleküle wurden dann mit Hilfe von Modellmembranen auf ihre Cardiolipin-Spezifität untersucht. Wir konnten ein Molekül identifizieren, das eine klare Präferenz gegenüber Cardiolipin aufweist. Dieses Molekül, das wir CliB genannt haben, wird es in Zukunft ermöglichen, die Rolle von Cardiolipin in biologischen Membranen und membrangebundenen Prozessen systematisch zu analysieren. Außerdem kann unser Arbeitsablauf auf andere Datenbanken angewendet werden und dabei helfen, weitere vielversprechende Cardiolipin-Binder zu identifizieren.

Im dritten Projekt haben wir ein *eYFP*-gekoppeltes Proteinkonstrukt konstruiert und als Cardiolipin-Marker etabliert. Mithilfe gentechnischer Methoden wurde das Konstrukt hergestellt und seine Spezifität gegenüber Cardiolipin mit Hilfe von Modellmembranen untersucht. Wir fanden eine klare Präferenz des Konstrukts für Cardiolipin im Vergleich zu anderen negativ geladenen Lipiden. Interessanterweise führt das Konstrukt zu strukturellen Veränderungen in den Modellmembranen. Dies wäre für das entsprechende Vollängenprotein zu erwarten, nicht aber für das Konstrukt. Um das Konstrukt als spezifischen Cardiolipin-Marker verwenden zu

können, muss geklärt werden, woher diese Veränderungen kommen und ob und wie sie eliminiert werden können.

Im letzten Projekt wurde die Membranassoziation von Tafazzin eingehender untersucht. Wir konnten zeigen, dass die vorhergesagte N-terminale Helix des Proteins an der Membranbindung beteiligt ist. Unsere Ergebnisse zeigen jedoch auch, dass dies nicht der einzige Teil des Proteins ist, der es mit der Membran assoziiert. Weitere Studien sind dringend erforderlich, um endgültig zu klären, wie Tafazzin an die Membran assoziiert.

# 1. Introduction

## 1.1. Membranes

Without biological membranes life as we know it today wouldn't exist. Biological membranes separate cells from their environment and delimit reaction spaces in higher organisms, such as organelles. They are highly selective permeable barriers that build closed compartments. Furthermore, they are responsible for the interaction between the cell/organelle and the environment. Besides their structural function, biological membranes contain receptors, enable signalling, induce enzymatic activity and are responsible for fusion-fission, endocytosis, and transport of molecules among others [1].

Biological membranes mainly consist of lipids. In addition, sugars and membrane proteins are among their main components [2]. Because function and properties of biomembranes control highly complex processes in organisms and play a key role in biological reactions, they are an important subject of current research activities.

### 1.1.1. Structure and Properties of Biological Membranes

Involvement of lipids in the cell structure were first described by Charles E. Overton in the 19<sup>th</sup> century. About 30 years later the first membrane organization models were postulated [1]. These models ranged from mono- to trilayers of lipids and proteins. The most accepted model, which in principle is still valid today, is the fluid mosaic model proposed by Singer and Nicolson in 1972 [3]. In this model membranes are described as lipid bilayers with embedded proteins. The lipids and proteins are in permanent motion free to switch between the bilayers, to rotate and to move laterally [4]. In the last decades further research led to a refinement of said model such as heterogeneity within the bilayer (membrane domains), introduction of curvature and pore formation, lipid interactions with its environment and a higher protein/lipid ratio [1,4,5].

Lipids are the main components of membranes. As amphipathic molecules they contain a hydrophilic (head) region and a hydrophobic (tail) region (Figure 1A) [2]. Many ways exist to categorize lipids. A common one is based on their functional backbone into acylglycerols, sphingolipids, prenols, polyketides and saccharolipids. Hereby, fatty acyls are separated from polyketides, sterols from prenols and glycerophospholipids (or short: phospholipids) from glycerolipids due to historical and

bioinformatic reasons [6]. Phospholipids, sphingolipids, and sterols are the main types of lipids found in eukaryotic membranes (Figure 1A) [2,7].

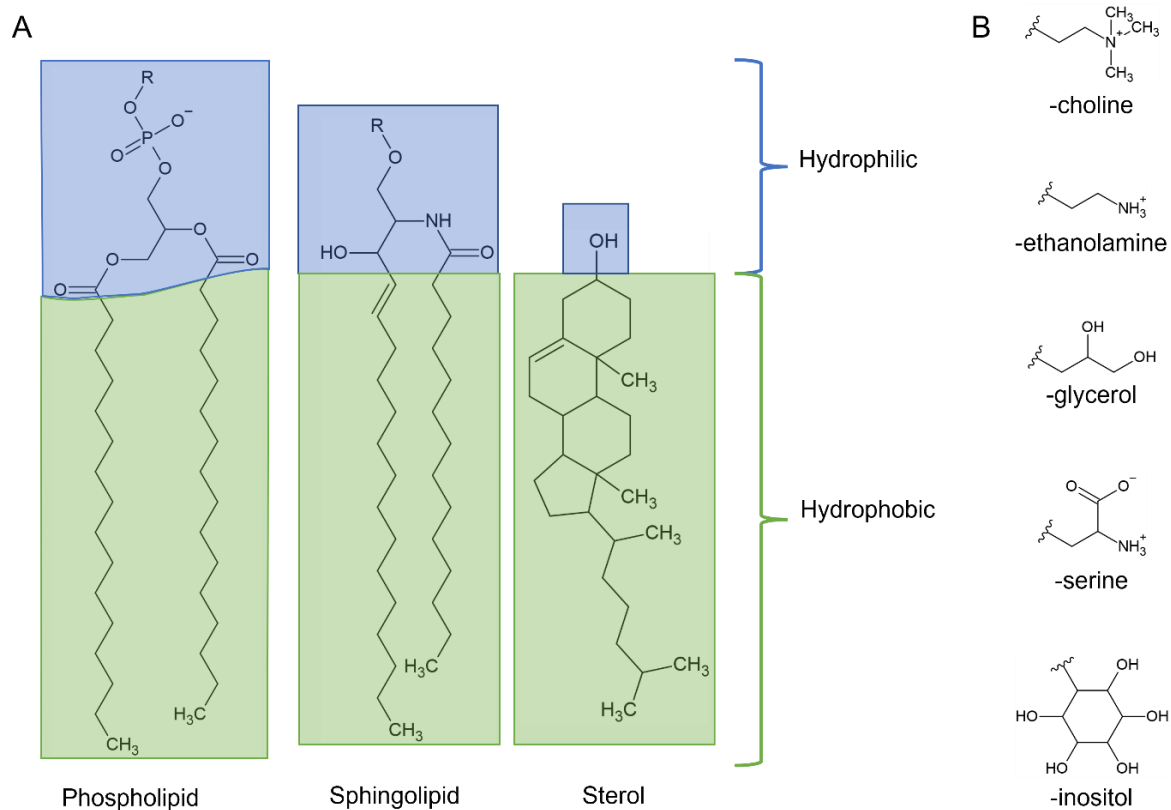


**Figure 1:** Structure of the most common eukaryotic lipid classes.

(A) Structures of a phospholipid, a sphingolipid, and a sterol (cholesterol). R can be replaced by different alcohols and sugars. In case of the sphingolipid the alcohol is linked by a phosphate group. The acyl chains can also differ in their length and their saturation (B) Different alcohols for esterification of the lipids. The structures were drawn with ChemSketch V5 (Freeware from ACD/Labs, Toronto, Ontario, Canada).

In phospholipids, two acyl chains are linked to a glycerol via an ester bond. These acyl chains may be saturated or unsaturated [7]. At the third C-atom of the glycerol backbone a phosphate group can be found, esterified with one of various head groups, such as ethanolamine, choline, serine, glycerol, inositol or oligosaccharides (Figure 1B). Choline and ethanolamine as a headgroup lead to zwitterionic lipids, serine, glycerol, and inositol to anionic ones [2,6]. Sphingolipids have an acyl chain linked to a sphingoid base via an amide group. They can show the same functional groups coupled via a phosphate group as phospholipids or glycosidically linked sugars. The most common sphingolipids are sphingomyelins showing a choline or an ethanolamine headgroup (Figure 1) [7]. All lipids with a directly linked sugar molecule without a



linking phosphate group belong to the group of glycolipids. Sterols have a hydrophobic sterol-base and with a hydroxy group a relatively small hydrophilic head group [8]. Cholesterol is probably the best known and most important human sterol [9].

Based on their head-to-tail ratio, the geometric shapes of lipids differ significantly. This can have a major impact on the curvature of the membrane (Figure 2A). Phosphatidylcholines (PC) and sphingomyelins have a cylindrical shape [10,11]. Lipids such as phosphatidic acid (PA), phosphatidylethanolamine (PE), phosphatidylserine (PS) are conical-shaped and form structures with a negative curvature. Other lipids, like lysophospholipids and polyphosphoinositides, have an inverted conical shape, form structures with a positive curvature (Figure 2B) [1,12,13]. Due to their amphiphilicity and the hydrophobic effect, lipids self-assemble in aqueous environments. This happens independently of their shape [2]. Only cylindrical lipids form a bilayer with the head group facing outward and the acyl chains forming a hydrophobic core [13,14]. Lipids that show an inverted conical shape or a conical shape form micelles with a hydrophobic core, or inverted micelles with a hydrophilic core, respectively (Figure 2B). These lipids are referred to as “non-bilayer forming lipids”. However, they can form bilayer structures when other lipids of other shapes are present [13].

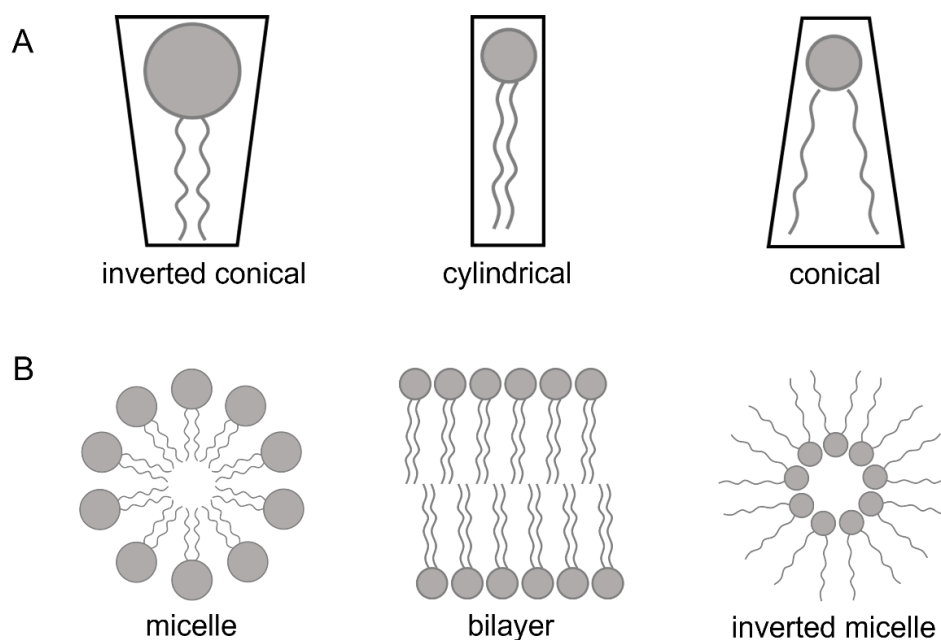


**Figure 2:** Lipid shapes and lipid self-assemblies.

(A) Due to their head-to-tail ratio, lipids show an inverted conical (left), cylindrical (middle), or conical (right) shape. (B) In aqueous environment lipids form spontaneously different assemblies due to their shape. Figure adapted from [15].

Basically, the lipid bilayer can exist in two main phases. The double bonds of unsaturated lipids are either in the *trans* or the *gauche* conformation in those phases (Figure 3A) [16]. In the gel solid ordered ( $S_o$ ) phase, the double bonds are in *trans*-conformation and the acyl chains are extended. In this phase lipids are arranged in a bilayer and they can interact tightly with each other resulting in a rigid membrane. On the other hand, in the liquid-disordered ( $L_d$ ) phase, the double bonds are in the *gauche*-conformation and the acyl chains are not stretched. In this case the membrane lipids are less packed and the membrane is more fluid. The temperature at which a transition from one phase to the other one is happening is the so-called transition temperature ( $T_m$ ). Below the  $T_m$ , the membrane is in the  $S_o$  phase and above the  $T_m$  it is in the  $L_d$  phase (Figure 3B) [1,16,17]. Some membrane lipids cause a pretransition in which the membrane is in the so-called ripple phase ( $P_\beta$ ). This phase is characterized by periodic one-dimensional ripples on the surface of the lipid-bilayer [18].

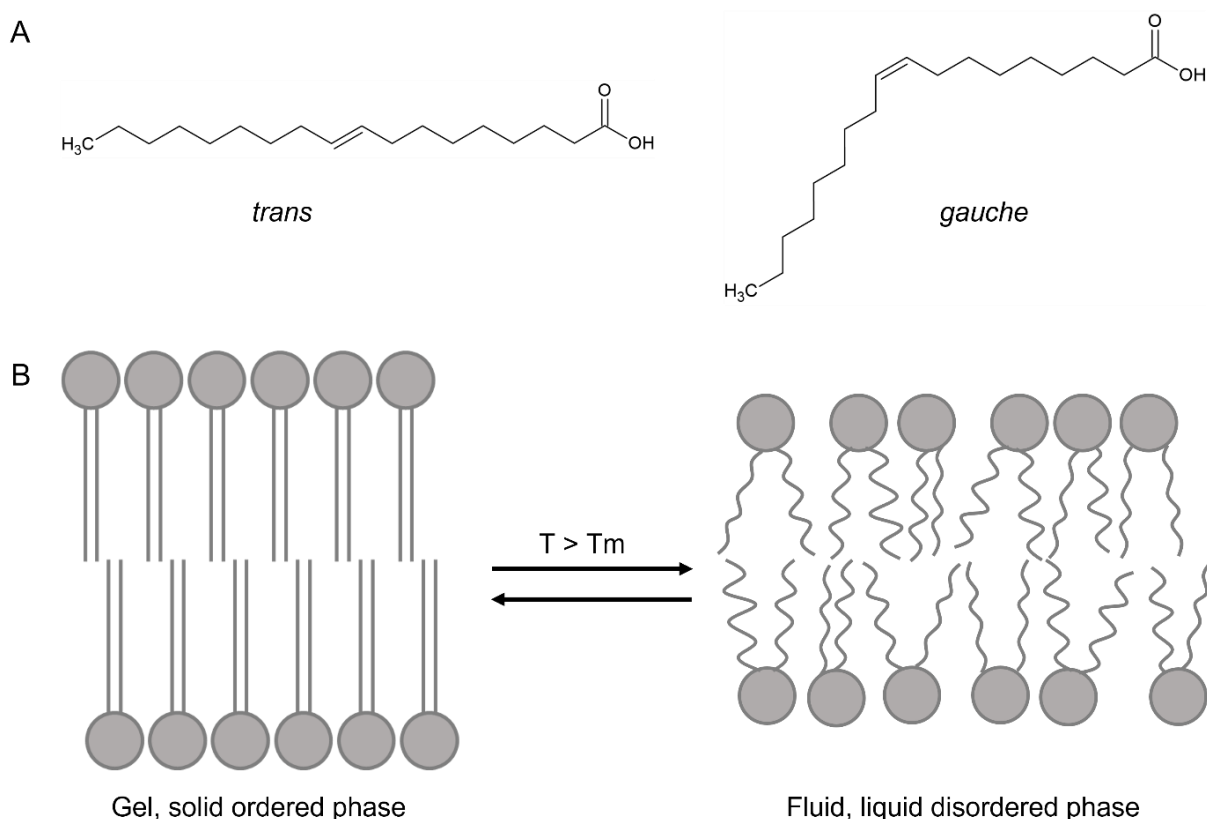


**Figure 3:** Acyl chain configurations and membrane phases.

(A) The *trans* and *gauche* configuration of a fatty acid ( $\Delta^9$ -octadecanoic acid). (B) The two phases of membranes. Below the  $T_m$ , the membrane is in the solid ordered phase (left), above the  $T_m$ , the membrane is in the liquid disordered phase (right). The figure is adapted and modified from [18], structures were drawn with ChemSketch.

The membrane fluidity and thus the  $T_m$  are mainly affected by two factors: the amount of unsaturated fatty acids and the cholesterol content. Fluidity is additionally affected by the temperature [19,20]. A high cholesterol content leads to a more tightly packed membrane and hence to a more rigid liquid-ordered bilayer ( $L_o$ ), if the membrane is in the  $L_d$  state. This phase can exist simultaneously with the  $L_d$  phase in a membrane [1,21,22]. Unsaturated lipids reduce lipid packing and improve fluidity, whereas saturated lipids favour ordered packing of the membrane due to their straight tails and van der Waals forces [1,19]. The fluidity of the membrane influences its permeability [23,24].

The lipid composition of a membrane varies a lot between different organisms. In contrast to eukaryotic membranes, the membranes of *E. coli* for example lack sterols and show a high amount (around 10 %) of the special lipid diphosphatidylglycerol (cardiolipin) [25]. However, the lipid composition of membranes varies not only from organism to organism, but also within organelles in the same organism [1,26]. Moreover, since the physicochemical properties of the membranes are related to the lipid composition, they also vary depending on their localization. Even the lipid compositions, and consequently the physicochemical properties of the inner and the outer leaflet of a lipid bilayer can differ and [1,5,12,13,27]. The protein content in membranes also varies substantially between different types of membranes [28].

## 1.2. Mitochondria

One type of eukaryotic organelles showing a unique lipid composition within their membranes are mitochondria. The composition is similar to those of bacteria, which is due to the endosymbiotic origin of these organelles [29–31]. The existence of mitochondria is conserved among all eukaryotes [32], nevertheless the amount of mitochondria within the cell varies among cell types and is tissue- and organ-dependent [31]. With their own DNA, RNA and protein synthesis machinery, mitochondria are partially autonomous organelles [33,34]. As highly dynamic organelles, they are constantly undergoing fusion and fission processes, regulating their morphology and their function [34,35]. Many important processes are linked to mitochondria, like energy production, metabolism, intracellular signalling, cell death, development, and immune responds [34]. Mitochondria function as the energy producers of the cell and nearly the whole required adenosine triphosphate (ATP) is

produced by mitochondria [30,32,36]. Additionally, mitochondria play a key role in adaptation during stress situations [37]. The involvement in so many important processes highlight the significance of healthy and well-functioning mitochondria. Defect mitochondria can lead to serious diseases, like cancer, autoimmune diseases, and neurodegenerative diseases [34].

### 1.2.1. Structure and Membrane Properties of Mitochondria

Mitochondria are one of the most specialized organelles. They show a two-membrane system, which divides the mitochondrion into four different compartments, namely the outer cell membrane, the inner cell membrane, the intermembrane space, and the matrix (Figure 4) [31–34].

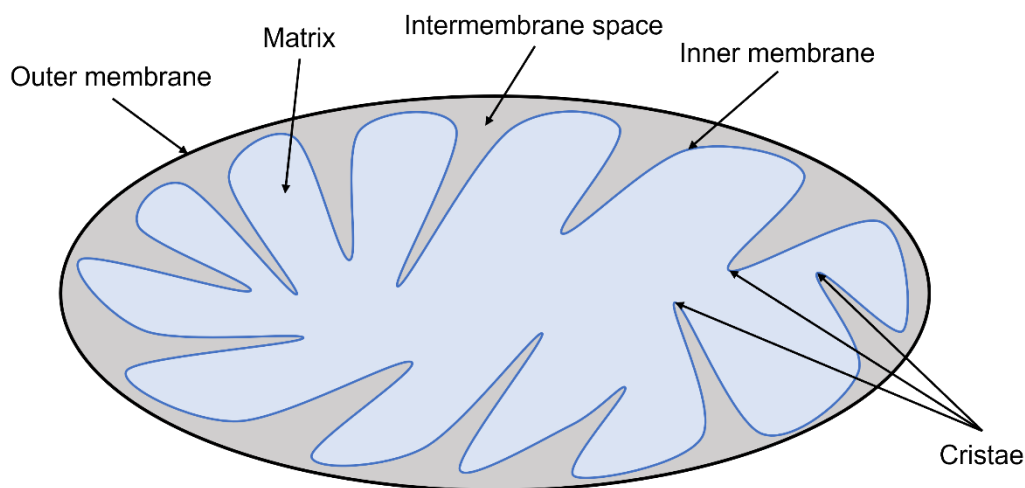


**Figure 4:** Schematic structure of a mitochondrion.

From outside to inside: Outer membrane, intermembrane space, inner membrane and matrix. The inner membrane is folded into so-called cristae. The figure was drawn using PowerPoint.

The outer membrane is the barrier to the mitochondrial environment and the entry port for many different molecules. It is rich in lipids and contains mainly the phospholipids phosphatidylcholine and phosphatidylethanolamine. Furthermore, it has a high number of porins and a high fluidity [31,33]. The inner membrane represents a tight diffusion barrier, and it shows a high protein density (76 %). The surface area of the inner membrane is significantly larger than the one of the outer membrane as it is highly folded into so-called cristae structures [31,33]. Both membranes, the inner and outer membrane, are in close contact via junctions [33]. The

intracellular or intermembrane space between the two membranes is around 20  $\mu\text{m}$  wide and differs from the cytosol in several physicochemical properties [31].

The overall shape and size of mitochondria is not fixed as they undergo constantly fission and fusion processes and can be almost round but also elongated [31,34].

Like any other subcellular compartment, mitochondria have their own specific lipid composition, which may vary depending on the cell type. However, compared to other subcellular fractions, all mitochondria have low phospholipid-to-protein ratios. As mentioned above, the major phospholipids in mitochondria are phosphatidylcholine and phosphatidylethanolamine. On the other hand, sterols and sphingolipids are present only in very small amounts. A unique characteristic solely found in mitochondria is the phospholipid cardiolipin [33,34].

### **1.3. Cardiolipin**

As mentioned before, the presence of cardiolipin makes the lipid composition of mitochondria unique [38]. For this reason, it is also called mitochondrial signature lipid. In the inner mitochondrial membrane, up to 20 % of the total lipid content is cardiolipin, one reason for this high content could be that the lipid is synthesized here. It is the major anionic phospholipid in mitochondrial membranes and plays a role in many important mitochondrial processes [37–39]. For example, it plays a role in stress, apoptosis, mitochondrial membrane dynamics, energy metabolism, metabolic carriers, and mitochondrial metabolism [33,34,37–41]. Cardiolipin also associates with several proteins, stabilizing them and/or altering their function [42].

Since cardiolipin is important for many processes, it is also associated with many medical conditions and diseases, such as the Barth's Syndrome (BTHS), Tangier's disease, diabetes, and heart disease [38,39]. In addition, loss of cardiolipin can lead to reactive oxygen species (ROS) and altered or decreased cardiolipin content leads to a disruption of mitochondrial homeostasis in various tissues. For this reason, it can be associated with various pathological conditions, including ischemia, hypothyroidism, aging, heart failure, ischemic reperfusion, and neurodegenerative disease [41,42].

Cardiolipin shows beside its unique occurrence also a unique structure (Figure 5). It contains three glycerol backbones and four acyl chains. The polar head of cardiolipin has two negative charges, which gives the lipid a dimeric and highly specific conical structure [38,42]. The acyl chain composition of cardiolipin is very diverse and differs

depending on its localization in an organism. In humans, cardiolipin mainly contains di-unsaturated acyl chains [38,39].

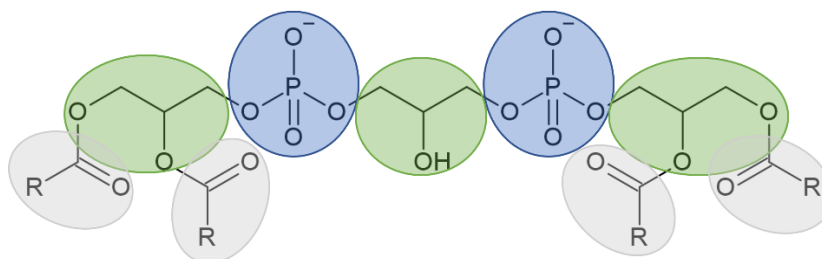


**Figure 5:** Structure of cardiolipin.

Head group of cardiolipin with the two phosphate groups (blue) with a negative charge each and three glycerol groups (green). Four acyl chains are coupled to the backbone (grey). R can be various saturated and unsaturated carbon chains. The structure is drawn with ChemSketch V5 (Freeware from ACD/Labs, Toronto, Ontario, Canada).

The biological formation of cardiolipin occurs in the inner leaflet of the inner mitochondrial membrane. It is formed from phosphatidylglycerol (PG) and cytidine diphosphate-diacylglycerol and undergoes at least two remodelling steps [37–40]. The condensation of PG and cytidine diphosphate-diacylglycerol is catalysed by the enzyme cardiolipin synthase which is encoded by *crd1*. A deletion of this gene results in complete depletion of cardiolipin in yeast [38,39].

The previously mentioned remodelling steps are an important part of receiving mature cardiolipin. There are two possible remodelling ways. One is Coenzyme A- (CoA) dependent and known as the Lands-cycle. Here, a deacylation-reacylation takes place. The other pathway is CoA-independent and a trans-acylation between two different phospholipids [38]. The only known enzyme involved in the second maturation pathway is tafazzin [38,39]. Tafazzin transfers a fatty acid from a phospholipid (*e.g.*, PG) to a lyso-phospholipid (mono-lyso cardiolipin (MLCL)). This reaction is unspecific, and it is still scientifically unexplained how the specific cardiolipin patterns in tissues arise [39].

In order to study the disease patterns associated with cardiolipin, it is important to determine and quantify cardiolipin. This is often done by thin-layer chromatography which is not very sensitive and limited to non-living systems. Another method is the visualization of cardiolipin with the help of specific dyes. 10-*N*-nonyl-acridine-orange (NAO) is often used as it has long been considered to be cardiolipin specific. While it is known already for a while that NAO also binds to other negatively charged lipids, it is

still frequently used [38]. This shows how important it is to find and establish new cardiolipin specific markers.

#### **1.4. Membrane Targeting and Modulation**

By using specific markers, membranes can be examined regarding disease patterns. Nowadays, many different naturally and synthetically occurring small molecules, macromolecules and proteins are known to interact with membranes. This interaction of a molecule with the membrane is a result of the interaction between functional groups, which can form hydrogen bonds, van der Waals, electrostatic and/or hydrophobic interactions. Many physical membrane properties, such as fluidity, membrane tension, hydrophobic thickness, electrostatics, and curvature, affect the interaction between these molecules and the membrane. However, the molecules can also influence and change the physicochemical properties of a membrane [43,44]. For this reason, many therapeutics act directly on the membrane. Some of them even regulate lipid composition or target lipids directly, while others target membrane proteins [45–47]. In order to find and establish new more specific molecules or substances which are binding to the membrane or influence its properties, it is important to know which molecular properties lead to an interaction between a molecule and the membrane.

#### **1.5. Model Membranes**

There are several approaches and possibilities to study membranes and their interaction with proteins, natural or synthetic molecules: *in silico* using calculations and simulation methods, or *in vitro* and *in vivo* including model membranes, bacteria or cells. In all cases, a situation as close as possible to the physiological one is favoured but can mostly not be realized. *In vitro* studies often use simple model systems, like lipid monolayers and bilayers, liposomes, small unilamellar vesicles, large unilamellar vesicles (LUVs), and giant unilamellar vesicles (GUVs). An advantage of these systems is that the environment of the experiment can be easily controlled and modified.

LUVs and GUVs are very common and efficient model systems for membrane studies. Both - their lipid composition and their size – are easy to control which is a great

advantage. Furthermore, GUVs have a size of several micrometres and can be easily visualized directly by a microscope and in real time [48–50].



## 1.6. Objectives of This Thesis

Biomembranes are essential for life. They are responsible for the appropriate interaction of different molecules to keep the biologically significant processes in the cells of an organism in line. Various small and large, natural and synthetic molecules are known to do so. For example, many pharmaceutical drugs have a positive effect on the organism if interacting with the membrane, but some molecules also have negative effects, and *e.g.* disrupt the membrane. How a substance interacts with a membrane depends on the type and properties of the molecule as well as on the structure of the membrane and the exact site of the interaction. Because of the great variety of the occurring effects, research on these interactions and influences is of great scientific interest as well as a targeted control and modulation of the membrane. Targeted visualization of specific membrane regions or components (lipids) can also help to understand the mechanism of certain processes.

In this thesis, four projects are presented with focus on either membrane modulation or cardiolipin binding and identification.

**I.** In the first project, the impact of the small molecule 2-phenylethanol (2-PEtOH) and some of its derivatives on model membranes was investigated. The aim was to identify molecular properties that can be used to predict their influence on a biological membrane. This could help in the future to screen different molecules with certain properties to achieve targeted control of different effects on the membrane. We focused on the ability of the substance to incorporate into the lipid bilayer and how it could influence the membrane order. Furthermore, we tested the bacteriotoxic effect of the substances and looked for a correlation between the incorporation and bacteriotoxic effect of the substance.

**II.** Mitochondria have a number of essential functions. Dysfunctions of mitochondria lead to aging of biological systems and are involved in the development of various serious diseases. Targeted modulation of the structure and dynamics of mitochondrial membranes by small molecules can help to directly influence these processes. One lipid is thought to play a key role in these mitochondrial processes, namely cardiolipin. Therefore, cardiolipin is a good starting point for these studies. In this project we used computer-assisted screening methods to find molecules directly and specifically

interacting with cardiolipin. After we identified some promising candidates, we tested their specific effect in *in vitro* and *in vivo* experiments.

**III.** Many mitochondrial proteins interact specifically with the cardiolipin. One of these proteins is the dynamin-related protein 1 (DRP1), which plays a role in mitochondrial fission processes. In this project the specificity of the protein was used to create and establish a new cardiolipin specific marker. For this purpose, the parts of DRP1 that are important for the specific cardiolipin interaction were coupled to a fluorescent protein. Subsequently, among other techniques the specific binding was investigated using GUVs and fluorescence microscopy.

**IV.** In this project, we focused on tafazzin and cardiolipin. The membrane associated protein tafazzin is an enzyme involved in cardiolipin maturation and mutations in this protein can lead to a disease called Barth syndrome (BTHS). The association of the enzyme with the membrane plays an important role for its function but is not yet clearly understood. For this reason, we investigated the membrane association of tafazzin using a construct lacking the region proposed to be necessary for binding to the membrane.

## 2. Materials

### 2.1. Chemicals and Expendable Material

All chemicals were purchased from Sigma-Aldrich (Munich, Germany), Merck (Darmstadt, GER) and Roth (Karlsruhe, GER). All lipids were purchased from Avanti Polar Lipids (Alabaster, ALA, USA). Enzymes were bought from New England Bio Labs (Frankfurt, GER). The substances (small molecules) from chapter 5 were purchased from MCULE (Budapest, HUN).

Expendable material was, if not declared otherwise, purchased from Bio-Rad (Munich, GER), Roth (Karlsruhe, GER), Sarstedt (Nürnberg, GER) and VWR (Darmstadt, GER).

### 2.2. Buffers and Solutions

The composition of all used buffers and solutions can be found in Table 1. They were all prepared with deionized and filtered water, if necessary.

**Table 1:** Composition of buffers and solutions.

<b>Notation</b>	<b>Composition</b>
<b><i>E. coli</i> culture</b>	
Ampicillin	100 mg/mL in 50 % Ethanol
Kanamycin	30 mg/mL in H <sub>2</sub> O
Streptomycin	50 mg/mL in H <sub>2</sub> O
IPTG	1 M in H <sub>2</sub> O
<b>SDS-PAGE</b>	
Stacking gel buffer	1.5 M TRIS 0.4 % SDS (w/v) pH 6.8
Separation gel buffer	0.5 M TRIS 0.4 % SDS (w/v) pH 8.8

10x SDS running buffer	0.25 M TRIS 1.92 M Glycine 1 % SDS (w/v) PH 8.3
5x SDS sample buffer	0.25 M TRIS 10 % SDS (w/v) 0.2 % Bromphenol blue 50 % Glycerol (v/v) 0.5 M DDT
Coomassie staining solution	0.125 % Coomassie Brilliant Blue G-250 (w/v) 40 % Ethanol (v/v) 2 % Phosphoric acid (v/v)
Coomassie destaining solution	30 % Ethanol (v/v) 2 % Phosphoric acid (v/v)

---

**Western Blot detection**

TBST buffer	0.25 M TRIS 0.125 M NaCl 0.05 % Tween 20 (v/v) pH 7.8
Transfer buffer	0.25 M TRIS 0.192 M Glycerol 30 % Methanol (v/v) pH 7.6
Blocking buffer	5 % Milk powder in TBST buffer
Antibody His Tag® Monoclonal Antibody	1:10 000 in TBST
ECL1 solution	90 % H <sub>2</sub> O 10 % TRIS (500 mM, pH 8) 1 % Luminol (250 mM DMSO) 0.44 % Coumaric acid (50 mM DMSO)
ECL2 solution	90 % H <sub>2</sub> O 10 % TRIS (500 mM, pH 8) 0.055 % H <sub>2</sub> O <sub>2</sub> (v/v)

---

---

**Gel electrophoresis**

TAE	400 mM TRIS 10 mM EDTA 200 mM acetic acid
6x loading buffer	50 % glycerin (v/v) 0.2 % bromophenol blue (w/v) 0.2 % xylene cyanole (w/v)

---

**Membrane association assay**

Buffer 1	25 mM Tris 2 mM EDTA pH 8
Buffer 2	10 mM HEPES pH 7.5
Buffer 3	50 mM HEPES pH 7.5
Buffer 4	50 mM HEPES 2 M NaCl pH 7.5
Buffer 5	50 mM HEPES 2 M CaCl <sub>2</sub> pH 7.5
Buffer 6	50 mM HEPES 2 M NaSCN pH 7.5
Buffer 7	50 mM HEPES 6 M Urea pH 7.5
Buffer 8	10 mM Caps pH 10.5
Buffer 9	10 mM Caps pH 11
Buffer 10	10 mM Caps pH 11.5

---

Buffer 11	10 mM Caps pH 12
Buffer 12	0,1 M NaOH pH 13
Buffer 13	50 mM HEPES 3 % SDS

---

### General buffers

HEPES buffer	10 mM HEPES 150 mM NaCl pH 7.4
PBS buffer	12 mM H <sub>3</sub> PO <sub>4</sub> 2.7 mM KCl 137 mM NaCl pH 7.4
Phosphate buffer	50 mM Sodium phosphate 150 mM NaCl 10 % Glycerol pH 8
GUV buffer	20 mM HEPES 150 mM NaCl 7.5 mM KCl 5 mM MgCl <sub>2</sub> pH 7.4

---

## 2.3. Kits and Standard Marker

Used kits are listed in Table 2. Used standard marker can be found in Table 3.

**Table 2:** Used kits.

Kit	Manufacturer
Plasmid preparation	Presto Mini Plasmid Kit NucleoSpin Plasmid Kit
	Geneaid Biotech, Taipei, TW Machery Nagel, Düren, GER

---

Agarose gel extraction Gel/PCR DNA Fragments Geneaid Biotech, Taipei, TW  
Kit

---

**Table 3:** Used marker.

<b>Marker</b>		<b>Manufacturer</b>
DNA Ladder	GeneRuler™ 1kb	Thermo Scientific, Darmstadt, GER
Protein Ladder	PageRuler™ Prestained PageRuler™ Unstained	Thermo Scientific, Darmstadt, GER

---

## 2.4. Media and Bacterial Strains

The used bacteria strains are listed in Table 5. *E. coli* MC4100 were cultivated in TB-Medium. All others were cultivated in LB-Medium (Table 4).

**Table 4:** Used media.

<b>Notation</b>	<b>Composition</b>
LB medium	1 % Tryptone (w/v) 5 % Yeast extract (w/v) 1 % NaCl (w/v)
TB medium	1.2 % Tryptone (w/v) 2.4 % Yeast extract (w/v) 0.4 % Glycerol
LB/TB agar	1.5 % Agar (w/v) in LB/TB medium

---

**Table 5:** Used bacteria strains.

<b>Bacteria strain</b>	<b>Genotype</b>
<i>E. coli</i> MC4100	<i>F<sup>-</sup> [araD139]<sub>B/r</sub> Δ(argF-lac)169 λ<sup>-</sup> e14<sup>-</sup> flhD5301 Δ(fruK-yeiR)725 (fruA25) relA1 rpsL150(strR) rbsR22 Δ(fimB-fimE)632(::IS1) deoC1</i>
<i>E. coli</i> Tuner(DE3)	<i>F<sup>-</sup> ompT hsdS<sub>B</sub> (r<sub>B</sub><sup>-</sup> m<sub>B</sub><sup>-</sup>) gal dcm lacY1(DE3)</i>
<i>E. coli</i> XL1 blue	<i>recA1 endA1 gyrA96 thi-1 hsdR17 supE44 relA1 lac</i>

## 2.5. Plasmids

**Table 6:** Used and generated plasmids.

<b>Plasmid</b>	<b>Origin</b>
pEYFP-C1-DRP1	addgene, Watertown, MA, USA Plasmid #45160
pEYFP-C1-DRP1 A1029G T1872C	This work
pET30b-5M SrtA	addgene, Watertown, MA, USA Plasmid #51140
pET30b-5M SrtA eYFP-DRP1	This work
pET30b-5M SrtA eYFP-stalk	This work
pET30b-5M SrtA eYFP-B-insert	This work
pCMV6-Entry wt taz	Eurofins Genomics, Ebersberg, GER
pCMV6-Entry taz C744T	This work
pCMV6-Entry taz C744T Nde1 Xho1	This work
pET30b-5M SrtA wt taz	This work
pET30b-5M SrtA ΔTM	This work



## 2.6. Instruments

**Table 7:** Used instruments.

<b>Instrument</b>	<b>Notation</b>	<b>Manufacturer</b>
Cell homogenizer	Maximator	Maximator GmbH, Nordhausen, GER
Centrifuges	Avanti J-26CP	Beckman Coulter, Krefeld, GER
	Centrifuge 5810 R	Eppendorf, Hamburg, GER
	Optima MaxXP	
	Ultracentrifuge	Beckman Coulter, Krefeld, GER
Chemoluminescence detection system	Stella	Raytest, Straubenhardt, GER
	Fusion FX	Vilber, Marne-la Vallée cedex 3, FRA
Electrophoresis chamber	Mini-Protean 3 cell	Bio-Rad, Munich, GER
Electrophoreses power supply	PowerPac Basic	Bio-Rad, Munich, GER
Fluorescence microscope	Axio observer.Z1	Carl Zeiss Microscopy, Jena, GER
Fluorescence spectrometer	Fluoro-Max-4	Horiba, Bensheim, GER
	FP-8500	Jasco Deutschland GmbH, Pfungstadt, GER
Gel scanner	ViewPix700	Biostep, Burkhardtsdorf, GER
Heating block	Thermomixer comfort	Eppendorf, Hamburg, GER
Incubator	B28	Binder, Tuttlingen, GER
	Multitron HAT	Infors, Bottmingen, CH
Microwave	R-234	Sharp, Köln, GER
Oxygen Sensitive Optrode and PreSens Fibox 3 Minisensor	DP-PSt3-L2.5-5510-YOP	Presens Precision Sensing GmbH, Regensburg, GER

pH-Meter	pH211 Microprocessor	HANNA Instruments, Vöhringen, GER
Photometer	Nanodrop 2000C	Thermo Scientific, Darmstadt, GER
Thermocycler	Thermocycler TGradient 96	Biometra, Göttingen, GER
UV table	Transilluminator	Stratagene, Heidelberg, GER
Western Blot system	Trans-Blot Turbo Transfer System	Bio-Rad, Munich, GER

## 2.7. Software

**Table 8:** Used software programs

<b>Application</b>	<b>Software</b>
Chemical structures	ChemSketch V5, Freeware from ACD/Labs, Toronto, Ontario, CAN
Data analysis	MicrosoftExcel (Office 365) Origin 2019b OriginPro 8.6, Northampton, MA, US
Calculation of the partition coefficient (logP)	Molinspiration v2016.10 (www.molinspiration.com, accessed on 21. June 2018)
Figure editing	Adobe Illustrator 2020 Adobe Photoshop CC 2018 Microsoft PowerPoint (Office 365)
Literature management	Mendeley 1.19.8
Text editing	Microsoft Word (Office 365)

## 3. Methods

In this section the general methodology of the experiments is described. The deviations for the different sections are highlighted.

### 3.1. Molecular Biological Methods

#### 3.1.1. Polymerase Chain Reaction and Site Directed Mutagenesis

Polymerase chain reaction (PCR) is used for the exponential amplification of a DNA region defined by two primers. Site-directed mutagenesis (SDM) is a form of PCR and used to introduce single or multiple mutations into plasmid vectors. For this purpose, primers are required that overlap with the plasmid DNA but have an altered base sequence at the desired location. In this work PCR and SDM were used for construct design (chapter 6 and chapter 7). Detailed experimental information can be found in chapters 3.1.2. and 3.1.3.

Table 9 shows the standard mixture for the PCR/SDM reaction and Table 10 the programs used.

**Table 9:** PCR reaction mixture.

	Concentration	Volume [ $\mu$ L]
<b>H<sub>2</sub>O (sterile)</b>		33.5
<b>Phusion GC-buffer</b>	5x	10
<b>MgCl<sub>2</sub></b>	25 mM	1
<b>DMSO</b>		1
<b>Plasmid</b>		1
<b>Primer (forward)</b>	10 $\mu$ M	1
<b>Primer (reverse)</b>	10 $\mu$ M	1
<b>dNTPs</b>	2 mM	1
<b>Phusion Polymerase</b>	2.5 U	0.5

**Table 10:** Programs used for polymerase chain reaction (PCR) and site-directed mutagenesis (SDM)

	Temperature [°C]	Time [min]	Cycles
<b>Initial denaturation</b>	98	1	
<b>Denaturation</b>	98	0.5	36 PCR 16 SDM
<b>Hybridization</b>	65	1	
<b>Elongation</b>	72	1000 number of base pairs	
<b>Final Elongation</b>	72	7.5	

In case of site-directed mutagenesis, parental DNA was digested by incubating the reaction mixture with *Dpn1* at 37 °C for 1 hour. The reaction mixture was then transformed into *E. coli* XL1 blue cells as described in chapter 3.2.2. A single colony was picked and used to inoculate 10 mL of Lysogeny broth (LB) medium (100 µg/mL ampicillin). The bacteria were incubated overnight at 37 °C and 180 rpm (Multitron). After harvesting the cells by centrifugation (16 000 g, 2 minutes, 4 °C) plasmid preparation was performed (chapter 3.1.3.).

### 3.1.2. Agarose Gel Electrophoresis

Gel electrophoresis was used for analytical and preparative separation of DNA fragments and plasmid DNA.

1 % (w/v) agarose was dissolved in TAE buffer by heating in a microwave. DNA samples were mixed 5:1 with 6x loading buffer and pipetted onto the gel. Separation was performed at 129-150 V.

For DNA visualization the gel was placed in a 1 µg/mL ethidium bromide solution for 15 – 30 minutes. The gel was then exposed to UV light. The gels were photographed using a transilluminator.

If preparative gel electrophoresis was performed, the parts of the gel that contained DNA of interest were excised and recovered using the Gel/PCR DNA fragment Kit.

### **3.1.3. Plasmid Preparation**

Plasmids were prepared using the Presto Mini Plasmid Kit or the NucleoSpin Plasmid Kit. This was done as recommended by the manufacturer. DNA concentration was determined by the absorption of 260 nm using the NanoDrop. The correct plasmid sequences were confirmed by sequencing (Eurofins Genomics, Ebersberg, GER).

### **3.1.4. Restriction Digest of DNA**

Various enzymes were used for the restriction digest of DNA. Hereby restriction endonucleases cut the DNA at specific sites. In this work, DNA digestion was used to generate specific DNA ends for cloning purposes and for verification of these clonings. In case of preparative experiments, a total volume of 50  $\mu\text{L}$  was used. The restriction endonucleases and buffers used were according to the manufacturer's instructions. The mixture was incubated at 37 °C for 4 hours °C. Subsequently, the desired DNA fragment was isolated using preparative agarose gel electrophoresis (chapter 3.1.2). For analytical control restriction, a total volume of 10  $\mu\text{L}$  was used. The result was analyzed by analytical agarose gel electrophoresis (chapter 3.1.2.).

### **3.1.5. Ligation**

Ligation allows the introduction of restricted foreign DNA into a restricted linearized plasmid vector. DNA strands with complementary ends were ligated using T4 DNA ligase. was used to ligate restricted/digested DNA into restricted vector. 100 ng of vector DNA

100 ng of vector DNA was used and the insert was added in a fourfold molar excess. The total volume of the reaction mixture was 20  $\mu\text{L}$  and was performed according to the manufacturer's introductions. The mixture was incubated for 2 hours at room temperature in the dark. Ligation products were monitored by analytical DNA restriction digest followed by analytical agarose gel electrophoresis and sequencing (Eurofins Genomics, Ebersberg, GER). The whole reaction mixture was used for transformation into *E. coli* bacteria.

### 3.1.6. Construct Design of DRP1 constructs (Chapter 6)

eYFP tagged human isoform 3 DRP1 was purchased from addgene (Watertown, MA, USA, Plasmid #45160, GenBank ID NM\_005690). Site-directed mutagenesis was performed to eliminate two *ssp1* restriction sites in the middle of the DNA encoding for the protein. The primers used can be found in Table 11.

PCR (chapter 3.1.1.) was used to amplify the eYFP-DRP1 construct and the PCR product was purified, digested, and ligated into a pET30b-5M SrtA vector/plasmid (addgene, Watertown, MA, USA, Plasmid #51140) (chapter 3.1.2-3.1.5)

The eYFP-stalk (amino acid 329 to 668 of full length DRP1) and eYFP-B-insert (amino acid 503 to 599 of full length DRP1) constructs were designed using standard protocols (chapter 3.1.1.) The primers used can be found in Table 11.

DRP1 was excised from eYFP-DRP1 using restriction enzymes (*EcoRI* and *BamHI*) and the Stalk (the B-insert, respectively) was ligated into it to receive eYFP-stalk and eYFP-B-insert.

**Table 11:** Primers used for DRP1 construct design

Primer	Use
forward: CAAATTTGCCACAGAGTATTGTAACACTATTG; reverse: CAATAGTGTTACAATACTCTGTGGCAAATTTG;	Elimination of the <i>ssp1</i> restriction site; A1029G
forward: CATTGTCAGAAAGAACATTCAAGACAGTGTG; reverse: CACTGTCTTGAATGTTCTTTCTGACAATG	Elimination of the <i>ssp1</i> restriction site; T1872C
forward: GCGCGCAATATTATGGTGAGCAAGGGC reverse: GCGCGCGGTACCTCACCAAAGATGAGTC	Amplification eYFP-DRP1
forward: GCGCGCGCGAATTCGAAAAGTGCTACTTTAC reverse: GCGCGCGGATCCTTAGTCCTCAGATTC	Amplification stalk domain
forward: GCGCGCGAATTCGGATGCTTGTGGGCTAATG reverse: GCGCGCGGATCCTTATAGTTTTTCGTGC	Amplification B-insert

### 3.1.7. Tafazzin Construct Design (Chapter 7)

Human wild type tafazzin isoform 1 was synthesized by and purchased from Eurofins Genomics (Ebersberg, GER). To get rid of a *Nde1* restriction site in the middle of the DNA encoding for the protein, site-directed mutagenesis (chapter 3.1.1.) was performed. The used primers can be found in Table 12.

New restriction sites (*Xho1* and *Nde1*) were introduced (primers: Table 12). Subsequently, full-length tafazzin was subcloned into a pET30b vector (addgene, Watertown, MA, USA, Plasmid #51140) by ligation (chapter 3.1.5.).

To obtain the  $\Delta$ TM construct (lacking the transmembrane helix [51]), the 35 N-terminal amino acids were deleted using standard PCR methods (chapter 3.1.1, primers: Table 12).

**Table 12:** Primers used for tafazzin construct design

Primer	Use
forward: GCCCTGCCTGTACTTGAGCGGCTCCGGG reverse: CCCGGAGCCGCTCAAGTACAGGCAGGGC	Elimination of the <i>Nde1</i> restriction site; C744T
forward: GCGCGCCATATGCCTCTGCACGTGAAG reverse: GCGCGCCTCGAGTCTCCCAGGCTGGAG	Creation of new restriction sites
forward: GCGCGCCATATGAAGTACATGAACCAC reverse: GCGCGCCATATGTATATCTCCTTCTTAAAG	Elimination of the transmembrane helix

## 3.2. Microbiological Methods

### 3.2.1. Transformation of Competent Bacteria

*E. coli* Tuner(DE3) and *E. coli* XL1blue cells were made transformation competent using ice-cold tryptic soy broth (TSB)-medium as described by Chung-Miller [52].

4 mL of LB medium were inoculated with a colony of the *E. coli* strain and incubated overnight at 37 °C and 180 rpm (Multitron). This preculture was used to inoculate 50 mL of LB medium at a 40:1 ratio. After the culture reached an optical density (OD<sub>600</sub>) of approximately 0.6 the cell suspension was centrifuged at 4 °C (3220 g,

10 minutes). The pellet was resuspended in 5 mL of ice-cold TSB medium and incubated on ice for 10 minutes. Aliquots of 100  $\mu$ L were frozen in liquid nitrogen and stored at -80 °C.

### **3.2.2. Plasmid Transformation**

In this work, transformation of plasmid DNA into *E. coli* by heat shock was used. An aliquot of 100  $\mu$ L of competent cells (chapter 3.3.1.) was thawed. Under sterile conditions, 1  $\mu$ L of the preferred plasmid solution was added and the cells were incubated on ice for 20 minutes. Heat shock at 43 °C for 90 seconds causes permeability of the membrane to the DNA plasmid. After incubation on ice for 5 minutes, 500  $\mu$ L of LB medium was added and the cells were incubated at 37 °C and 180 rpm (Multitron) for 1 hour. 200  $\mu$ L of the cell suspension was applied to an agar plate. The agar plate was incubated over night at 37 °C (B28)

### **3.2.3. Heterologous Expression of Proteins**

All protein constructs in this work were heterologously expressed in *E. coli* Tuner(DE3). For this purpose, the corresponding expression plasmid was transformed into the expression strain (chapter 3.2.2.). Subsequently, 50 mL of LB medium containing 100  $\mu$ g/mL kanamycin were inoculated with a single colony of the transformed cells and incubated overnight at 37 °C and 180 rpm (Multitron). Subsequently, 2 L of LB medium containing 100  $\mu$ g/mL kanamycin were inoculated with the precultures and the cells were cultured at 37 °C under constant movement (120 rpm, Multitron). At an OD<sub>600</sub> of 0.7, protein expression was induced by adding 2 mL of 1 mM Isopropyl  $\beta$ -D-1-thiogalactopyranoside (IPTG), followed by another 4 hours of incubation at 37 °C and 120 rpm (Multitron). Cells were harvest by centrifugation (10 minutes, 4 °C, 2346 g, Avanti J-26CP) The resulting pellet, from 2 L culture was resuspended in approximately 30 mL phosphate buffer and stored at -20 °C.



### 3.2.4. Growth Assay and Determination of Minimal Inhibitory Concentrations 50 (MIC<sub>50</sub>) (Chapter 4)

This chapter is an unchanged section of my 2020 in MDPI membranes published article “The Bacteriostatic Activity of 2-Phenylethanol Derivatives Correlates with Membrane Binding Affinity”. The entire article can be found in Appendix 13.2. The style was adapted to this thesis.

*Escherichia coli* strain MC4100 was grown in a terrific broth (TB)-medium buffered with 10 % K<sub>2</sub>HPO<sub>4</sub>/KH<sub>2</sub>PO<sub>4</sub> (0.17 M/0.72 M). 20 mL TB medium with 1:1000 streptomycin (50 mg/mL) was prepared, and the tested substance was dissolved in the medium at the given concentration. From an overnight culture, *E. coli* MC4100 was diluted in fresh medium to an OD<sub>600</sub> of 0.2. The cultures were incubated at 37 °C and 200 rpm for four hours, the OD<sub>600</sub> of a 5fold diluted sample was measured, and the real value was calculated. The highest tested concentration was defined by the solubility of the tested substances in TB medium or was the concentration where the *E. coli* were not able to grow anymore. A dose-response curve was fit to the data with a modified Hill equation using OriginPro 8.6 (Northampton, MA, US),

$$y = c + \frac{d-c}{1+(\frac{x}{e})^b} \quad (1)$$

[53], with the concentration of the substance  $x$  and the parameter  $e$  reflecting the MIC<sub>50</sub> for each tested substance (Figure 9). In order to get an idea about the concentration of the substance incorporated into the *E. coli* membrane, we calculated the overall surface area presented by the bacteria and, based on the partition coefficient, calculated the concentration of the lipids required to obtain the corresponding area/ml as liposomes. According to [54], an OD of 0.2 corresponds to about  $2 \cdot 10^8$  *E. coli* cells/ml. The surface area of an *E. coli* cell is about  $3 \mu\text{m}^2$  [55], corresponding to about  $4.2 \cdot 10^6$  lipid molecules, assuming  $0.7 \text{ nm}^2/\text{lipid}$  [56]. Thus, the concentration of the lipids necessary to create the corresponding area of a lipid bilayer is about  $3 \mu\text{M}$ .

### 3.2.5. Oxygen Consumption of *E. coli* (Chapter 5)

For *E. coli* oxygen consumption measurements, a PreSens Fibox 3 Minisensor and an Oxygen Sensitive Optrode (DP-PSt3-L2.5-5510-YOP, PreSens Precision Sensing

GmbH, Regensburg, Germany) was used. *E. coli* MC4100 cells from an overnight culture (prepared as described above) were diluted and grown until an OD<sub>600</sub> of around 0.6 was reached. The cells were harvested, and the pellet was resuspended in 200 µL PBS Puffer (137 mM NaCl, 2.7 mM KCl, 12 mM H<sub>3</sub>PO<sub>4</sub>, pH=7.4) containing 10 mM ethylenediaminetetraacetic acid (EDTA). Upon incubation for 5 minutes, cells were pelleted and resuspended in TB media (OD<sub>600</sub> = 0.2). SM<sub>19</sub> was added up to a final concentration of 10 µM. 3 mL cells were placed in the reaction chamber, the chamber was closed airtight, and the measurement was started at 37 °C. The measurement was stopped when the oxygen amount reached 0 µmol/L.

### **3.2.6. Fluorescence Microscopy of *E. coli* (Chapter 6)**

10 mL *E. coli* Tuner(DE3) in LB media containing the construct were grown at 37 °C to an OD<sub>600</sub> of 0.45. Protein production was induced by adding 5 µL of 1 M IPTG. After 15 minutes, 20 µL were transferred to an agarose pad and visualized under a fluorescence microscope (Axio observer.Z1). Bright channel and TagYFP channel pictures were taken using the 63x objective. Pictures were merged using Adobe Photoshop CC 2018.

## **3.3. Biochemical Methods**

### **3.3.1. Purification of Proteins**

The eYFP constructs (chapter 6) were purified by immobilized metal affinity chromatography using nickel-nitrilotriacetic acid (Ni-NTA)-agarose. Sigma protease inhibitor cocktail, (1:1000) was added to thawed cells from the heterologous protein expression (chapter 3.2.3.). The cells were homogenized using a maximator (Maximator GmbH) Cells were centrifuged at 13776 g for 10 minutes (Centrifuge 5810 R). The supernatant was incubated with 4 mL Ni-NTA-agarose (Machery-Nagel, Düren, GER) for 1 hour at room temperature. After transferring to a disposable column (5 mL polypropylene column) four wash steps were performed. One with 40 mL phosphate buffer, one with 60 mL phosphate buffer and 10 mM imidazole, one with 60 mL phosphate buffer and 20 mM imidazole, and one with 60 mL phosphate buffer and 40 mM imidazole. The protein was eluted with 10 mL phosphate buffer containing 200 mM imidazole. The imidazole was removed and the buffer was exchanged using a

PD10 desalting column (GE Healthcare, Chicago, IL, USA). For this purpose, the protein solution was concentrated to 2.5 mL and added to the column. Elution was performed with 3.5 mL of HEPES buffer. Small molecules such like imidazole remained on the column, while large molecules (such as proteins) were eluted.

Protein quality was checked using sodium dodecyl sulfate polyacrylamide gel electrophoresis (SDS-PAGE) and Western blot analysis. The absorbance of the protein solution at 280 nm was determined using the NanoDrop (ThermoScientific). Protein concentration was calculated using the specific extinction coefficient of the protein. For direct use, the protein was stored at 4 °C, for later use, 50 % (v/v) glycerol was added and the protein was stored at -20 °C.

### 3.3.2. SDS-PAGE

SDS-PAGE was used to separate proteins based on their molecular weight [57]. Two different gel compositions were used in this work. For the eYFP constructs from chapter 6 a 10 % acrylamide gel and for the tafazzin constructs from chapter 7 a 12 % acrylamide gel. The composition of the separation gels and the stacking gel can be found in Table 13.

**Table 13:** Composition of the separation and stacking gels

	Separation gel	Separation gel	Stacking gel
	12 %	10 %	
<b>H<sub>2</sub>O</b>	4.5 mL	5 mL	6 mL
<b>Acrylamide 40 %</b>	3 mL	2.5 mL	1.5 mL
<b>Specific buffer</b>	2.5 mL	2.5 mL	2.5 mL
<b>APS 10 %</b>	100 µL	100 µL	100 µL
<b>TEMED</b>	40 µL	40 µL	40 µL

Protein samples were mixed with 5x sample buffer and incubated at 80 °C for 20 minutes for denaturation. The gel was placed in a gel chamber containing SDS running buffer (Table 1) and the samples were loaded. A standard was also loaded to determine the molecular weight. A voltage of 200 V was used to separate the proteins. Electrophoresis was stopped when the running front reached the end of the gel.

After electrophoresis the gel was placed in Coomassie brilliant blue R250 solution to visualize the proteins in the gel. This dye interacts with basic amino acids of the protein. The gel was incubated for 1 hour in the Coomassie solution. The excess dye was removed by incubating the gel in the Coomassie destaining solution (Table 1) until the protein band was clearly visible. For documentation the gel was scanned after a short incubation in water.

### **3.3.3. Western Blot Analysis**

Western blot analysis was performed to identify proteins. Proteins were transferred to a nitrocellulose membrane after SDS-PAGE and identified using a specific antibody. In this work an anti-histidine tag (HisTag) antibody was used.

For transferring the protein on the nitrocellulose membrane the Trans-Blot Turbo Transfer system from Bio-Rad was used. An electric field (25 V) was applied for 30 minutes. The membrane was then incubated in blocking buffer for 1 hour and then washed three times with TBST buffer for 5 minutes each. After the washing step the membrane was incubated with the antibody for one hour and then washed again with TBST buffer (3x 5 minutes). To visualize the protein 10 mL of ECL1 solution was added for one minute followed by the addition of 10 mL ECL2 for 1 minutes. Luminescence was detected using the detection system Stella (Raytest). Figure 28 was detected with the detection system Fusiom FX (Viler).

### **3.3.4. Membrane Association Assay (Chapter 7)**

Cells were disrupted by using a Maximator (Maximator GmbH) (about 18000 psi) and the lysate was centrifuged for 10 minutes at 14000 g and 4 °C (Centrifuge 5810 R, Eppendorf (Hamburg, GER)). The supernatant was transferred into another tube and the pellet was discarded. The supernatant was replenished to 100 mL and divided into 13 ultracentrifuge tubes (7.5 mL each) following ultracentrifugation for 1 hour at 100000 g (Optima L-100K Ultracentrifuge). This time, the supernatant was discarded and the pellets were resuspended in 7.5 mL of 13 different buffers (Table 1). The samples were incubated and stirred for 30 minutes at room temperature. Subsequently, the samples were centrifuged again for 1 hour at 100000 g and 4 °C. A sample of the supernatant was taken. The pellet was resuspended in 2 mL of the

appropriate buffer. For relative protein quantification, Western blot analysis was performed (chapter 3.3.3.).

### **3.3.5. Liposome Preparation**

#### *Large unilamellar vesicles (LUVs)*

For liposome preparation, the lipid or lipid mixture of interest (dissolved in chloroform) was pipetted into a reaction tube. The solvents were removed under a gentle nitrogen stream and vacuum desiccation overnight.

The next day HEPES-buffer was added, and the lipid film was rehydrated. The LUVs used for the experiments in chapter 5 and 6 were prepared by vortexing the mixture twice for 1 minute. Subsequently, five freeze-thaw cycles were performed. To obtain the LUVs used in chapter 4, the mixture was vortexed and then incubated for 30 minutes at 37 °C and 1000 rpm in a thermoblock mixer comfort from Eppendorf. Five freeze thaw cycles were performed. The liposomes were again incubated for 30 minutes at 37 °C and 1000 rpm on a thermoblock mixer comfort from Eppendorf.

#### *Giant unilamellar vesicles (GUVs) (Chapter 6)*

GUVs were prepared using a polyvinyl alcohol (PVA) swelling method. 25 µL of 1 % PVA was dried on round coverslips. The coverslips were transferred into a multiwell plate and 8 µL of the desired lipid mixture was added. Lipid mixtures contained 50 % 1,2-dioleoyl-sn-glycero-3-phosphocholine (DOPC) and either 50 % 1,2-dioleoyl-sn-glycero-3-phosphoglycerol (DOPG) or 50 % cardiolipin. All mixtures contained PE-Atto336 (0.01 g/L) to stain the GUVs. To get rid of all solvents, the lipid film was dried for 30 minutes under vacuum. 400 µL of GUV buffer was added and the sample was incubated for 1 h. The GUVs were transferred into a 1.5 mL reaction tube and diluted 1:5. After transferring the GUVs into a glass chamber they set for 1 hour. GUVs were documented using a fluorescence microscope and the AF647 channel (Axio observer.Z1). Protein (eYFP-stalk) was added to a concentration of 0.1 g/mL and again GUVs were documented via the microscope, this time additionally using the TagYFP channel to visualize the protein.

### 3.3.6. Sedimentation Assay (Chapter 6)

20  $\mu\text{L}$  of 4.5 mM lipid in chloroform were used to prepare LUVs. Protein in HEPES buffer was added to the prepared liposomes, resulting in 0.05 mM protein, and incubated for 1 hour. 50  $\mu\text{L}$  were taken as a sample for SDS-PAGE analysis. The remaining sample was centrifuged for 30 minutes at 139104 g and 4  $^{\circ}\text{C}$  (Optima MaxXP ultracentrifuge). The supernatant was discarded, except for 50  $\mu\text{L}$ , which were kept as a sample for subsequent SDS-PAGE analysis. The pellet was resuspended in 150  $\mu\text{L}$  HEPES buffer and 50  $\mu\text{L}$  were collected for SDS-PAGE analysis.

## 3.4. Biophysical Methods

### 3.4.1. Laurdan Fluorescence Spectroscopy and Generalized Polarization Values

LUVs were prepared as described in chapter 3.3.5. Lipids were mixed with Laurdan (dissolved in methanol) in a 500:1 molar ratio before drying.

Laurdan spectra were recorded at 25  $^{\circ}\text{C}$  using a fluorescence spectrometer. The methods and the used instrument can be found in Table 14. Each lipid composition was measured at least three times using freshly prepared liposomes. Generalized polarization (GP) values were calculated from the fluorescence emission spectra using the following equation [58]:

$$GP = \frac{I_{440} - I_{490}}{I_{440} + I_{490}} \quad (2)$$

$I_{440}$  and  $I_{490}$  are the emission intensities at 440 and 490 nm, respectively.

**Table 14:** Instrument and methods used for Laurdan fluorescence spectroscopy.

	<b>Instrument</b>	<b>Method</b>
<b>Chapter 4 (PEtOH)</b>	Fluoro-Max-4 fluorescence spectrometer	excitation and emission band widths: 2 nm Excitation: 350 nm Recording: 400 - 550
<b>Chapter 5 (CliB)</b>	Jasco Spectrofluorometer FP-8500	excitation and emission band widths: 2.5 nm Excitation: 360 nm Recording: 400 - 600

**Chapter 4:** 25  $\mu\text{L}$  of 10 mM *E. coli* polar lipid (EPL) in chloroform and methanol (2:1) was used for liposome preparation. 250  $\mu\text{L}$  of the substances dissolved in HEPES-buffer at the desired concentrations were added for the rehydration of the lipid film. Depending on their solubility in aqueous buffer, methyl phenylacetate was measured up to 15 mM, 1-hexanol up to 70 mM, phenylacetic acid and phenyllactic acid up to 80 mM and Tyrosol and 2-phenylethanol up to 100 mM.

**Chapter 5:** If needed, a substance (dissolved in methanol) was added at the indicated concentration before drying. 300  $\mu\text{L}$  HEPES-buffer were added resulting in a solution with 300  $\mu\text{M}$  total lipid.

For easier comparison, the  $\Delta\text{GP}$  value was calculated using mean GP values determined in presence (+ $\text{SM}_{xx}$ ) or absence (- $\text{SM}_{xx}$ ) of the small molecules with the following equation.

$$\Delta\text{GP} = \text{GP}_{+\text{SM}_{xx}} - \text{GP}_{-\text{SM}_{xx}} \quad (3)$$

$xx$  is a number between 1 and 22.

For each mean value, the standard error of the mean (SEM) was calculated, and the error for  $\Delta\text{GP}$  and  $\Delta\text{GP}_{\text{cardiolipin}} / \Delta\text{GP}_{\text{PG}}$  was calculated based on Gaussian error propagation.

### 3.4.2. Fluorescence Measurements Using the Emission of SM19 (Chapter 5)

LUVs containing different amounts of DOPC and DOPG or cardiolipin (1,3-bis[1,2-dioleoyl-*sn*-glycero-3-phospho]-glycerol (TOCL)), respectively, were prepared as described (chapter 3.3.5.). 3  $\mu\text{M}$  SM<sub>19</sub> (2-[(*E*)-2-[4-(dimethylamino)phenyl]ethenyl]-3-ethyl-1,3-benzothiazol-3-ium iodide) was mixed with the lipids during liposome preparation. Fluorescence spectra were measured using a Jasco Spectrofluorometer FP-8500 (Jasco Deutschland GmbH). The sample was excited at 500 nm and spectra were recorded from 520 to 680 nm. The band widths were set to 2.5 nm.

### 3.4.3. Fluorescence Measurements of SM19 in Presence of *E.coli* (Chapter 5)

*E. coli* strain MC4100 was grown in TB-medium buffered with 10 % K<sub>2</sub>HPO<sub>4</sub>/KH<sub>2</sub>PO<sub>4</sub> (0.17 M/0.72 M). From an overnight culture, containing 10 mL TB medium with 1:1000 streptomycin (50 mg/mL), *E. coli* MC4100 were pelleted. The cells were washed three times with HEPES buffer and resuspended in buffer to a final OD<sub>600</sub> of 2. Different concentrations of SM<sub>19</sub> (dissolved in water) were added to 500 µL of cells and incubated for 5 minutes. The emission spectra of SM<sub>19</sub> were recorded between 520 and 680 nm with a Jasco Spectrofluorometer FP-8500 (Jasco Deutschland GmbH), upon excitation at 500 nm. The intensity at 592 nm was plotted.

### 3.4.4. LogP Correlation (Chapter 4)

This chapter is an unchanged section of my 2020 in MDPI membranes published article “The Bacteriostatic Activity of 2-Phenylethanol Derivatives Correlates with Membrane Binding Affinity”. The entire article can be found in Appendix 13.2. The style was adapted to this thesis.

It can be expected that the effect of a given compound on a membrane correlates with its tendency to incorporate into the membrane, represented by the corresponding partitioning coefficient P. This type of correlation is probed as [59]

$$\log \frac{1}{C} = a \times \log P + b \quad (4)$$

if only logP is considered as the predictor for the activity of the substance, with a and b being constants and C the concentration relevant for the effect to be tested, here: Minimal inhibitory concentration 50 (MIC<sub>50</sub>; see [59] for a recent discussion of the approach).














## 4. The Bacteriostatic Activity of 2-Phenylethanol Derivatives Correlates with Membrane Binding Affinity

### 4.1. Author Contributions

This chapter is a shortened version of my 2020 in MDPI membranes published article “The Bacteriostatic Activity of 2-Phenylethanol Derivatives Correlates with Membrane Binding Affinity”. It contains the unchanged text and figures of the Abstract, Introduction and Results and Discussion parts. The entire article can be found in Appendix 13.2. Materials and Methods used and performed by me can be found in chapter 2 and 3. Methods performed by others can be found in Appendix 13.1.1. The authors’ affiliations are listed in chapter 12 and the authors’ contributions are listed in Table 15

**Table 15:** Author contributions to “The Bacteriostatic Activity of 2-Phenylethanol Derivatives Correlates with Membrane Binding Affinity”

<b>Conceptualization</b>	Complete study	████████████████████
<b>Methodology</b>	Complete study	████████████████████
<b>Software</b>	Complete study	██████████
<b>Validation</b>	Complete study	████████████████████ ██████
<b>Formal analysis</b>	Complete study	████████████████████
<b>Investigation</b>	Complete study	████████████████████
<b>Writing</b>	Original draft preparation	████████████████████
	Review and editing	████████████████████

<b>Supervision, funding acquisition, resources, and project administration</b>	Complete study	
<b>Figures</b>	<b>Methodology, Investigation, Formal analysis</b>	<b>Data visualization</b>
<b>Figure 6</b> <b>Figure 7</b> <b>Figure 8</b> <b>Figure 9</b> <b>Figure 10</b>	    	    

## 4.2. Abstract

The hydrophobic tails of aliphatic primary alcohols do insert into the hydrophobic core of a lipid bilayer. Thereby, they disrupt hydrophobic interactions between the lipid molecules, resulting in a decreased lipid order, i.e., an increased membrane fluidity. While aromatic alcohols, such as 2-phenylethanol, also insert into lipid bilayers and disturb the membrane organization, the impact of aromatic alcohols on the structure of biological membranes, as well as the potential physiological implication of membrane incorporation has only been studied to a limited extent. Although diverse targets are discussed to be causing the bacteriostatic and bactericidal activity of 2 phenylethanol, it is clear that 2-phenylethanol severely affects the structure of biomembranes, which has been linked to its bacteriostatic activity. Yet, in fungi some 2-phenylethanol derivatives are also produced, some of which appear to also have bacteriostatic activities. We showed that the 2-phenylethanol derivatives phenylacetic acid, phenyllactic acid, and methyl phenylacetate, but not Tyrosol, were fully incorporated into model membranes and affected the membrane organization. Furthermore, we observed that the propensity of the herein-analyzed molecules to partition into biomembranes positively correlated with their respective bacteriostatic

activity, which clearly linked the bacteriotoxic activity of the substances to biomembranes.

### 4.3. Introduction

Due to their amphipathic properties, alcohols affect numerous biological processes, many of which are related to cellular membranes. The hydrophobic tails of alcohols insert into the hydrophobic core region of a lipid bilayer and disrupt hydrophobic interactions between the lipid molecules, resulting in a decreased lipid order, i.e., an increased membrane fluidity [60,61]. The exact impact of alcohol on the structure of a lipid bilayer depends on the length and overall hydrophobicity of the alcohol alkyl chain, and it is predicted that the effect of alcohols on membranes increases with increasing alkyl chain lengths [62]. Thus far, the impact of alcohols on biomembranes has been studied to a great extent using, aliphatic primary alcohols, albeit aromatic alcohols, such as 2-phenylethanol (2-PEtOH), also insert into lipid bilayers and disturb the membrane organization [63].

2-PEtOH, a compound also known as phenylethyl alcohol or benzylcarbiol, is a colorless liquid with a rose-like odor. 2-PEtOH occurs widely in nature and is—besides in rose extracts—a major component in a variety of plant extracts from carnations, hyacinths, jasminum, geranium species, and others [64]. 2-PEtOH has been shown to affect cell proliferation in bacteria, yeast, plants, fungi, and mammalian cells, albeit its exact mode of action is still under debate [65–68]. Due to its bactericidal effect, 2-PEtOH is frequently used in concentrations of up to 100 mM to protect pharmaceuticals, cosmetics, and other personal care products from spoilage. However, 2-PEtOH is already bacteriostatic at vastly lower concentrations, starting at concentrations as low as 8 mM with explicit effects at 12–16 mM [66].

2-PEtOH appears to affect DNA, RNA, and protein synthesis in bacteria [69–71]. Additionally, it has been suggested that the bactericidal activity of 2-PEtOH in fact depends on its conversion into phenylacetaldehyde, which is way more toxic to bacteria than 2-PEtOH [71]. Yet, while diverse targets are discussed to be causing the bacteriostatic activity of 2-PEtOH, it is clear that 2-PEtOH partitions into bacterial membranes and severely affects the structure of biomembranes [63,66,72]. As observed with other alcohols, the interaction of 2-PEtOH with the model as well as with biological membranes results in a drastic change of the lipid acyl-chain order [73–75].

This 2-PEtOH-induced change in the lipid order significantly affects the dimerization of transmembrane helices in the model, as well as in cellular membranes [73]. Thus, 2-PEtOH-induced lipid disordering might crucially affect the structure of transmembrane proteins in general, and this effect on the structure of biological membranes might be the first and ultimate line of the 2-PEtOH bacteriostatic activity. Further, 2-PEtOH is also produced by some fungi, which can significantly retard their growth and development [65,68]. Yet, fungi also produce some 2-PEtOH-derivatives, such as Tyrosol, phenyllactic acid, and phenylacetic acid (Figure 6), some of which appear to also have bacteriostatic activities. Already decades ago, a correlation between the bacteriostatic activity of phenyl-substituted alcohols (other than analyzed here) and their partitioning between an aqueous phase and an organic layer was described, and it was suggested that the compounds acted on cellular membranes [72]. Thus, it is reasonable to assume that the 2-PEtOH derivatives also act on cellular membranes and affect cell viability.

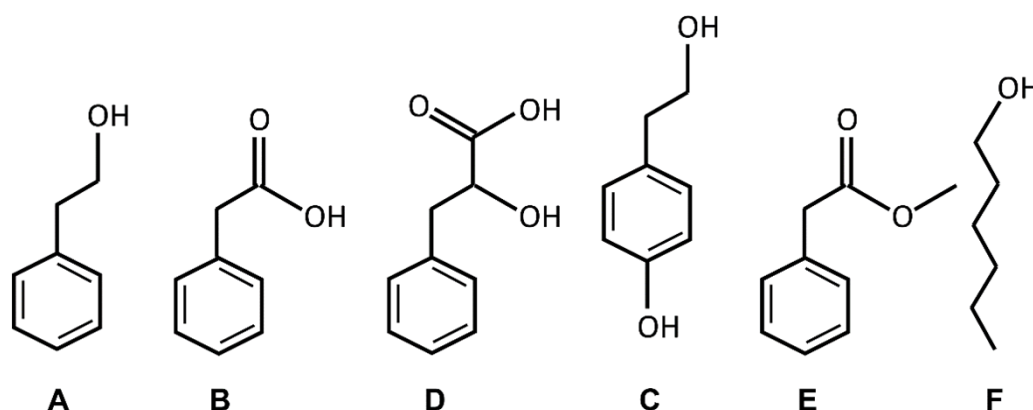


**Figure 6:** Chemical structures of 2-phenylethanol (2-PEtOH) and derivatives.

2-phenylethanol (A), phenylacetic acid (B), phenyllactic acid (C), Tyrosol (D), methyl phenylacetate (E), and 1-hexanol (F). The structures were drawn with ChemSketch V5.

Similar to 2-PEtOH, phenyllactic acid, the metabolite of phenylethylamine that occurs in the phenylalanine metabolism [76–78], also appears to have antimicrobial properties, targeting fungi and bacteria [73,74,79–81]. Just as for 2-PEtOH, also for phenyllactic acid, diverse modes of actions are discussed, and the compound appears to affect the integrity of the bacterial cell wall [73,79], and/or it might intercalate into the DNA and hinder DNA replication [82].

Yet, just as 2-PEtOH, it has been suggested that phenylacetic acid does also act at the cell membrane, albeit not knowing the mode of action [76]. Clearly, phenylacetic acid

can passively cross liposomal membranes *in vitro* [83], and a correlation between the membrane partition coefficients of some of its para-substituents and their bacteriostatic properties is described [84], and phenyllactic acid potentially makes the outer membrane of *Escherichia coli* more permeable, without disrupting it [82]. In contrast to 2-PEtOH and phenylacetic acid, membrane interaction of methyl phenylacetate, the methyl ester of phenylacetic acid, which is produced by several plants, has not been analyzed yet.

Tyrosol belongs to the most widely distributed compounds in plants [75]. It is the major phenolic compound found in olive oil, red wine and white wine [85,86].

While membrane interaction of 2-PEtOH has been studied to some extent and the bacteriostatic activity of 2-PEtOH has been linked to its membrane activity, the interaction of 2-PEtOH derivatives with model and biomembranes has only marginally been studied, if at all. Given that most compounds have an amphipathic nature, membrane interaction is expected, and it is well possible that membrane interactions affect bacterial homeostasis. In the present study, we showed that the 2-PEtOH derivatives phenylacetic acid, phenyllactic acid, and methyl phenylacetate (Figure 6) were incorporated into the model membranes and affected the membrane structure. The higher the overall hydrophobicity of a 2-PEtOH derivative, the higher its fluidizing impact on a membrane. Furthermore, we observed a positive correlation between membrane partitioning and the bacteriostaticity of the here analyzed 2-PEtOH derivatives.

#### **4.4. Results and Discussion**

The impact of 2-PEtOH on the structure and the stability of the model, as well as biological membranes, were studied in the past [65–67,73–75]. Nevertheless, plants, some fungi, as well as some bacteria produce and secrete the 2-PEtOH derivatives phenylacetic acid permeabilizes the outer membrane of bacteria (by a yet unknown mechanism) [82], the membrane activity of the 2-PEtOH derivatives is largely unexplored. All molecules are amphiphilic and have a polar region with hydroxyl or carboxyl groups and a nonpolar phenyl ring. An exception is Tyrosol, which has an extra hydroxyl group at the phenyl ring that renders the molecule non-amphiphilic [75]. Furthermore, in the present study, we additionally analyzed methyl phenylacetate, the methyl ester of phenylacetic acid produced in some plants, as it

allows separating effects of the polar group from effects potentially caused by the negative charge of the carboxylate group. Furthermore, 1-hexanol, whose membrane interaction is well studied [60,61], was used as a non-aromatic control.

#### 4.4.1. Membrane Partitioning and the Impact of 2-PEtOH Derivatives on the Membrane Structure

To estimate the membrane-binding affinity of the here-analyzed substances, we first calculated logP values (Table 16), which provide information as to the partitioning of the substances between water and octanol (which is typically used as a mimic of the hydrophobic membrane core). This calculation is based on the hydrophobicity and polarity of a substance, and the less hydrophobic a molecule, the lower the logP value. [87].

**Table 16.** LogP and MIC<sub>50</sub> values of 2-PEtOH and derivatives.

Substance	logP	MIC <sub>50</sub>
phenyllactic acid	0.72	44.97
Tyrosol	1.00	29.74
phenylacetic acid	1.36	20.28
2-phenylethanol	1.49	14.89
methyl phenylacetate	1.98	6.30
1-hexanol	2.13	7.05

The partition coefficient (logP) values of the substances, which provide information as to membrane partitioning of a molecule, were calculated with the online Molinspiration software v2016.10. The higher the value, the more hydrophobic the molecule and the higher will be the fraction of the membrane incorporated substance. The minimal inhibitory (MIC<sub>50</sub>) value provides information as to the bacteriostatic potential of a molecule (compare Figure 9). The higher this value, the less bacteriostatic a substance.

Phenyllactic acid has the lowest logP value and, thus, is the least hydrophobic molecule analyzed here, and 1-hexanol is the most hydrophobic molecule with the highest logP value of our studied substances.

Based on the definition of the logP, it is evident that a substance with a negative logP has a higher affinity to the aqueous phase, and a positive logP denotes a higher concentration in the lipid phase. Thus, based on this analysis, we expected all our tested substances to incorporate into the membrane (the lipid phase) as all the

#### 4. The Bacteriostatic Activity of 2-Phenylethanol Derivatives Correlates with Membrane Binding Affinity

calculated values are positive [88]. Indeed, computer simulations clearly indicated that all substances incorporated around the lipid head groups (Figure 7). The ring lies deeper in the membrane than the side chain for all substances except Tyrosol. In fact, the angle distribution shown below (Figure 7) indicated that Tyrosol did not intercalate into a membrane but rather bound parallel on a membrane surface, in line with previous assumptions [75,89]. The angle between the membrane bilayer normal and the orientation of Tyrosol was just about  $90^\circ$ , while all other compounds showed much larger angles (Figure 7F).

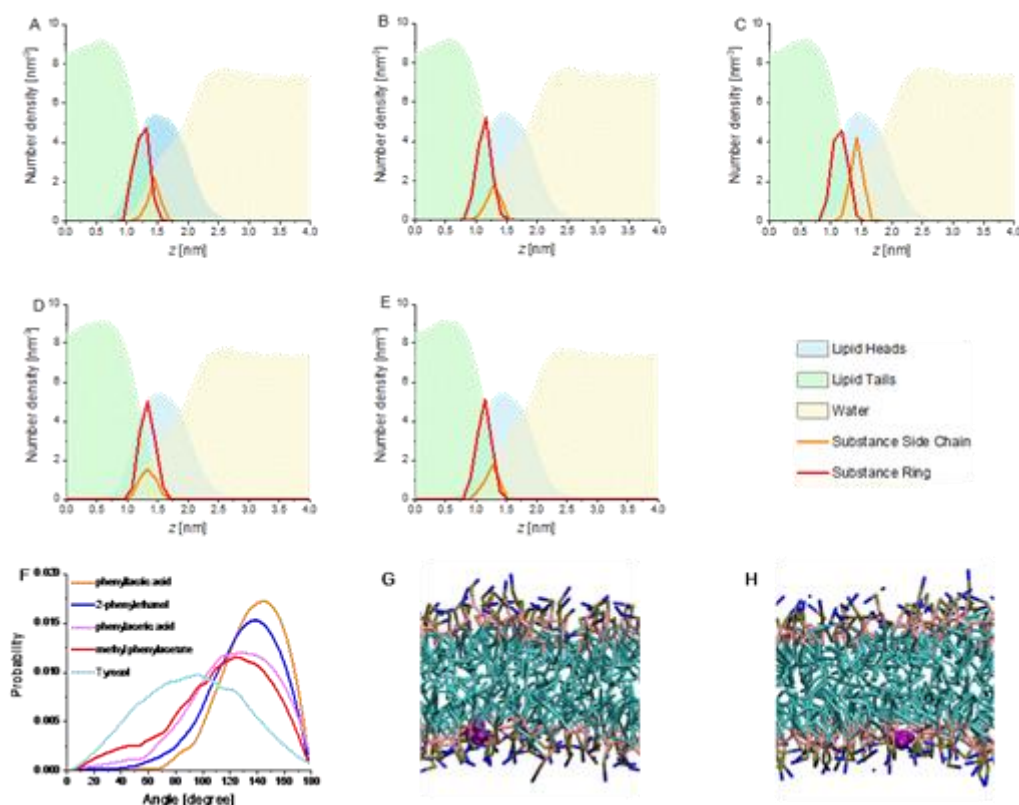


**Figure 7:** Number–density profiles, compound orientation relative to the membrane normal and simulation snapshots.

(A–E) The number–density profiles report the molar fraction of different chemical groups in the simulation box, perpendicular to the bilayer. (A) 2-PEtOH, (B) phenylacetic acid, (C) phenyllactic acid, (D) Tyrosol, and (E) methyl phenylacetate. All substances have shifts between the side chain and ring, except Tyrosol. Molar fractions of the solutes have been multiplied by 50 for clarity. All substances spontaneously insert close to the lipid head groups. (F) The angle between membrane normal and compound orientation (defined from side chain to aromatic ring) shows large values for methyl phenylacetate, phenylacetic acid, 2-PEtOH, and phenyllactic acid, indicative of their intercalation in the membrane. Smaller values are reported for Tyrosol, indicating its binding parallel to the membrane surface. (G,H) Representative simulation snapshots of 2-PEtOH and Tyrosol (purple) inserted in the headgroup region of the phospholipid membrane. Water is not shown for clarity.

Thus, all 2-PEtOH derivatives intercalated into a lipid monolayer, except Tyrosol, where direct interactions with the lipid acyl chains were not expected.

As membrane integration and membrane activity of 2-PEtOH had been demonstrated in the past, we next determined the impact of 2-PEtOH derivatives on the structure of model membranes via laurdan fluorescence spectroscopy [60,61,67,68,73,76,79]. Laurdan is a fluorescent dye that incorporates in lipid bilayers. Changes in the laurdan fluorescence emission spectrum reflect changes in the dye's ultimate environment, e.g., caused by altered lipid packing. To quantify the impact of a molecule on the structure of a lipid bilayer, the generalized polarization (GP) value was calculated [90]. A high GP value ( $\approx + 0.4$ ) is characteristic for a rigid lipid bilayer with densely packed lipid molecules, i.e., the membrane gel state, whereas a low GP value ( $\approx - 0.2$ ) is characteristic for less densely packed lipid bilayers, i.e., the fluid membrane state. As these values are largely independent of the lipid head groups and acyl chains, changes in the GP value can provide information about changes in the lipid order upon the addition of substances [91].

To this end, unilamellar liposomes were prepared from *E. coli* lipids containing 2  $\mu$ M Laurdan as well as increasing concentrations of the substances analyzed here. Changes in lipid packing were determined via laurdan fluorescence spectroscopy and illustrated as changes in the GP values (Figure 8). For further details, see Materials and Methods. 2-PEtOH and 1-hexanol are well known to increase membrane fluidity [60,61,67]. In line with this, the GP values measured here with increasing 2-PEtOH and 1-hexanol concentrations, respectively, are constantly decreasing (Figure 8), indicating a membrane fluidizing effect of all substances. For the maximal tested concentrations of the two substances, 70 mM for 1-hexanol and 100 mM for 2-PEtOH, the GP value is around  $- 0.2$ . This value is characteristic of a bilayer in the fluid (liquid crystalline) phase [90,91]. Here, 2-PEtOH acts like 1-hexanol, although the impact of 1-hexanol on the lipid acyl chain order was more pronounced already at lower concentrations.



#### 4. The Bacteriostatic Activity of 2-Phenylethanol Derivatives Correlates with Membrane Binding Affinity

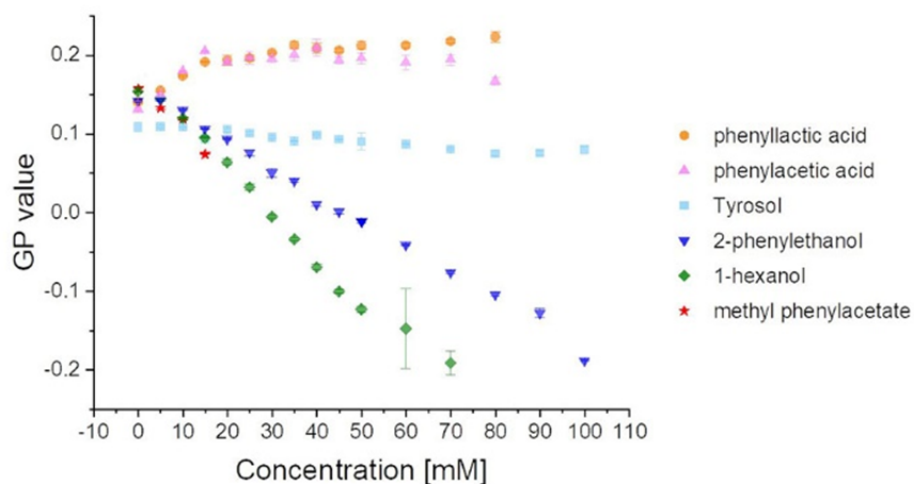


**Figure 8:** 2-PEtOH and derivatives affect the structure of the model membranes.

GP values determined at increasing substance concentrations are shown. The values indicate a fluidizing effect for the more hydrophobic substances 1-hexanol, 2-PEtOH, and methyl phenylacetate. Tyrosol seems to be largely ineffective, while phenyllactic acid and phenylacetic acid seem to have a slight ordering effect.

Yet, even though Tyrosol binds solely to membrane surfaces, an impact on the lipid order might be expected. However, we did not see any change of the GP values with increasing Tyrosol concentrations, and thus, apparently, surface adhesion of Tyrosol does not (significantly) affect the membrane structure.

Further, for phenylacetic acid and phenyllactic acid, it was suggested that they could incorporate into membranes [73,76,79,83], which is in line with the calculated logP values (Table 16). Yet, in contrast to 2-PEtOH, the addition of both phenyllactic acid as well as phenylacetic acid to *E. coli* lipid membranes did result in increasing GP values, which remained constant at concentrations larger than 15 mM. Thus, phenylacetic acid and phenyllactic acid both appeared to increase rather than decrease the membrane lipid order creating a more rigid membrane. Nevertheless, the membrane ordering effect was much lower than the disordering effect of 2-PEtOH or 1-hexanol.

To estimate whether the reverse impact of the two acids, compared to 2-PEtOH, might be caused by the negative charge, we additionally analyzed the impact of the methyl ester of phenylacetic acid, methyl phenylacetate, on the membrane structure. The addition of methyl phenylacetate to the model membranes resulted in decreasing GP values, as observed with 2-PEtOH or 1-hexanol. Consequently, membrane incorporation of methyl phenylacetate increased the membrane fluidity, and thus

masking the negative charge of phenylacetic acid seemed to have a significant impact on the membrane activity (as further discussed below).

#### 4.4.2. 2-PEtOH and Derivatives are Bacteriostatic

For all substances, except for Tyrosol, we showed that membrane binding had an impact on the membrane structure. Next, to test whether this membrane activity correlates with a potential bacteriostatic activity of the substances, the impact of 2-PEtOH, phenylacetic acid, phenyllactic acid, methyl phenylacetate, Tyrosol, and 1-hexanol on the growth of the bacterium *E. coli* was tested. For 2-PEtOH, it was already shown that it decreases bacterial growth starting at concentrations as low as 8 mM with explicit effects at 12–16 mM [66]. We followed bacterial growth in presence of increasing substance concentrations to calculate the (non-lethal) amount of substance that inhibits 50% bacterial growth (Figure 9).

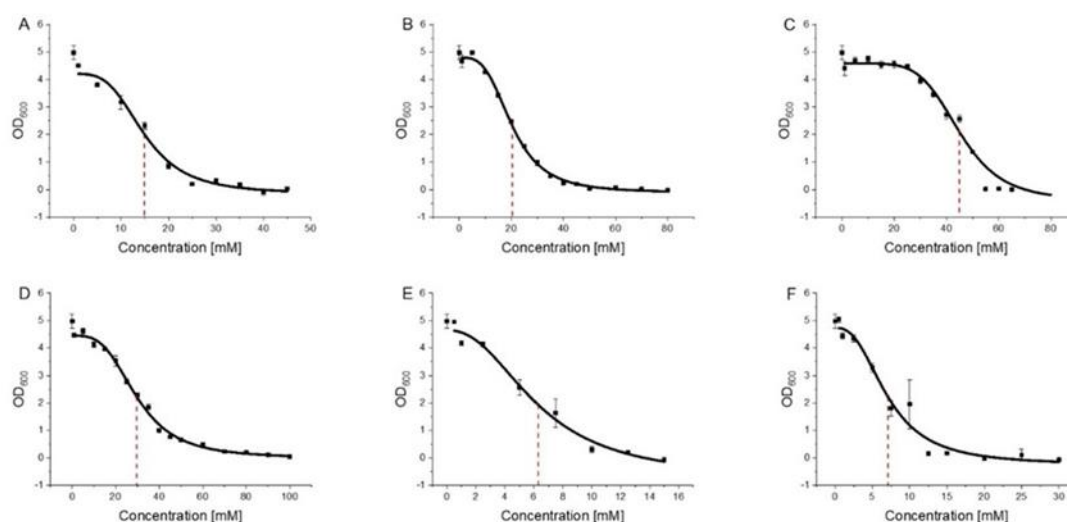


**Figure 9:** Determination of MIC<sub>50</sub> values.

The OD<sub>600</sub> was plotted against the substance concentration and a dose-response fit was performed for (A) 2-PEtOH, (B) phenylacetic acid, (C) phenyllactic acid, (D) Tyrosol, (E) methyl phenylacetate, and (F) 1-hexanol ( $n = 3$ ,  $\pm$ SD). The corresponding MIC<sub>50</sub> values are given in Table 16.

This minimal inhibitory (MIC<sub>50</sub>) value is a measure of the antimicrobial activity of compounds [92].

In excellent agreement with literature values, we here observed a clear effect of 2-PEtOH on *E. coli* growth with an MIC<sub>50</sub> value of  $\sim 15$  mM [5–9]. As for phenylacetic acid, we likewise observed a bacteriostatic effect with an MIC<sub>50</sub> value of  $\sim 20$  mM. However, when we masked the negative charge and analyzed the methyl phenylacetate

instead, the MIC<sub>50</sub> value was lowered to ~ 6.3 mM, a value lower than 2-PEtOH and in the same range as observed with 1-hexanol. This showed that masking the negative charge not only considerably affected the membrane activity of (methyl) phenylacetate (Figure 8) but also significantly enhanced its bacteriostatic efficiency. Surprisingly, while Tyrosol did not integrate into and affect the structure of biomembranes but rather lies flat on membrane surfaces (Figure 7H), it still affected the *E. coli* growth with an MIC<sub>50</sub> value of ~ 30 mM [75,88]. The naturally produced 2-PEtOH derivative phenyllactic acid was least active with an MIC<sub>50</sub> as high as ~ 45 mM. The determined MIC<sub>50</sub> values are summarized in Table 16 for each of the tested substances.

#### **4.4.3. Hydrophobicity, Membrane Fluidity, and Bacterial Growth Correlate**

The here-analyzed molecules with the highest logP values decreased the membrane order with increasing concentration, whereas phenylacetic acid and phenyllactic acid, which both have a low logP value, showed increasing GP values with increasing concentration. Thus, the higher the overall hydrophobicity of a molecule, the higher its fluidizing impact on a membrane. Nevertheless, as all molecules, except the control 1-hexanol as well as Tyrosol, had a methylene benzene group, the chemistry of the substituents was evidently important for the membrane activity of 2-PEtOH derivatives. In contrast to 2-PEtOH, phenylacetic acid and phenyllactic acid did not decrease but slightly increased the order of a lipid bilayer. Yet, when masking the negative charge via the formation of a methyl ester, methyl phenylacetate showed an even increased membrane fluidizing activity compared to 2-PEtOH. Thus, the incorporation of the hydrophobic methylene benzene group into the hydrophobic membrane core region, as well as (polar) interactions within the lipid head group region, likely together affect the membrane activity of 2-PEtOH derivatives (as well as of other substances). This appears to be nicely reflected by the calculated overall hydrophobicity, i.e., the calculated logP values.

Based on several subsequent studies, the bacteriostatic activity of 2-PEtOH was linked to biological membranes, albeit the exact mode of action is still unclear, and other target structures were also discussed [63,66–68]. Yet, the calculated logP values nicely correlated with the determined MIC<sub>50</sub> values (Figure 10), and with an increasing logP value, the MIC<sub>50</sub> decreased. In fact, when we plot the logarithm of the MIC<sub>50</sub> values determined for the 2-PEtOH derivatives against the calculated logP values, we

#### 4. The Bacteriostatic Activity of 2-Phenylethanol Derivatives Correlates with Membrane Binding Affinity

obtained a linear correlation with an  $r^2$  value of 0.987 (Figure 10). Thus, the hydrophobicity of the molecules, i.e., their calculated propensity to partition into biomembranes, correlated with the bacteriostatic activity, which indicated that the partition coefficient significantly determined the biological activity of the substances and links the bacterotoxic activity of the substances to biomembranes.

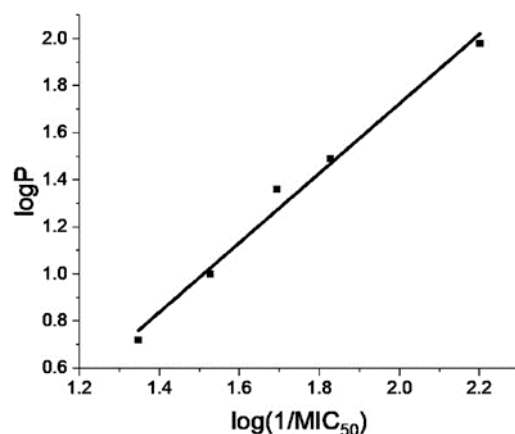


**Figure 10:** The  $\log P$  values of 2-PEtOH linearly correlate with the  $\log(1/MIC_{50})$  values.

The  $\log P$  values of 2-PEtOH and derivatives is plotted against the respective  $\log(1/MIC_{50})$  values. The correlation coefficient is  $r^2 = 0.987$ .

In most cases, a clear effect on membrane lipid order was already observed in the liposome-based assay at the  $MIC_{50}$  values, and, thus, changes in general membrane properties could well have an important impact on the bacteriostatic activity of the 2-PEtOH derivatives. Yet, there was no general correlation between the bacteriostaticity and the observed effect on the membrane structure: All substances clearly had an impact on bacterial growth, yet some substances increased the lipid order (phenylacetic acid, phenyllactic acid), Tyrosol did essentially not affect the membrane structure, whereas the remaining substances decreased the lipid order. Furthermore, it has to be noted that all molecules analyzed here might also have additional cellular targets.

In summary, our results indicate a correlation between the hydrophobicity of the 2-PEtOH derivatives analyzed here and their respective bacteriostatic activity, and our results link the biological activity of the molecules to cellular membranes.



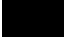
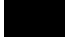


















## 5. CLiB - a Novel Cardiolipin-Binder Isolated via Data-Driven and *In Vitro* Screening

### 5.1. Author Contributions

An extended version of this chapter has been submitted to RSC Chemical Biology. Materials and Methods used and done by me can be found in chapter 2 and 3. Methods performed by others can be found in Appendix 13.1.2 and 13.1.3. The authors' affiliations are listed in chapter 12 and the authors' contributions are listed in Table 17.

**Table 17:** Author contributions to CLiB – a novel cardiolipin-binder isolated via data-driven and *in vitro* screening.

<b>Conceptualization</b>	Complete study	████████████████████
<b>Methodology</b>	Computer simulations <i>P. anserina</i> /mitochondria <i>In vitro</i> and rest	████ ████ ████
<b>Software</b>	Complete study	████████████████
<b>Validation</b>	Complete study	████████████████ ████████████████
<b>Formal analysis</b>	Computer simulations <i>P. anserina</i> /mitochondria <i>In vitro</i> and rest	████ ████ ████████
<b>Investigation</b>	Computer simulations <i>P. anserina</i> /mitochondria <i>In vitro</i> and rest	████ ████ ████
<b>Writing: Original draft preparation</b>	Introduction Results and Discussion: Computer simulation part Mitochondrial part <i>In vitro</i> and rest	████ ████ ████ ████ ████

<b>Review and editing</b>	Complete study	
<b>Supervision, funding acquisition, resources and project administration</b>	Complete study	
<b>Figures</b>	<b>Methodology, Investigation, Formal analysis</b>	<b>Data visualization</b>
<b>Figure 11</b>		
<b>Figure 12</b>		
<b>Figure 13</b>		
<b>Figure 14</b>		
<b>Figure 15</b>		
<b>Figure 16</b>		
<b>Figure 17</b>		
<b>Figure 18</b>		
<b>Figure 19</b>		
<b>Figure 29</b>		

## 5.2. Summary

Cardiolipin, the mitochondria marker lipid, is crucially involved in stabilizing the inner mitochondrial membrane and is vital for the activity of mitochondrial proteins and protein complexes. Directly targeting cardiolipin by a chemical-biology approach and thereby altering the cellular concentration of “available” cardiolipin eventually allows to systematically study the dependence of cellular processes on cardiolipin availability. In the present study, physics-based coarse-grained free energy calculations allowed us to identify the physical and chemical properties indicative of cardiolipin selectivity and to apply these to screen a database of natural compounds for putative cardiolipin-binders. The membrane binding properties of the 22 most promising molecules identified in the *in silico* approach were screened *in vitro*, using model membrane

systems finally resulting in the identification of a single molecule, CLiB (**C**ardio**L**ipin-**B**inder). CLiB clearly affects respiration of cardiolipin-containing intact bacterial cells as well as of isolated mitochondria. Thus, the structure and function of mitochondrial membranes and membrane proteins might be (indirectly) targeted and controlled by CLiB for basic research and, potentially, also for therapeutic purposes.

### 5.3. Introduction

Cellular membranes separate intracellular processes from the environment and surround defined intracellular structures within cells, resulting in formation of defined intracellular reaction compartments, the organelles, a basis for the evolution of complex life [93,94]. Biomembranes consist of a scaffold of multiple membrane lipids, albeit the concentration of membrane-attached and/or integrated protein can be high. Biological membranes can contain more than 1000 different lipid species, where the main membrane constituents belong to three classes of lipids: phospholipids, glycolipids, and cholesterol, with glycerophospholipids being the major class [8,94]. The exact lipid composition varies significantly between the diverse intracellular membrane systems in eukaryotes, with the membrane lipid composition of organelles differing from each other as well as from the composition of the plasma membrane [8]. Even within a membrane, regions with diverse lipid compositions can co-exist, such as the basolateral and apical regions of epithelial plasma membranes, and in eu- as well as in prokaryotes the formation of defined lipid domains is discussed, regions where distinct lipid species segregate. It is assumed that specific proteins diffuse into such domains and thereby form signaling platforms. (Targeted) disturbance of such lipid domains can severely affect cellular functions, resulting in missignaling [25].

While the relative concentrations of individual lipid species within the eukaryotic membrane systems varies, and thus the exact lipid composition appears to define the membranes' physico-chemical properties, several lipids are restricted to chloroplasts and mitochondria, the organelles with an endosymbiotic origin. *E.g.*, galactolipids are solely found in chloroplasts, as expected due to their cyanobacterial origin [95]. Many bacteria contain significant amounts of cardiolipin (around 10 % in *E. coli*) [25], whereas in eukaryotes this "bacterial lipid" can only be found in significant amounts in mitochondria [96,97]. In the inner membrane of mitochondria, cardiolipin typically constitutes 10-20 % of the total lipid [98,99], whereas in the outer mitochondrial membrane only minor amounts of cardiolipin are found [39,100]. Consequently,

cardiolipin is a marker for the mitochondrial inner membrane. In contrast, in fungi the cardiolipin content in mitochondria can be much lower [101–103], and especially in mitochondria from *P. anserina* the cardiolipin level is very low (1.5 %) [104].

Besides its unique origin and subcellular localization, also the structure of cardiolipin is uncommon (Figure 1): two phosphatidyl backbones are linked via a glycerol head group, and thus one cardiolipin molecule contains two negative charges [40,97,105]. Four fatty acid chains are attached to this backbone, which typically differ in their respective length and saturation [38,97,106]. Because of its overall cone-shaped structure, cardiolipin is primarily found in high curvature membrane regions, for example at the poles of rod-shaped bacteria [107,108] or at highly curved regions of the mitochondrial inner membrane [97]. Consequently, alterations in the mitochondrial cardiolipin content can result in an altered morphology of the mitochondrial inner membrane [109].

Mitochondria are the dominant generator of ATP in most eukaryotic cells and crucially involved in several metabolic processes [97]. Cardiolipin is essential for the activity of several mitochondrial enzymes [38,97], such as the glycerol-3-phosphate dehydrogenase [110], creatine kinase or phosphate carriers [111,112], and the activity of the respiratory chain complexes depends to some extent on cardiolipin [38]. Additionally, during apoptosis, interaction of cardiolipin with cytochrome c appears to trigger intracellular signal propagation [113,114]. Accordingly, cardiolipin deficiency or alterations in the mitochondrial cardiolipin levels has pathophysiological consequences in humans, such as ischemia or reperfusion and results in diabetes, heart disease or the BTHS [38,109,115]. All these observations indicate that molecular engineering of drugs that target cardiolipin is an innovative chemical concept that potentially allows controlled analysis of physiological consequences caused by cardiolipin abnormalities. In general, when a membrane-active compound binds a defined lipid and/or acts as an inhibitor of lipid heterogeneity, this can (indirectly) affect the activity of proteins or protein networks that need the specific lipid and/or lipid-containing membrane platforms to perform their cellular functions [38]. Based on this concept, the structure and function of mitochondrial membrane proteins might be indirectly controlled for basic research and, potentially, also for therapeutic purposes using engineered, cardiolipin-binding drugs (“cardiolipin-binders”).

Presently, molecules that specifically bind cardiolipin are still rare. The antibiotic Daptomycin appears to bind more specifically to cardiolipin than to the



glycerophospholipid PC, yet with even higher affinity to PG [116]. The fluorophore 1,1,2,2-tetrakis[4-(2-trimethylammonioethoxy)-phenylethene] (TTAPE-Me) has been introduced as a promising candidate for binding cardiolipin [117], yet here binding also appears to be rather non-specific [118]. 10-*N*-nonylacridine orange (Figure 11) has already been introduced decades ago as a mitochondrial surface marker, as it was suggested to specifically interact with cardiolipin [119].

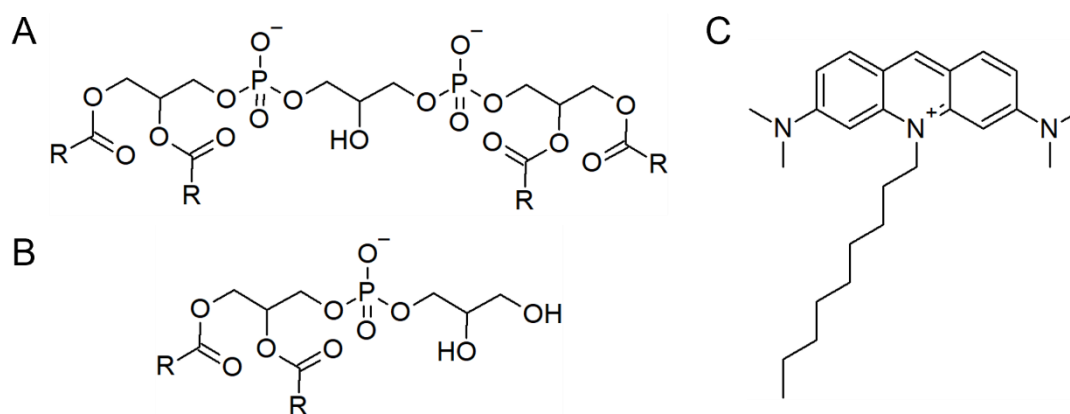


**Figure 11:** Molecular structures of (A) cardiolipin, (B) PG and (C) NAO.

In (A) and (B) R represents the fatty acid chains not relevant for this work. CL: cardiolipin, PG: phosphatidylglycerol, NAO: 10-*N*-nonyl acridine orange

NAO intercalates into the inner mitochondrial membrane in a membrane potential independent manner and thereby poisons mitochondrial respiration [120]. At low concentrations, it inhibits ATP synthesis and at increased concentrations it additionally inhibits the respiratory electron transfer, potentially via competitively capturing cardiolipin [119]. In line with this, at high doses, NAO alters the structure of mitochondrial membranes [121,122]. The positively charged NAO likely electrostatically interacts with the negatively charged cardiolipin head group, and the cardiolipin fatty acid composition appears not to affect this binding specificity [123,124]. Upon cardiolipin-binding, a shift in the NAO fluorescence emission spectrum is observed. NAO is able to diffuse spontaneously across membranes, and can thus be well used *in situ*, in whole cells [123], and consequently, NAO is used to visualize and quantify the cardiolipin content of and/or clustering within bacterial cells and/or mitochondria. Nevertheless, while a cardiolipin specificity has been postulated many times, it has turned out in recent years that NAO is not cardiolipin-specific. In fact, NAO still properly accumulates in mitochondria in cardiolipin-deficient yeast mutants [125] and using model membranes it has been shown that NAO binds with

high affinity to PG, which is chemically similar to cardiolipin (Figure 11A, B). In summary, cardiolipin-selective molecules are urgently needed for future research.

In the present study, we set up an efficient pipeline to screen for novel specific cardiolipin-binders. Computational screening methods are gaining increasing recognition in materials modelling and drug design for efficient identification of molecular candidates that feature desired properties [126–131]. A microscopic picture not only provides the means to resolve the main physicochemical interactions at play, but it can also directly connect chemical structure with property [132]. This connection allows the identification of several candidate molecules with structural features linked to desired properties that can be investigated in more detail. Molecular dynamics (MD) simulations can provide microscopic insight into macromolecular structure-property relationships that are difficult to gain experimentally [133–139]. Coarse-graining (CG) reduces the complexity of molecular representations by averaging over the chemical and physical properties of adjacent heavy (non-hydrogen) atoms represented by a single bead. The result is a considerable reduction in computational complexity, while still reproducing the underlying chemical and physical properties sufficiently well [140–144]. Here we show that CG modelling is an efficient strategy to discover cardiolipin-binding small molecules (SM). Starting from the reference compound NAO, we employ a series of free-energy calculations to unravel the physicochemical interactions that lead to specific binding to cardiolipin. Free energy calculations via alchemical transformations explicitly compare differences in stability between cardiolipin and PG membranes. The calculations lead to the establishment of physicochemical design rules. We subsequently applied these design rules to screen a natural compound database. In a separate study, we employed a more elaborate combination of CG simulations, free-energy calculations, deep representation learning, and Bayesian optimization to tackle the same cardiolipin-binding SM discovery problem [145]. The results of this parallel study provide a more detailed description of the chemical space of putative cardiolipin-binders yet resulted in consistent physicochemical design rules. Via computational screening we have identified 22 SMs which potentially bind cardiolipin with high specificity. Subsequent *in vitro* analyses of these SMs, using model membranes, resulted in the identification of a single molecule, CLiB (**C**ardio**L**ipin-**B**inder) with a high preference for cardiolipin over PG. *In vivo* analyses indicate that interaction of CLiB with cardiolipin affects respiration in bacteria as well as in mitochondria. Thus, we here introduce CLiB as a

new chemical biology tool for studying the physiological role of cardiolipin in cells and/or organelles.

## 5.4. Results and Discussion

Typically, the impact of cardiolipin on the physiology of mitochondria is analyzed in organisms or isolated mitochondria using strains in which cardiolipin synthesis is inhibited due to deletion of genes coding for cardiolipin-synthesizing enzymes. Yet, it remains an open question as to how far any physiological consequences observed in such deletion strains *de facto* reflect cardiolipin-dependent processes or are due to an altered membrane, the composition of which has been adjusted in the organisms when cardiolipin is absent. Thus, it clearly is desirable to manipulate the cellular cardiolipin content in a more controlled way using a chemical biology approach.

cardiolipin, the mitochondrial marker lipid, is crucially involved in stabilization of the inner mitochondrial membrane as well as in the stabilization and activity of mitochondrial proteins and protein complexes. Furthermore, the cardiolipin content of mitochondria is altered during cellular adaption to defined stress conditions, as well as during aging [37,39]. Directly targeting cardiolipin by a chemical-biology approach and thereby altering the cellular concentration of “free” cardiolipin eventually allows to systematically study the dependence of mitochondrial processes on cardiolipin availability. Therefore, we aimed at identifying a previously unrecognized small molecule that interacts specifically with cardiolipin and can be used in future research on mitochondrial physiology. To do so, we set up a workflow involving two initial computational steps, (i) the identification of physical and chemical properties crucial for cardiolipin selectivity of a small molecule and (ii) screening of a vendor database for possible candidates. This was done by applying a physics-based CG model of a known cardiolipin probe, reducing the complexity of chemical space, and thereby allowing us to systematically observe the change in selectivity caused by the introduction of new interaction types into the CG model. The observations were formulated as design rules describing which substructures in candidate molecules are indicative of the properties required for cardiolipin selectivity. The pre-selected candidate molecules were subsequently *in vitro* screened to identify promising candidate substances. Finally, the activity of the top cardiolipin-binders identified in

the present study on the physiology of a cardiolipin-containing bacterium as well as on mitochondria was evaluated.

#### 5.4.1. Rational Identification of 22 Candidate Molecules with a Putative Cardiolipin-Binding Propensity

Due to its claimed cardiolipin-selectivity, NAO is commonly used to stain cardiolipin-containing membranes, or cardiolipin-containing membrane domains. Yet, its specificity and sensitivity towards cardiolipin is not high (as often proposed), as it also interacts with other negatively charged lipids, such as PG, PS and phosphatidylinositol (PI) [117,146]. Nevertheless, the chemical structure of NAO can serve as a reasonable starting point to search for new cardiolipin-binders.

The physical and chemical properties of the CG representation of NAO were systematically varied by exchanging individual bead types, for instance by altering the number of hydrophobic sites or charged groups by calculating the relative partitioning free energy  $\Delta\Delta G$  of the altered CG NAO from the water phase into each lipid membrane. This is accomplished through two different free-energy methods, performing alchemical transformations, and calculating the potential of mean force (PMF), see Figure 29 in the appendix. Negative  $\Delta\Delta G$  and minima of the PMF curve represent energetically favorable processes, i.e., insertion at the membrane-water interface, selectivity to the targeted cardiolipin. We monitored the influence of the bead-type exchanges on the preferential stability for cardiolipin compared to PG. The resulting partitioning free energy differences  $\Delta\Delta G_{\text{PG} \rightarrow \text{cardiolipin}} = \Delta\Delta G_{\text{cardiolipin}} - \Delta\Delta G_{\text{PG}}$  between the same bead-type transformation in both the cardiolipin membrane and the PG membrane are shown in 3A. The modified NAO structures are represented on the horizontal axis, the color code indicates the position in the CG structure a specific bead was assigned to (Figure 12B). Due to the symmetry of the reference NAO structure along its vertical axis, for the pink and blue bead positions, no distinction was made whether a specific bead was placed on the left or on the right side. The cardiolipin-selectivity  $\Delta\Delta G_{\text{PG} \rightarrow \text{cardiolipin}}$  is represented on the y-axis. The compounds are sorted by their resulting  $\Delta\Delta G_{\text{PG} \rightarrow \text{cardiolipin}}$ , from left (low selectivity) to right (high selectivity). The Martini coarse-grained force field defines 14 neutral bead types sorted by increasing polarity, from **C1-C5** (very apolar) via **N**-types (neutral) to **P**-types (polar). Additionally, it provides four charged bead types (**Q**). From here on, we denote all CG

Martini bead types in bold and italics. It becomes clear that increased hydrophobicity brought on by replacing the two **C5** beads on the outer sides of the original CG NAO structure (blue) by **C1** or **C2** beads shifted the selectivity of the resulting CG structure away from cardiolipin and towards PG ( $\Delta\Delta G_{PG \rightarrow \text{cardiolipin}} > 0$ ). Adding a neutral **Na** bead with hydrogen-bond acceptor properties instead of the original **No** beads to the top of the structure (pink) had no noticeable effect on cardiolipin-selectivity. In contrast, introducing hydrogen-bond donor properties to the pink beads (**Nda/Nd**) together with weak hydrophobicity (**C5**) in the blue beads resulted in an increased cardiolipin-selectivity. This trend was increased further by replacing the hydrophobic **C**-types at the blue positions with neutral beads with added hydrogen-bond donor sites (**Nda/Nd**). Finally, the biggest increase in cardiolipin-selectivity was obtained in the calculations by replacing the central charged bead (yellow) with a neutral hydrogen-bond donor bead type, keeping the same bead types at the pink bead positions, and introducing two positively charged hydrogen-bond donor beads (**Qd/Qda**) at the blue positions on the outside of the molecule.

In summary, slightly shifting the overall hydrophobicity of the CG NAO representation towards a more amphiphilic character, adding hydrogen bond donor properties, and doubling the positive charge while simultaneously moving the charged beads from the center to the outsides of the CG structure led to a larger negative  $\Delta\Delta G_{PG \rightarrow CL}$ , indicating increased cardiolipin selectivity. Example PMFs for three of those molecules are shown in Figure 12C. Here, the solid lines represent PMFs calculated in the cardiolipin membrane, the dashed lines PMFs in the PG membrane. The grey PMF curve resulted from the original NAO representation to provide a reference for our introduced bead-type changes. The red and the blue lines represent the bead-type conformations circled in the same colors in Figure 12A. The increased depths of the minima of the PMF curves indicate an increased selectivity of the candidate compounds for both the PG and the cardiolipin membranes, and the increased distance at the minima of the PMF curves for the same compound indicate an increased selectivity for cardiolipin over PG. Overall, the umbrella sampling results show the same trend as found in the alchemical transformation results shown in Figure 12A. Due to the increase in computational cost, umbrella sampling calculations with more than one charged bead were not performed. Our observations now allowed us to express three design rules of molecules that selectively bind to cardiolipin and prefer cardiolipin over PG:

1. Positively charged beads: At least one, ideally two sites that will carry a positive charge at physiological pH (pH $\approx$ 7.3).
2. Neutral and charged beads (**N**- and **Q**-types) with hydrogen-bond donor properties: Functional groups able to form hydrogen bonds with the cardiolipin headgroup.
3. Apolarity (represented by the **C1** beads in the tail): Hydrophobic areas in the molecule that induce alignment with or insertion into the lipid bilayer.

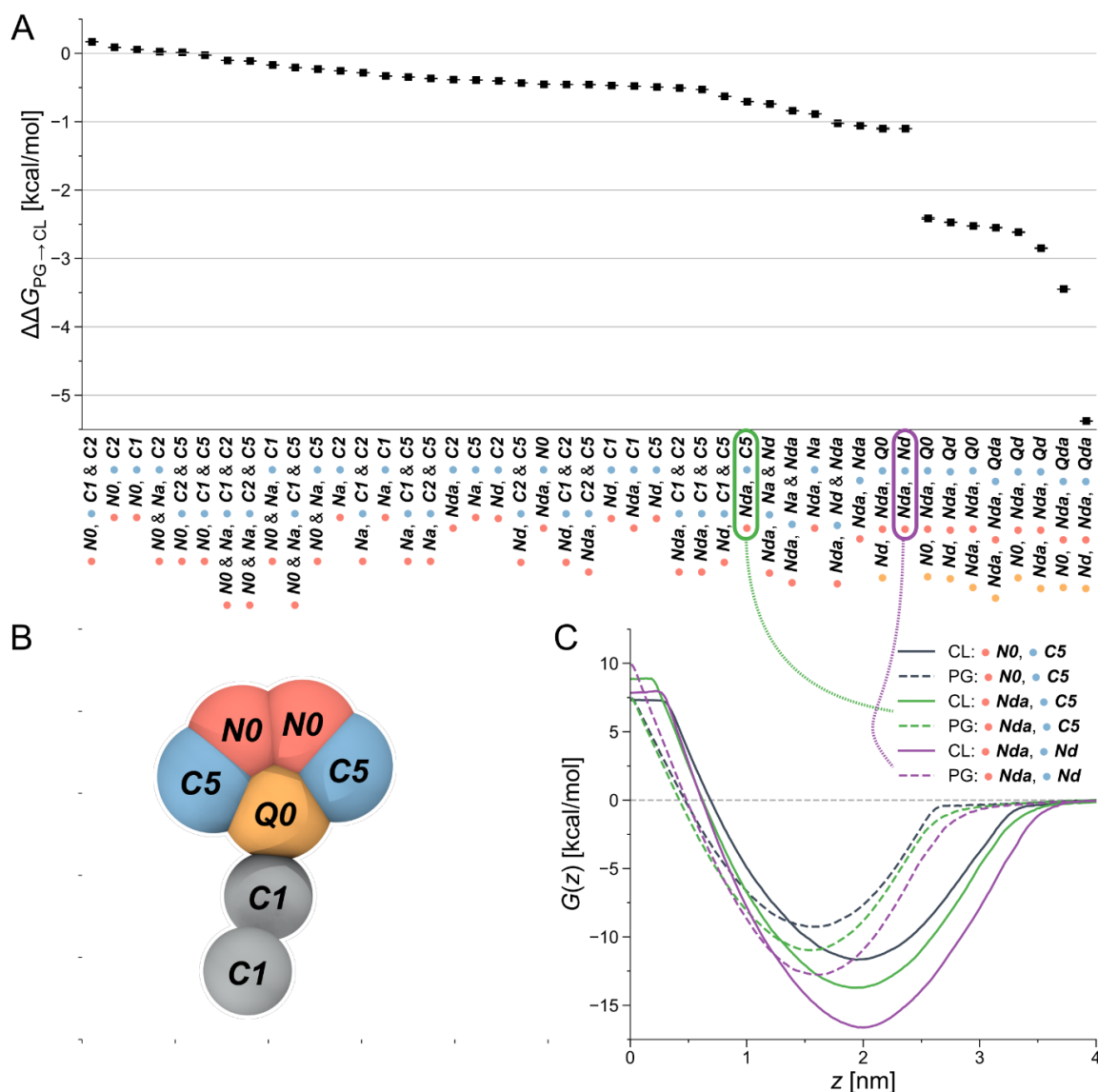


**Figure 12:** Results of the computational investigation.

(A) Differences in partitioning free energies  $\Delta\Delta G_{PG \rightarrow \text{cardiolipin}}$  from alchemical transformations of one or more beads in the CG-representation of NAO. (B) Original CG representation of NAO color-coded to visualize the locations of bead changes in the free energy calculations. (C) Exemplary PMFs of CG structures with different bead types in the cardiolipin membrane (solid lines) and the PG membrane (dashed lines). Connections show which PMF curve corresponds to which partitioning free energy difference  $\Delta\Delta G_{PG \rightarrow \text{cardiolipin}}$ .

The design rules allowed us to select candidate molecules for cardiolipin selectivity from the MCULE database [147] (Figure 12C). As NAO is described in the literature as a cardiolipin probe, the Tanimoto similarity coefficients [148,149] of NAO at the level of fingerprint representations was used for comparison. Candidate molecules with a Tanimoto coefficient  $> 0.39$  (lower threshold for similarity, identity is 1.0) were extracted. We further screened the candidates for the presence of positively ionizable sites and aromaticity [150]. From the resulting 93 molecules, a subset of 16 candidates with a Tanimoto coefficient  $> 0.44$  were subjected to experimental validation (SM<sub>1</sub> to SM<sub>7</sub>, SM<sub>10</sub> to SM<sub>12</sub>, SM<sub>16</sub> and SM<sub>18</sub> to SM<sub>22</sub>).

Eight of the 16 molecules had at least one hydrogen-bond acceptor site identified using the RDKit [151] chemical features definition, and one of those eight had both hydrogen-bond donor and acceptor sites. Six molecules with a lower Tanimoto coefficient were also added to cover the aspects of the design rules in more detail (SM<sub>8</sub>, SM<sub>9</sub>, SM<sub>13</sub> to SM<sub>15</sub> and SM<sub>17</sub>). Only hydrogen-bond donor- and no acceptor sites were identified in SM<sub>13</sub> to SM<sub>15</sub>, SM<sub>8</sub> showed five positively ionisable sites, SM<sub>9</sub> four hydrogen-bond acceptor sites and one donor site. Additionally, SM<sub>14</sub> and SM<sub>15</sub> are structurally very similar to SM<sub>16</sub>, even though their Tanimoto similarity to NAO is lower. SM<sub>17</sub> follows the design rules, even though the similarity to NAO was lower than that of the 16 initially selected candidates. It was included to probe the role of the structural similarity to the detected cardiolipin selectivity. The 22 molecules are shown in Figure 13, all descriptors used to select them can be found in Table 18.

**Table 18:** Descriptors used to select the 22 molecules for experimental validation.

<b>SM</b>	<b>Tanimoto</b>	<b>+ ionizable sites</b>	<b>acceptor sites</b>	<b>donor sites</b>	<b>aromaticity</b>
1	0.4444	1	1	0	True
2	0.4737	1	0	0	True
3	0.4857	1	1	0	True
4	0.439	1	0	0	True
5	0.4722	1	1	0	True
6	0.439	1	1	0	True
7	0.4359	1	1	0	True
8	0.1818	5	1	0	True
9	0.0909	1	4	1	True
10	0.5312	1	0	0	True
11	0.4615	1	0	0	True
12	0.4848	1	0	0	True
13	0.1159	1	0	1	True
14	0.325	1	0	1	True
15	0.3333	1	0	1	True
16	0.4474	1	1	1	True
17	0.2391	1	1	0	True
18	0.439	1	1	0	True
19	0.4615	1	0	0	True
20	0.439	1	0	0	True
21	0.4524	1	2	0	True
22	0.5588	1	0	0	True
NAO	1.0	1	0	0	True



We successfully applied a combination of physics-based coarse-grained representations of molecules to reduce the combinatorial complexity of chemical space together with efficient free-energy calculation methods, thereby greatly increasing the efficiency of examining the influence of different physical and chemical properties on our targeted cardiolipin selectivity. We were able to formulate design rules describing the identified properties on the CG level and linking back to related characteristics in molecular structures. The design rules were successfully used to screen the MCULE database of purchasable, in-stock compounds for potential cardiolipin-binders (Figure 13).

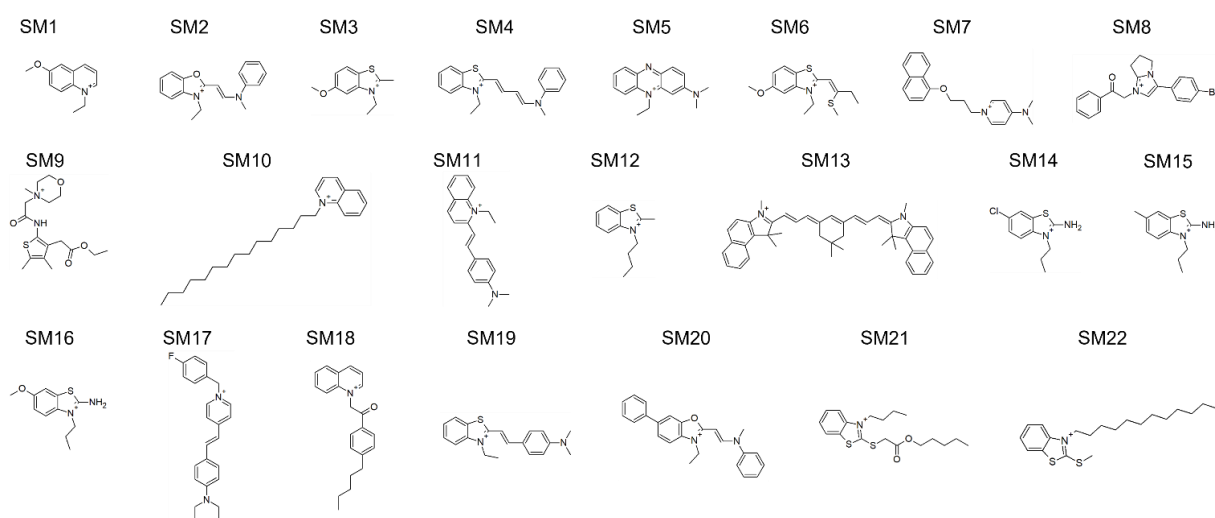


**Figure 13:** Structures of the 22 molecules further analyzed.

The chemical names of the substances can be found in Table 19.

The systematic names of the 22 molecules can be found in Table 19.

**Table 19:** Systematic names of the 22 small molecules.

SM	Systematic name
1	1-ethyl-6-methoxyquinolin-1-ium iodide
2	3-ethyl-2-[(E)-2-[methyl(phenyl)amino]ethenyl]-1,3-benzoxazol-3-ium ethyl sulfate
3	3-ethyl-5-methoxy-2-methyl-1,3-benzothiazol-3-ium 4-methylbenzene-1-sulfonate
4	3-ethyl-2-[(1E,3E)-4-[methyl(phenyl)amino]buta-1,3-dien-1-yl]-1,3-benzothiazol-3-ium iodide
5	3-(dimethylamino)-5-ethylphenazin-5-ium iodide
6	3-ethyl-5-methoxy-2-[2-(methylsulfanyl)but-1-en-1-yl]-1,3-benzothiazol-3-ium methyl sulfate
7	4-(dimethylamino)-1-[3-(naphthalen-1-yloxy)propyl]pyridin-1-ium chloride
8	3-(4-bromophenyl)-1-(2-oxo-2-phenylethyl)-5H,6H,7H-pyrrolo[1,2-a]imidazol-1-ium bromide
9	4-({[3-(ethoxycarbonyl)-4,5-dimethylthiophen-2-yl]carbamoyl}methyl)-4-methylmorpholin-4-ium chloride
10	1-pentadecylquinolin-1-ium iodide
11	2-[(E)-2-[4-(dimethylamino)phenyl]ethenyl]-1-ethylquinolin-1-ium iodide
12	3-butyl-2-methyl-1,3-benzothiazol-3-ium iodide
13	2-[(1E)-3-[(1E)-5,5-dimethyl-3-[(1E)-3-[(2E)-1,1,3-trimethyl-1H,2H,3H,4H,5H-benzo[e]indol-2-ylidene]prop-1-en-1-yl]cyclohex-2-en-1-ylidene]prop-1-en-1-yl]-1,1,3-trimethyl-1H-benzo[e]indol-3-ium perchlorate
14	2-amino-6-chloro-3-propyl-1,3-benzothiazol-3-ium iodide
15	2-amino-6-methyl-3-propyl-1,3-benzothiazol-3-ium iodide
16	2-amino-6-methoxy-3-propyl-1,3-benzothiazol-3-ium iodide
17	4-[(E)-2-[4-(diethylamino)phenyl]ethenyl]-1-[(4-fluorophenyl)methyl]pyridin-1-ium iodide
18	1-[2-oxo-2-(4-pentylphenyl)ethyl]quinolin-1-ium bromide
19	2-[(E)-2-[4-(dimethylamino)phenyl]ethenyl]-3-ethyl-1,3-benzothiazol-3-ium iodide
20	3-ethyl-2-[(E)-2-[methyl(phenyl)amino]ethenyl]-5-phenyl-1,3-benzoxazol-3-ium bromide
21	3-butyl-2-{{[2-oxo-2-(pentyloxy)ethyl]sulfanyl}}-1,3-benzothiazol-3-ium bromide
22	3-dodecyl-2-(methylsulfanyl)-1,3-benzothiazol-3-ium methyl sulfate

#### 5.4.2. Membrane Binding Properties of SM<sub>1-22</sub>

The CG free energy calculations allowed us to identify the physical and chemical properties indicative of cardiolipin selectivity, to formulate design rules and to apply those to screen a database for candidate molecules conforming to those design rules. To experimentally verify our *in silico* results, we next screened the membrane binding properties of the 22 molecules identified in the *in silico* approach *in vitro*, using liposomal systems.

When a small molecule integrates into a hydrophobic lipid bilayer due to its amphipathic character, this will affect lateral lipid packing, an effect often observed *e.g.*, with alcohols or other small, hydrophobic molecules [152]. Additional specific interactions with certain lipid headgroups will lead to an increase in the effective substance concentration at the surface of the bilayer, and therefore to an increased effective partitioning coefficient (see *e.g.* [153]). Furthermore, the effect on order and packing of the hydrophobic part might be altered, *e.g.*, due to a different orientation of the small molecule when specifically binding to a defined lipid species. Thus, comparing the impact of a small molecule on the membrane structure in a system where the molecules merely partition into the membrane with a system where the molecules additionally (more or less) specifically interact with a defined lipid species will allow parallel screening of multiple molecules for their potential to bind to cardiolipin. We rationalized that the molecules pre-selected in the computational screen will “only” integrate into net uncharged pure PC membranes but will (in the best of all cases) specifically interact with cardiolipin in cardiolipin-containing membranes. To delineate general membrane partitioning from specific lipid binding, we additionally tested the structure of a model membrane system where PG is present to isolate selectivity to cardiolipin by direct comparison. For monitoring changes in the membrane lipid structure, we utilized Laurdan, an environment-sensitive fluorescent dye that incorporates into lipid bilayers. From the Laurdan fluorescence emission spectra the GP values were calculated (Equation 2) [90] for membranes in absence *vs.* presence of the 22 substances identified in our computational screening. Besides pure PC and the PG- or cardiolipin-containing PC membranes, respectively, we also monitored the Laurdan fluorescence emission in PC liposomes containing PE, another net-uncharged phospholipid. PE introduces membrane curvature stress, and these measurements enabled us to test whether any observed effects on the Laurdan fluorescence spectra were mainly due to changes in the lateral membrane pressure.

This would result in changes observed in the PC/PE system being unequal to the pure PC system.

The Laurdan GP value is largely independent of the lipid head group and its acyl chain chemistry, and therefore any changes of this value upon the addition of a substance provides information about changes in the lipid order [91]. Thus, if the GP value in presence of a substance is altered, one can infer that binding/incorporation of the substance has occurred. Indeed, for several substances large positive  $\Delta$ GP values were observed (Figure 14).

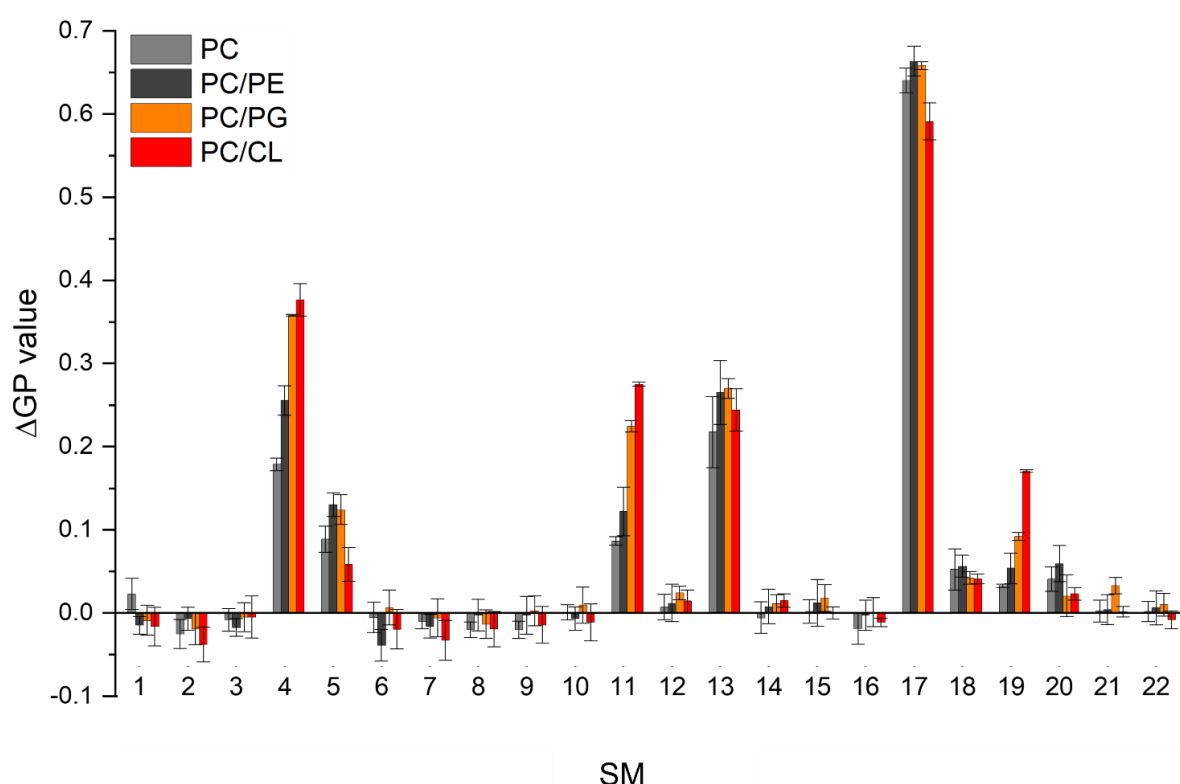


**Figure 14:**  $\Delta$ GP values of the preselected 22 SMs in various model membrane systems.

GP values were measured using pure PC liposomes, as well as liposomes containing PC/PG, PC/PE and PC/cardiophilin, all in a molar ratio of 80/20 (mol-%/mol-%) at 300  $\mu$ M total lipid. Low  $\Delta$ GP values indicate no influence of the respective SM on the membrane structure, when using Laurdan as a probe. The more a  $\Delta$ GP value deviates from 0.0, the higher is the respective impact of a given SM on the membrane structure. Positive  $\Delta$ GP values indicate increased lipid ordering due to the presence of a SM within a membrane.

Addition of SM<sub>4</sub>, SM<sub>5</sub>, SM<sub>11</sub>, SM<sub>13</sub>, SM<sub>17</sub> and SM<sub>19</sub> resulted in substantial changes in the GP values (high  $\Delta$ GP values) in all lipid systems, which clearly indicates considerable interaction of these SMs with the membranes. Noteworthy, while we did not observe

$\Delta$ GP changes for the remaining SMs, this does not finally exclude that these SMs do interact with membranes. We only limited the selection and further analysis in the screening pipeline developed and presented here, to substances which had a measurable impact on membrane lipid packing, as sensed by Laurdan. While all six molecules affected the Laurdan fluorescence emission spectrum, for SM<sub>5</sub>, SM<sub>13</sub> and SM<sub>17</sub> the results did not indicate a specificity towards charged lipids, as anticipated, as the  $\Delta$ GP values were similarly affected in membranes containing solely zwitterionic or additionally negatively charged lipids. Thus, a specific interaction with negatively charged lipids is unlikely. In contrast, SM<sub>4</sub>, SM<sub>11</sub> and SM<sub>19</sub> showed higher  $\Delta$ GP values in cardiolipin- and PG-containing PC membranes, indicating a specificity towards negatively charged lipids.

The objective of our research was to identify membrane-active compounds with a putative specificity towards cardiolipin. Thus far, our initial computational and *in vitro* screens limited our further analyses to three compounds, for which we next analyzed in greater detail their respective impact on the GP values of cardiolipin-containing liposomes compared to PG-containing liposomes. The magnitude of a GP value change observed upon SM binding might be specific for the substance and the lipid environment. Yet, with increasing amounts of negatively charged lipids but at a constant SM concentration, the  $\Delta$ GP values are affected more substantially when an observed change is due to a specific interaction of the substance with the lipid and thus information about the relative specificity can be extracted: a steeper relative increase of GP values is an indicator for a higher affinity. Therefore, we next monitored how the GP values determined in a (neutral) PC background are differentially affected when the mole fractions of the two negatively charged lipids PG or cardiolipin, respectively, increase (Figure 15), yielding a binding isotherm. In presence of all three SMs, increasing  $\Delta$ GP values were observed with increasing amounts of negatively charged membrane lipids. Yet, in case of SM<sub>4</sub> the shape of the relative increased is similar for cardiolipin- and PG-containing membranes, and also the  $\Delta$ GP values are similar. Thus, SM<sub>4</sub> (Figure 15) does not significantly discriminate between liposomes containing PG or cardiolipin, indicating about similar interaction with the negatively charged membrane lipids. For SM<sub>11</sub> (Figure 15B), a difference between liposomes containing PG and those containing cardiolipin was observed at all PG/cardiolipin concentrations. Furthermore, the curve is slightly steeper at the initial part in case of cardiolipin, indicating a specificity of SM<sub>11</sub> for cardiolipin. Finally, in case of SM<sub>19</sub>, the  $\Delta$ GP values

are overall lower than for the other two substances, yet the difference in the values obtained for cardiolipin- vs. PG-containing liposomes is larger. More importantly, the binding isotherm is steeper in case of cardiolipin-containing liposomes. Thus, SM<sub>19</sub> (Figure 15C) clearly discriminates best between cardiolipin- or PG-containing liposomes.

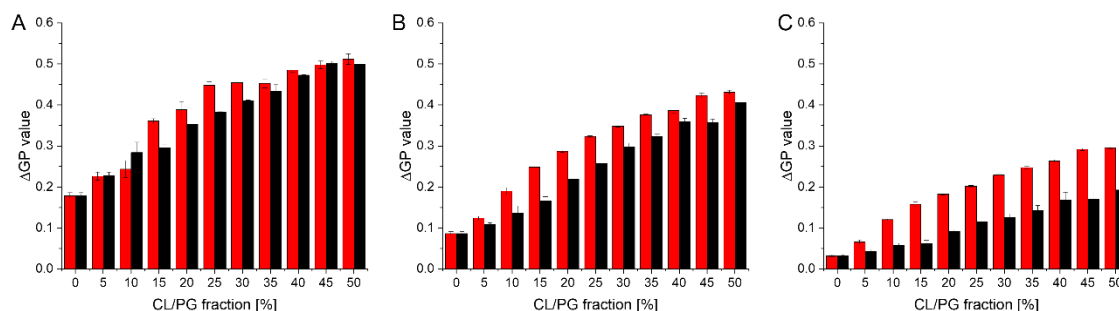


**Figure 15:**  $\Delta GP$  values in presence of the three most promising cardiolipin-binders determined in cardiolipin- or PG-containing model membranes.

$\Delta GP$  values were determined in liposomes, containing increasing amounts of the negatively charged lipids PG (black) or cardiolipin (red), respectively, in a PC background (300  $\mu M$  total lipid) at a constant concentration (3  $\mu M$ ) of SM<sub>4</sub> (A), SM<sub>11</sub> (B) and SM<sub>19</sub> (C). All SMs induce an increase in  $\Delta GP$  values with increasing amounts of the negatively charged lipids. The most significant difference between PG- vs. cardiolipin- containing membranes was observed for SM<sub>19</sub>.

In order to visualize the differences in shape of the binding isotherms more clearly, the ratio between the  $\Delta GP$  values obtained in presence of cardiolipin or PG, respectively, was calculated (Figure 16).

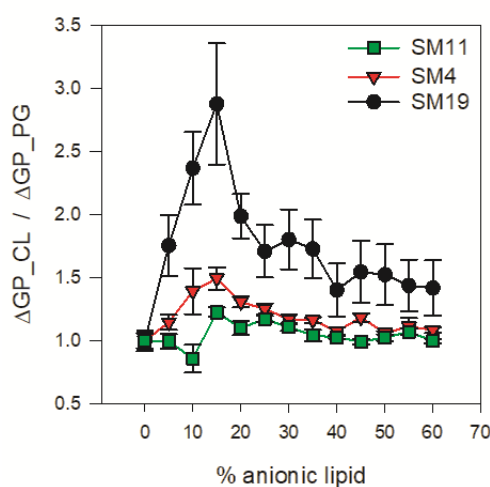


**Figure 16:** Ratio between the  $\Delta GP$  values in DOPC/DOPG and DOPC/cardiolipin containing liposomes.

The large deviation from constant ratio for SM<sub>19</sub> clearly indicates the highest specification towards cardiolipin for this molecule.

If the shapes of the binding isotherms were identical, yet differ in their  $\Delta GP$  value, the same ratio (within error limits) is expected at all mole fractions of anionic lipids. The data obtained in presence of  $SM_{19}$  clearly show the largest deviation from a constant ratio, and thus, based on these analyses,  $SM_{19}$  has the highest specificity towards cardiolipin (compared to PG).

To obtain an estimate of the  $SM_{19}$  affinity for cardiolipin, changes in the membrane lipid order were monitored at a constant lipid- but at varying  $SM_{19}$  concentrations (Figure 17A). The cardiolipin content in the liposomes was 10 %, approximately mirroring the cardiolipin concentration in *E. coli* and mitochondrial membranes [39]. In agreement with the above presented results, addition of increasing amounts of  $SM_{19}$  lead to higher  $\Delta GP$  values in case of cardiolipin-containing membranes when compared to PG-containing membranes. However, the shape of the curves does not allow to estimate the affinity constant. In agreement with the data in Figure 14 and Figure 15, the  $\Delta GP$  value is consistently higher in case of cardiolipin compared to PG.

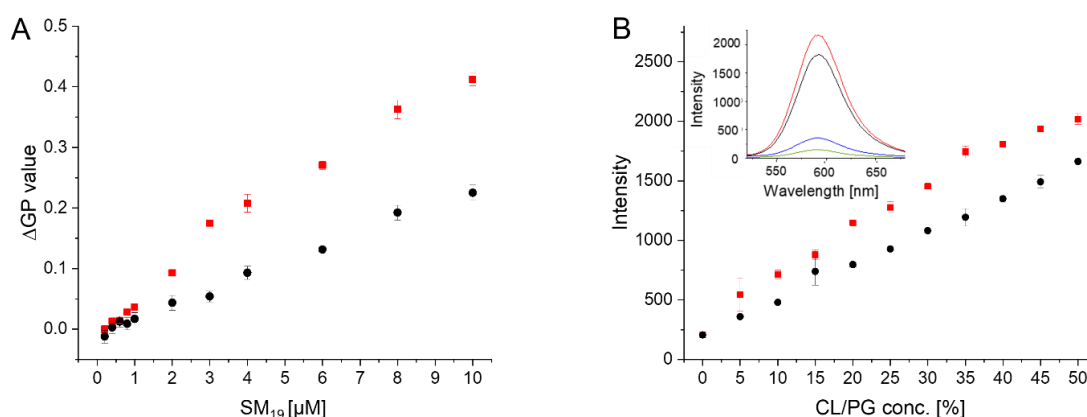


**Figure 17:** Specificity of  $SM_{19}$ -binding to cardiolipin-containing PC membranes.

(A)  $\Delta GP$  values determined in PG- or cardiolipin- containing model membranes in presence of increasing  $SM_{19}$  concentrations.  $\Delta GP$  values were measured using liposomes containing a fixed lipid composition of 90 % PC and 10 % cardiolipin (red) or PG (black), respectively, at increasing amounts of  $SM_{19}$ . At low  $SM_{19}$  concentrations no significant differences were observed. (B) The inherent  $SM_{19}$  fluorescence properties are affected by the membrane lipid composition. The fluorescence emission at 592 nm increases with increasing fractions of negatively charged lipids (PC/PG (black), PC/cardiolipin (red)). The intensity increases more and reaches a higher level in cardiolipin-containing membranes. (B inlet) Emission spectrum of pure  $SM_{19}$  in buffer (green), or in pure PC (blue), PC/PG (50/50) (black) and PC/cardiolipin (50/50) liposomes (red) ( $SM_{19}$  concentration: 3  $\mu M$ ).

As  $SM_{19}$  is intrinsically fluorescent (Figure 17B, inlet), we next additionally analyzed  $SM_{19}$  interaction with negatively charged lipids via following the  $SM_{19}$  fluorescence. In both PG- as well as cardiolipin-containing PC liposomes, the intensity of the  $SM_{19}$

fluorescence is rising with increasing concentrations of negatively charged lipids, which is perfectly in line with the Laurdan measurements (Figure 17A). Already when SM<sub>19</sub> was added to pure PC liposomes, the fluorescence emission increased (Figure 17B), indicating that membrane incorporation of SM<sub>19</sub>, *i.e.*, placing the dye in a more hydrophobic environment, affects the SM<sub>19</sub> fluorescence properties. When the liposome surface charge was increased via increasing the amount of PG or cardiolipin, respectively, the fluorescence emission intensity steadily increased. Thus, interaction of SM<sub>19</sub> with negatively charged lipids can also be monitored via the substances' inherent fluorescent properties and, as observed before using Laurdan as a probe, this effect is more pronounced in cardiolipin-containing liposomes.

### 5.4.3. Impact of SM<sub>19</sub> on Cardiolipin-Containing Cellular Membranes

Similar to mitochondria (10 – 20 %), *E. coli* cells contain ~10 % cardiolipin in their membrane as well as around 20 % PG [25]. When SM<sub>19</sub> was added to *E. coli* cells at increasing concentrations, the SM<sub>19</sub> fluorescence emission intensity at 592 nm increased (Figure 18), indicating membrane incorporation.

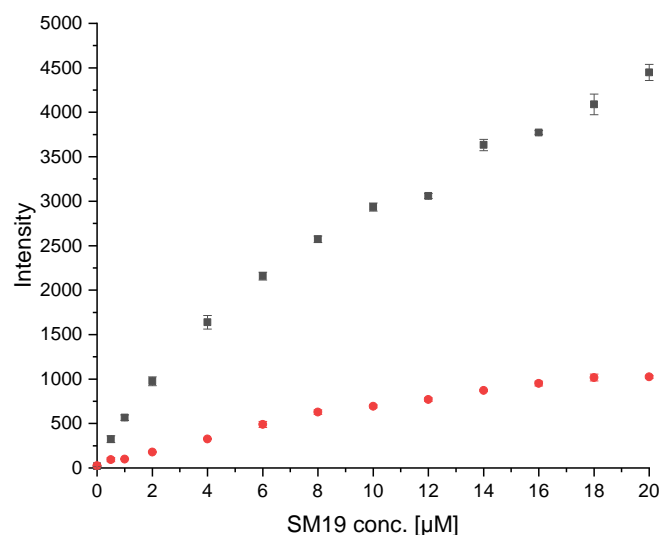


**Figure 18:** Membrane incorporation of SM<sub>19</sub> in cardiolipin-containing *E. coli* bacteria.

The SM<sub>19</sub> fluorescence emission is affected in presence of *E. coli* cells. In presence of bacteria (black), the SM<sub>19</sub> fluorescence emission at 592 nm increases, indicating proper membrane incorporation of the dye.



To next study the impact of a SM<sub>19</sub>-induced cardiolipin tethering on the physiology of *E. coli* cells, the impact of SM<sub>19</sub> addition on *E. coli* respiration was analyzed. In fact, SM<sub>19</sub> addition significantly affected respiration of *E. coli* cells and the respiration rates. Without the substance the respiration rate was around  $-19 \pm 0.7 \mu\text{mol oxygen/ min}^*\text{L}$ , which decreased in the presence of SM<sub>19</sub> to  $-15 \pm 0.5 \mu\text{mol oxygen/ min}^*\text{L}$ .

As these initial observations indicated a direct impact of SM<sub>19</sub> on the activity of proteins embedded in cardiolipin-containing membranes, we then ultimately analyzed the impact of SM<sub>19</sub> on mitochondrial respiration determined using mitochondria isolated from the fungus *P. anserina*. In presence of SM<sub>19</sub>, the relative oxygen consumption was decreased by around 40 % in wild type mitochondria (Figure 19), indicating that SM<sub>19</sub> efficiently tethers cardiolipin in mitochondrial membranes. To finally test whether this impact of SM<sub>19</sub> on mitochondrial respiration was due to a specific interaction of the compound with cardiolipin, we next used a cardiolipin-free *P. anserina* strain [104] and tested the impact of SM<sub>19</sub> on mitochondrial oxygen consumption using cardiolipin-free mitochondria. While the respiration rate is already reduced in cardiolipin-free mitochondria, addition of SM<sub>19</sub> showed only marginal effects. To also exclude that the non-responsiveness of cardiolipin-free mitochondria is due to their general impairment in respiration, we additionally tested whether they respond to inhibition of the two terminal oxidases present in *P. anserina* [154]. While complex IV (COX) is inhibited by KCN, SHAM inhibits the alternative oxidase AOX. Thus, mitochondrial respiration should be completely blocked when both inhibitors are given in combination. In fact, both in wild type and  $\Delta PaCrd1$  mitochondria the respiration rate was significantly decreased after addition of KCN/SHAM (Figure 19). Thus, the non-responsiveness of  $\Delta PaCrd1$  to SM<sub>19</sub> was indeed due to the lack of cardiolipin in this strain. These observations strongly indicate that SM<sub>19</sub> specifically interacts with cardiolipin as the substance clearly has an impact on the oxygen consumption rates (OCR) in wild type but not in cardiolipin-free mitochondria.

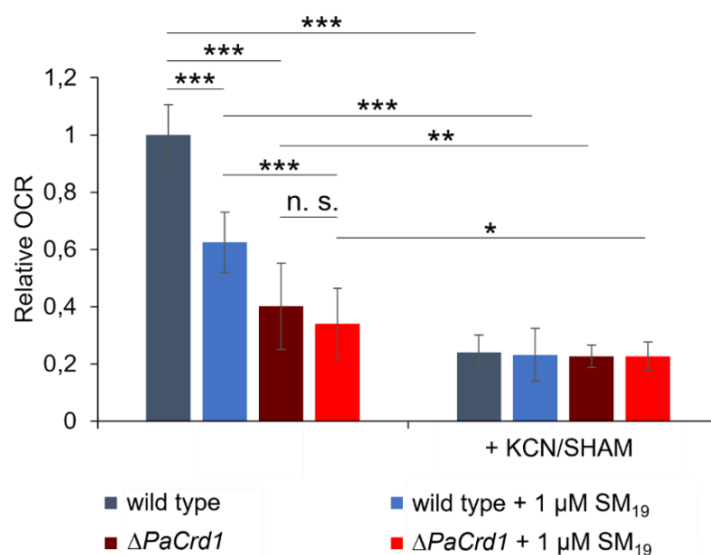


**Figure 19:** Oxygen consumption measured with mitochondria isolated from 6 days old wild-type and  $\Delta PaCrd1$  isolates.

Measurements were performed in absence vs. presence of 1  $\mu\text{M}$  SM<sub>19</sub>. Oxygen consumption rate (OCR) in the phosphorylating respiration state (in the presence of ADP) of the wild type was set to 1. In the wild-type, SM<sub>19</sub> treatment significantly reduced phosphorylating respiration by 40 % compared to the control. In contrast, in the mutant, addition of SM<sub>19</sub> had only marginal effects. In contrast, upon addition of KCN/SHAM a significant reduction in oxygen consumption was observed, independent of the strain and SM<sub>19</sub>. (Measurements of the phosphorylating respiration of wild type (n=15), of wild type + 1  $\mu\text{M}$  SM<sub>19</sub> (n=8), of  $\Delta PaCrd1$  (n=14) and of  $\Delta PaCrd1$  + 1  $\mu\text{M}$  SM<sub>19</sub> (n=9) and with additional adding KCN/SHAM wild type (n=3), wild-type + 1  $\mu\text{M}$  SM<sub>19</sub> (n=4),  $\Delta PaCrd1$  (n=4) and  $\Delta PaCrd1$  + 1  $\mu\text{M}$  SM<sub>19</sub> (n=5); mean values  $\pm$  standard deviation are shown; significant differences are marked with "\*", p < 0.05); "\*\*", p < 0.01; "\*\*\*", p < 0.001; n. s.: not significant).

SM<sub>19</sub> clearly affects respiration of intact *E. coli* cells as well as of isolated *P. anserina* mitochondria. As an impact of SM<sub>19</sub> was not observed when cardiolipin-free mitochondria were analyzed, the observed effects on respiration were very likely caused by cardiolipin-tethering via SM<sub>19</sub>.

Thus, after having identifying 22 putative cardiolipin-binders *in silico* and further analyzed them *in vitro*, we finally identified a single small molecule, 2-[(E)-2-[4-(dimethylamino)phenyl]ethenyl]-3-ethyl-1,3-benzothiazol-3-ium iodide (SM<sub>19</sub>) (Figure 13) which interacts with negative charged lipids and prefers cardiolipin over PG. Therefore, we will from now on name this molecule CLiB (**C**ardiolipin-**B**inder).

The interaction of CLiB with cardiolipin might be due to its quaternary ammonium ion (Figure 11), an interaction known to drive binding of NAO to cardiolipin and PG [36].

While the structures of PG *vs.* cardiolipin are very similar (Figure 11), the main difference is their respective charge. Thus, a specificity of a given substance would probably be based on a change in entropy: binding to a single cardiolipin molecule might be thermodynamically more favorable than binding two PG molecules due to a reduced loss in entropy. This is reflected in the design rules calling for two positively charged sites in the candidate structures to increase selectivity. The two positive charges correspond to the two negatively charged phosphate groups present in a cardiolipin molecule. Yet, this effect is likely very small, and thus it is potentially a deleterious task trying to isolate a substance with 100 % specificity towards cardiolipin. In summary we have identified and introduce here CLiB, a novel small molecule able to bind to negatively charged phospholipids, with a clear preference for cardiolipin (over PG). CLiB now allows to systematically analyze the role of cardiolipin in biological membranes and in membrane-harbored physiological processes, as with this chemical biology tool cardiolipin can be specifically targeted. We are optimistic that the identification of CLiB will now trigger new analyzes of mitochondrial processes, involving aging and dysfunction.



## **6. A Cardiolipin Detector Based on an eYFP-Coupled Dynamin Related Protein 1 Fragment**

### **6.1. Summary**

Cardiolipin is essential for many mitochondrial processes and alterations in its content have severe consequences for the cell and the organism. The localization of this lipid can help to study mitochondrial processes. Up to now, specifically interacting molecules are lacking. Some proteins are known to interact with this unique phospholipid. One is dynamin related protein 1 (DRP1), a large GTPase that plays an important role in mitochondrial fission and fusion processes. A defined region in DRP1, the B-insert, interacts with the mitochondrial specific lipid cardiolipin. In the present study, we coupled the cardiolipin-interacting region of DRP1 to an enhanced Yellow Fluorescent Protein (eYFP) to investigate and establish a specific fluorescent cardiolipin marker. Our construct shows a clear specificity towards cardiolipin as well as induces to structural changes in giant unilamellar vesicles.

### **6.2. Introduction**

Mitochondria are necessary for eukaryotic cell viability, plus they are crucially involved in key metabolic reactions and cellular processes, such as energy metabolism and apoptosis [35,97]. Thus, dysfunction of mitochondria leads to cell death and results in severe problems for the cell and the organism [32]. Mitochondria are highly dynamic and are frequently moving within the cell, thereby undergoing fusion and fission processes [155,156]. Many diseases are linked to defects in these morphological mechanisms of mitochondria, showing how important their optimal functioning is [155].

A group of proteins mainly regulating these mitochondrial morphological dynamics are dynamin related GTPases. One of these “large” GTPases of the dynamin superfamily is the 80 kDa human dynamin-related protein 1 (DRP1) [157]. By using the energy gained via GTP binding and hydrolyzing, it remodels the mitochondrial membrane [158,159].

DRP1 is predominantly involved in mitochondrial fission and can be found within the cytosol as a di- or tetramer [48,157,160–162]. If recruited to the fission sites, DRP1

forms large oligomeric assemblies, which then lead to membrane scission [48,157,160-163]. This happens through a lipid-induced self-assembly of DRP1, which also stimulates its GTPase activity [157,160,163]. The proteins self-assembly is driven by intermolecular dimerization of the so called G domain and intermolecular interactions within the stalk regions [160]. Besides the G domain and the stalk domains, DRP1 also contains bundle signaling elements (BSEs) and a region called the B-insert [157,164,165]. The G domain is responsible for the GTPase activity of DRP1, the BSEs are crucial for transmitting the conformation changes from the G domain to the stalk, and the stalk is, as mentioned, implicated in DRP1 multimerization [157]. The B-insert is an unstructured region that plays an important role in DRP1 regulation as well as its membrane association. Four lysine residues located in the B-insert of DRP1 are involved in membrane association, stimulation of the GTPase activity and are proposed to be responsible for the preferred interaction of DRP1 with cardiolipin [157,160].

In eucaryotes, the lipid cardiolipin can be exclusively found in the membrane of mitochondria (up to 20 % of total lipid in the inner mitochondrial membrane). The unique phospholipid is, aside from mitochondria, also present in significant amounts in many bacteria (e.g. about 10 % in the inner membrane of *E. coli*) [25], which underlines the endosymbiotic origin of mitochondria [98,99,166].

In addition to its unique occurrence, the chemical structure of cardiolipin is unique among phospholipids. It is an anionic, non-bilayer forming lipid with two negative charges at its polar head and four acyl chains, which can vary in their length and saturation [33,38,40,97,105,106,167]. Due to its conical structure, it is predominantly found at regions of high curvature [97]. Mitochondrial cardiolipin is crucially involved in many different processes, such as apoptosis, fission and fusion, mitochondrial protein imports as well as it is essential for the function of many enzymes involved in mitochondrial key processes [38,40,97,167]. Studies showed that alterations in the mitochondrial cardiolipin content led to morphological problems, which can have pathological consequences for the whole organism. Ischemia or reperfusion with the result of diabetes, heart disease or the BTHS are often found in patients with decreased cardiolipin content [38,109,115]. Naturally, the mitochondrial cardiolipin level constantly decreases during human aging [166].

Based on these observations, specific staining and localization of cardiolipin levels in mitochondria would drastically facilitate studying the processes resulting in

mitochondrial dysfunction. Due to a lack of a chromophore in the structure of cardiolipin, specific interacting and easy to detect compounds are needed for cardiolipin visualization and quantification. Thus far, such compounds are rare. An often-used small molecule in cardiolipin quantification is NAO, although this molecule also binds to other negatively charged phospholipids and consequently is not cardiolipin specific [119,125]. In an earlier project (chapter 5 of this thesis) we additionally introduced a new synthetic molecule specifically binding to cardiolipin. In this work, we show the ability to specifically stain model membranes with a modified DRP1 construct via specific cardiolipin interactions. This construct contains the B-insert, necessary for binding to cardiolipin and is coupled to an eYFP for autofluorescence and easy visualization.

### **6.3. Results and Discussion**

The mitochondrial specific lipid cardiolipin plays an important role in physiological activities and morphology of mitochondria [48,106]. Being able to specifically detect this lipid can help to better study its role in crucial cellular processes. Thus far, molecules specifically binding to cardiolipin are rare. The most prominent cardiolipin binder is NAO, a small synthetic molecule, which, however, does not specifically bind to cardiolipin but also to other negatively charged lipids [119,125]. Furthermore, in chapter 5 we introduced CLiB, a new promising small molecule specifically binding to cardiolipin.

Another approach is to look for proteins specifically interacting with cardiolipin, which are abundant. One advantage is that proteins can be expressed directly and easily in bacteria. For this reason, we aimed to establish a protein that allows specific detection of cardiolipin and visualization of cardiolipin-enriched membrane regions. In the process we came across DRP1 (Figure 20A), which is proposed to interact via its B-insert specifically with cardiolipin [33,157,160,165].

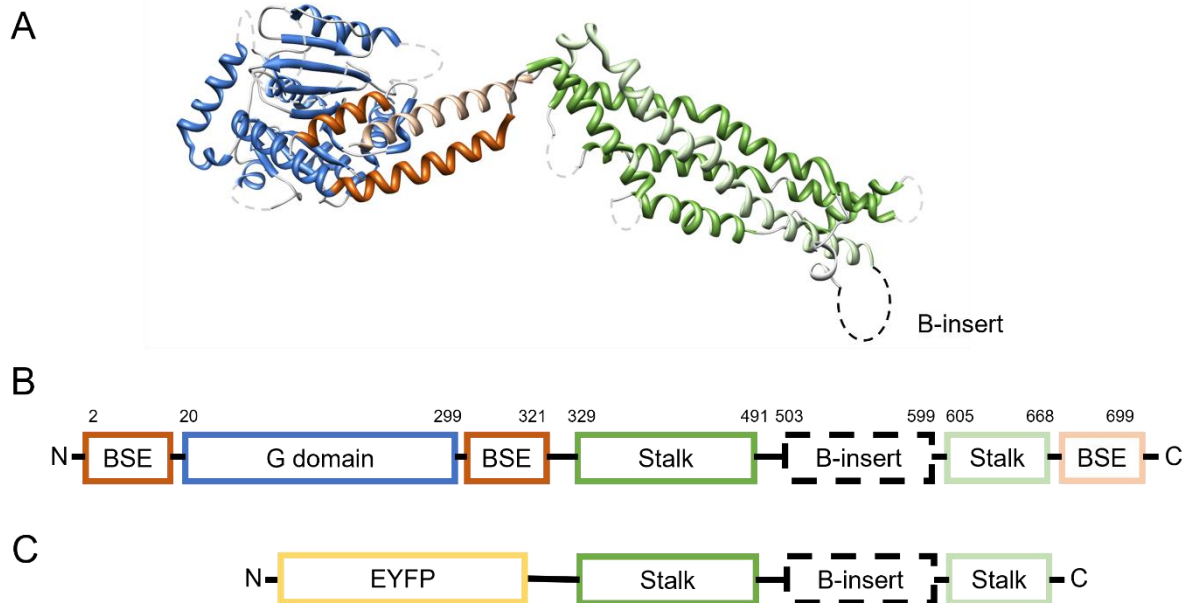


**Figure 20:** Scheme and structure of human DRP1 isoform 3 and our construct.

(A) Structure of DRP1 (PDB 4BEJ). Blue the G domain; red the bundle signaling elements (BSE) and green the stalk elements (B) Scheme of DRP1 structural elements. (C) Scheme of the generated construct. It contains the important B-insert and two stalk domains for stabilization. At its N-terminal site an eYFP is coupled. BSE: Bundle signaling elements.

The G domain contains the GTP-binding site and is important for GTPase activity. The bundle signaling elements and the stalk elements both play roles in multimerization of DRP1. The B-insert is responsible for the specific interaction with cardiolipin and is embraced by the stalk elements [165].

Thus, we genetically fused the cardiolipin-interacting domain of DRP1 to a fluorescent protein (here eYFP) for *in vitro* as well as *in vivo* detection and visualization of cardiolipin-enriched membranes and/or membrane regions. Yet, the B-insert is an unstructured region, and while heterologous expression of this isolated domain coupled to eYFP was successful, the protein turned out being unstable and degraded during the purification (data not shown). Consequently, we next expressed a fusion protein containing the crucial B-insert but lacking the G domain as well as the BSEs (Figure 20C). We named this protein, with the eliminated dynamin-specific activity, “stalk”. Via expression of the stalk region the cardiolipin-interacting B-domain is stabilized (Figure 20) and coupling this region to an eYFP resulted in generation of a promising fluorescent cardiolipin binder. Figure 20 shows schematically the domain structure of wild type DRP1 (B) and the final construct created and further analyzed in this study (C). The construct (C, eYFP-stalk) includes the amino acids K329 to D668 of the DRP1 wild type isoform 3 and is coupled to an eYFP at its N-terminal site. In Figure 20A the structure of DRP1 is seen and it is recognizable that a depletion of the G domain



and the BSEs will not affect the interaction of the two stalk regions and thus their stabilization of the B-insert.

### 6.3.1. Expression of eYFP-Stalk in *E. coli*

eYFP is one of the most widely used fluorescence proteins and can easily be visualized by using fluorescence microscopy.

For initial characterization, we expressed the chimeric protein eYFP-stalk heterologous in *E. coli* to visualize the location of the protein in living cells (Figure 21).

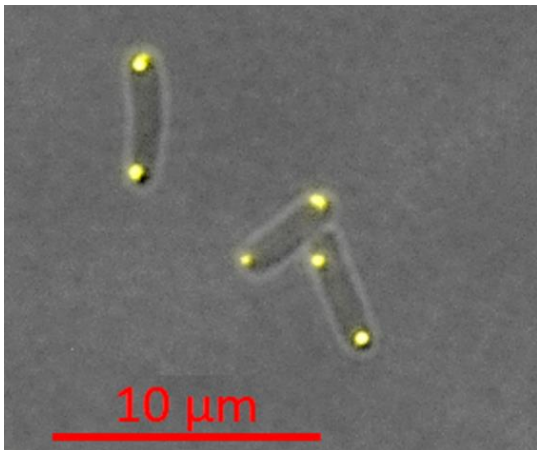


**Figure 21:** Fluorescence microscopy picture of *E. coli* MC4100/eYFP-stalk.

The picture was taken 15 minutes after induction with 0.5 mM IPTG. The bacterial cells were visualized using a fluorescence microscope (63x). The *E. coli* cells were visualized using the bright channel and for the eYFP the TagYFP channel of the microscope was used. Both pictures were merged.

The *E. coli* membrane comprises of about 10 % cardiolipin [25], however the eYFP-stalk construct is mostly localized at both poles of the bacteria and does not distribute over the whole cell membrane. This might be due to an accumulation of cardiolipin specifically at highly curved membrane parts, i.e. the cell poles [168]. Another reason for the accumulation at the cell poles could be the misfolding of the protein and the formation of inclusion bodies, which could lead to a malfunction of the protein [169]. Nevertheless, the fluorescence of the eYFP of our construct is still detectable, indicating that at least this part of the protein is correctly folded and/or not influenced in its fluorescence by misfolding. Whether misfolding of the construct affects the binding to cardiolipin cannot be assessed yet. To find this out, we next tested eYFP-stalk for its cardiolipin-recognition and -binding *in vitro*, using model membrane systems.

### 6.3.2. The eYFP-Stalk Construct Binds to Cardiolipin-Containing LUVs

A sedimentation assay is a simple way to check, whether a protein binds to liposomes of a specific lipid composition. Here, liposomes and the protein were incubated and after high-speed centrifugation, the liposomes can be found in the pellet. Consequently, protein bound to the liposomes will be found in the pellet after ultracentrifugation as well. In contrast, free or unbound protein is located in the supernatant. The results for the eYFP-stalk are shown in Figure 22.

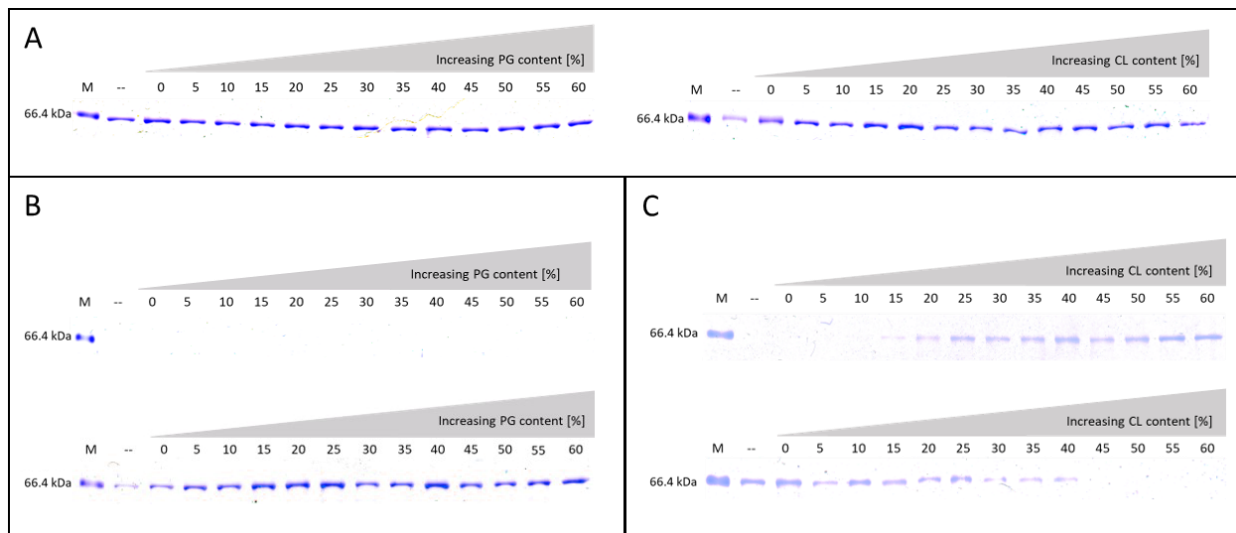


**Figure 22:** SDS-PAGE analysis of the sedimentation assay before (A) and after high-speed centrifugation (B and C).

(A) eYFP-stalk incubated with liposomes. Left: DOPC-DOPG liposomes with increasing amounts of DOPG in a DOPC background. Right: Increasing amounts of cardiolipin (CL) in a DOPC background. (B) Samples of DOPG containing liposomes. Top: the pellet; Bottom: the supernatant. If the protein binds to the liposomes, it is found in the pellet fraction. (C) Liposomes containing cardiolipin. Top: the pellet Bottom: the supernatant. With increasing amounts of cardiolipin more protein binds to the liposomes. M: Marker, -: without liposomes, o pure DOPC

As there is no other protein in the reaction approach than the eYFP-stalk, SDS-PAGE analysis was used to visualize the fraction containing the protein. In the experiment, increasing amounts of negatively charged lipid was used in a DOPC background as well as a pure DOPC control (o) and a control without any lipid (-). All samples taken before ultracentrifugation inevitably contain eYFP-stalk (Figure 22A). The sedimentation assay showed for the DOPC-DOPG liposomes no protein in the pellet, but in the supernatant (Figure 22B). This clearly shows that the protein neither binds to DOPC (control) nor to DOPG, indicating that the negative charge of the lipid *per se* is not enough for the eYFP-stalk to bind to the liposome.

In contrast, using increasing amounts of cardiolipin in DOPC-cardiolipin liposomes, the protein can be found in the supernatant as well as in the pellet. eYFP can be found in the pellet starting from around 10 % cardiolipin content and increases with increasing amounts of this lipid (Figure 22C). The opposite is seen for the supernatant and so goes hand in hand with the results from the pellet. This clearly indicates that eYFP-stalk exclusively binds to cardiolipin-containing liposomes. The slowly increasing intensity with increasing amounts of cardiolipin state that a minimal level of around 10 % cardiolipin is needed before the protein binds. As *E. coli* contains about 10 % of cardiolipin and the mitochondrial membrane comprise a higher percentage of cardiolipin, the use of the eYFP-stalk as a cardiolipin specific marker could be utilized *in vivo*.

### **6.3.3. The eYFP-Stalk Construct Binds to GUVs and Changes Their Structure**

Since the eYFP fused to the DRP1 construct could be detected *in vivo*, in living *E. coli* cells by fluorescence microscopy (Figure 21), membrane binding of the protein was further tested using GUVs containing different lipid compositions to determine its specificity. Due to the giant nature of GUVs, these can be seen as well under a microscope. For this reason, GUVs are a good way to study binding of a molecule or protein to a model membrane. The binding of the eYFP-stalk towards cardiolipin was studied using cardiolipin-containing GUVs in a 50/50 mixture with DOPC. And, to exclude binding to another negatively charged lipid, we used DOPG containing liposomes in a 50/50 mixture with DOPC as a control. The lipid mixture contained the dye PE-atto336, which incorporated into the GUVs and thus allowed visualization of GUVs with the AF647 channel of the microscope. The eYFP-stalk can be visualized using the TagYFP channel.

Figure 23 shows the result of staining the different GUVs with the protein.

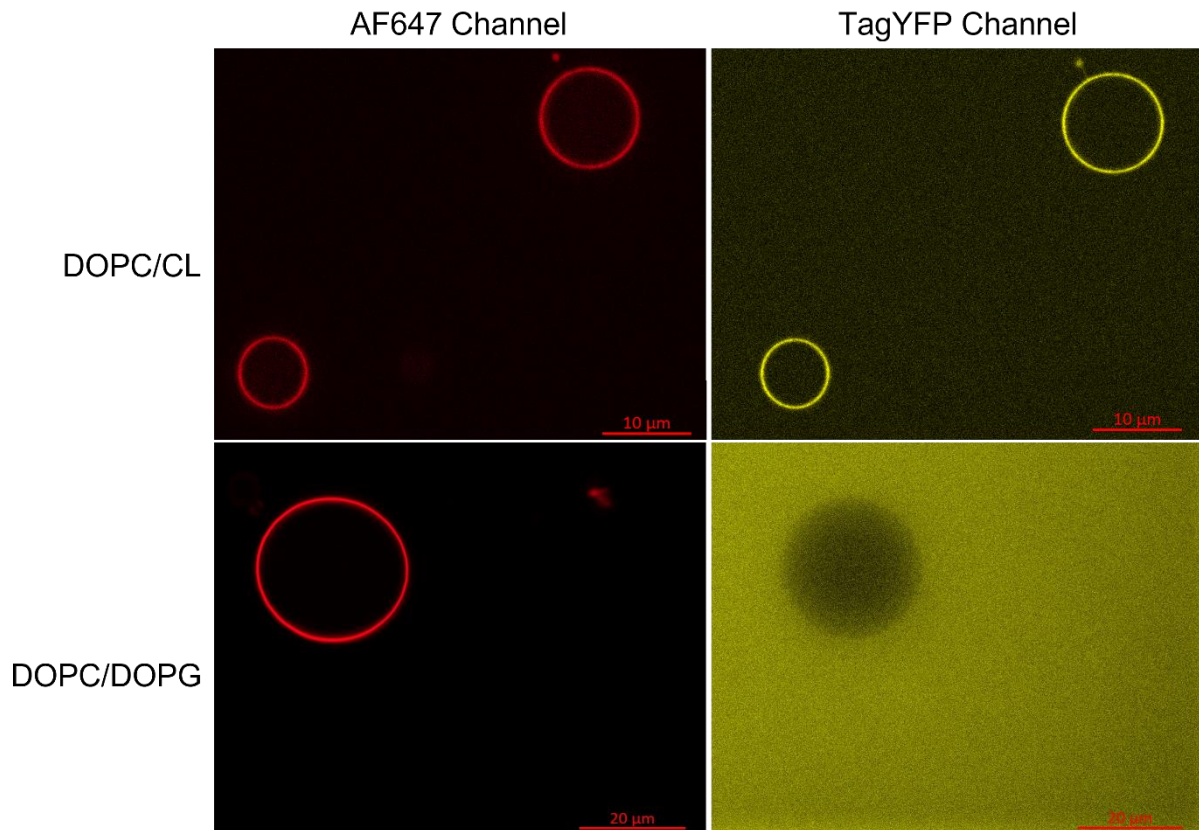


**Figure 23:** DOPC/cardiolipin (CL) or DOPC/DOPG GUVs incubated with eYFP-stalk.

Left: GUVs visualized using the AF647 channel. Right: Visualization of the construct using the TagYFP channel. eYFP-stalk bound to cardiolipin containing GUVs can be seen as well as the DOPC/DOPG containing GUVs without any protein bound.

Figure 23 shows uniformly round shaped DOPC/cardiolipin and DOPC/DOPG GUVs. In case of the cardiolipin containing GUVs, this shape is also nicely seen in the channel visualizing the eYFP, whereas this is not the case for DOPG containing GUVs. Indicating here that we can see a close to 100 % specificity of the protein towards cardiolipin, which perfectly supports the results gained from the sedimentation assay (Figure 22).

Another, yet unexpected observation was the change of the GUV structure after adding eYFP-stalk (Figure 24). This structural change was not observed for all GUVs studied (Figure 23). As seen, tube-like structures and smaller vesicle form on the surface of the GUVs (Figure 24). This structural change was seen in cardiolipin- as well as in DOPG-containing GUVs.

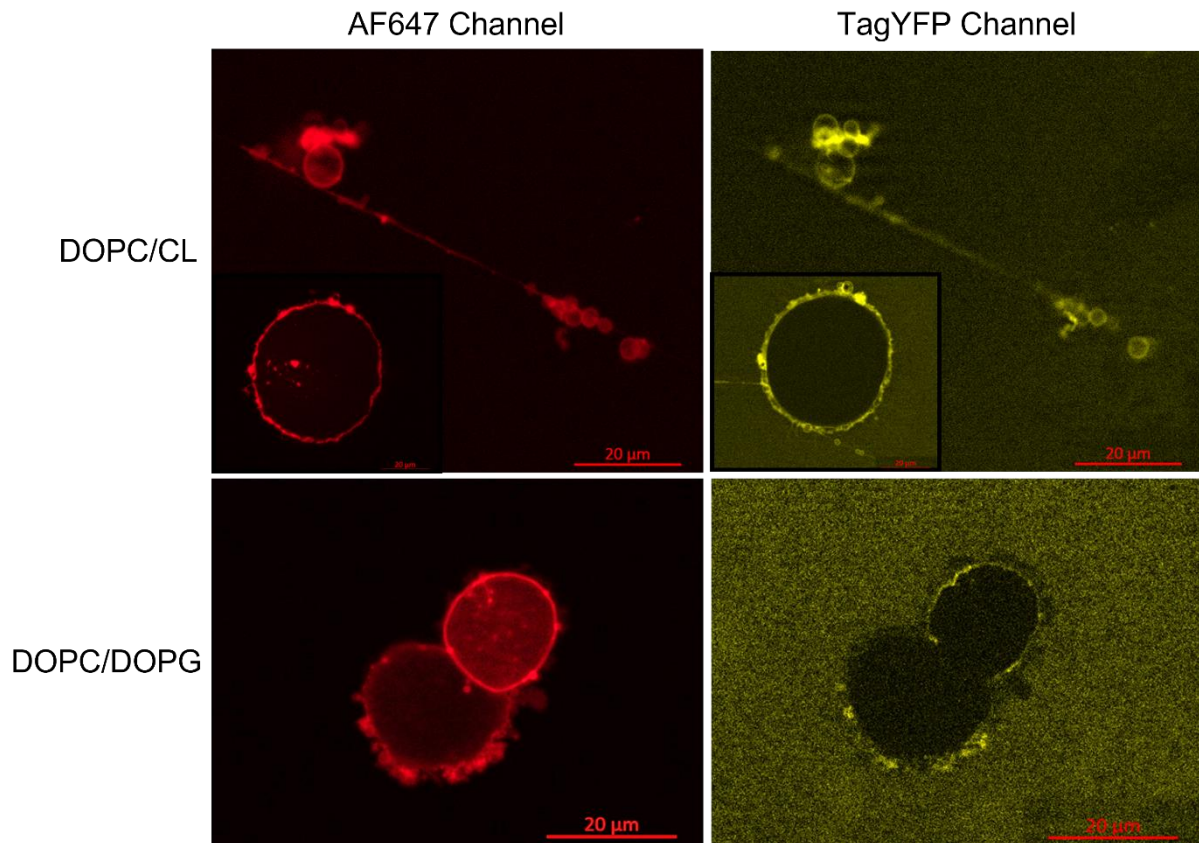


**Figure 24:** Structural change of GUVs after adding eYFP-stalk.

GUVs containing cardiolipin show some tubulations. eYFP-stalk is distributed all over the GUV surface. DOPG containing GUVs also show a change in structure, but the binding pattern of eYFP-stalk looks more patch like.

Changes in the structure of GUVs due to the full-length DRP1 were previously seen by different groups [48,162]. As seen in those publications, long tube-like structures could be observed, when interacting with cardiolipin, which we also observed in our approach (Figure 24). These structural changes in the GUVs occur shortly after adding the protein without any incubation time.

As seen in Figure 23, some GUVs do not undergo structural changes. Furthermore, we could observe that upon the initial structural changes, typical shaped GUVs formed again. Cardiolipin containing GUVs that exhibit a structural change also show binding of the protein, appearing to be completely covered with the construct. Interestingly, for GUVs containing DOPG and showing a structural change the binding of the protein is also seen. Hereby, the binding pattern of the protein looks more incomplete, which was as well previously seen by other groups and suggesting cardiolipin is needed for optimal DRP1 binding. *Ugarte-Urbe et al.* concluded in their publication that the binding of DRP1 is not only due to the negative charge of cardiolipin but also to its

specific structure. However, it can be at least partially substituted by DOPG. [48]. Our observations of GUVs undergoing structural changes support this statement.

A structural change of the GUVs due to the interaction with the eYFP-stalk was not expected, as it is suspected that the energy from GTP hydrolysis is necessary for this membrane remodeling process. [158,164,165,170]. Since the G domain is not existing in the eYFP-stalk protein, we consequently expected no ability to hydrolyze GTP and thus should not be able to remodel the membrane/GUV. However, our results indicate that the remodeling activity of DRP1 is not or only partially linked to the G domain and GTP hydrolysis.

Why we do not observe structural changes of all GUVs is not clear yet. Since binding of the protein induces the structural change, it is no surprise that no protein is bound to DOPG containing GUVs who do not undergo structural changes. More interesting is the binding of the protein to cardiolipin containing GUVs and not inducing any structural changes. The reason for this still needs to be clarified and further investigations are needed to answer this question.

Overall, we were able to generate a construct based on human DRP1 that showed a clear cardiolipin specificity in the sedimentation assay and which is a promising candidate for further research. We also showed that the remodeling properties of DRP1 might not be completely dependent on the G domain. Nevertheless, for *in vivo* utilization, where membrane remodeling is not desired, further refinement of the construct is needed, respectively it must be checked if the structural changes also occur under altered conditions. The question of why it sometimes binds to DOPG containing GUVs and sometimes does not needs to be addressed, as does the question of why we only sometimes observe a structural change of the GUVs.

## **7. Human Tafazzin is a Membrane-Attached, but not a Transmembrane Protein**

### **7.1. Summary**

Tafazzin, a mitochondrial transacylase, is involved in maturation of cardiolipin, the mitochondrial marker lipid. Alterations in the cardiolipin content are known to lead to severe problems for the organism, consequently showing that functional tafazzin is of great importance. Crucially important for the function of tafazzin is its association with the mitochondrial membrane. Yet, it is not clear how the protein attaches to the membrane but there are two possible membrane associating regions discussed in the literature. Within the protein, both regions are found at very distinct places. One is predicted to be a transmembrane helix, the other one is predicted to be a membrane “anchor” (extending into, but not through the membrane). In the present study, we investigated the membrane association of tafazzin. We were able to show that the predicted helix plays a role in membrane association of tafazzin but is not the only part that connects the enzyme to the membrane.

### **7.2. Introduction**

Cardiolipin is the signature phospholipid of mitochondria. Within eukaryotic cells, it occurs in significant amounts solely within the inner mitochondrial membrane (up to 20 % of total lipid) [98,99], whereas in the outer mitochondrial membrane only traces of cardiolipin are found. In contrast to eukaryotes, bacterial cytoplasmic membranes typically contain significant amounts of this lipid. For example, the inner (cytoplasmic) membrane of *E. coli* contains up to 10 % cardiolipin [171]. Beside its distinctive occurrence, cardiolipin additionally shows a unique structure: Due to two glycerol-linked phosphatidylglycerol backbones and four acyl chains, which can show different lengths and saturations. The cardiolipin head group contains two negative charges, a characteristic of this untypical phosphoglycerolipid [38,40,97,105,106]. A decrease or depletion of cardiolipin has severe consequences in mitochondria and in consequence for the whole organism. Alterations in the cardiolipin content is linked to several diseases, such as diabetes, heart disease or the BTHS [38,109,115].

BTHS is an X-linked disease and leads to multisystem disorders. BTHS patients must deal with symptoms like cardiac and skeletal myopathies, delayed growth until

puberty, 3-methylglutaconic aciduria and cyclic neutropenia. Consequently, undiagnosed, BTHS leads to an early death caused by cardiac failure. Nevertheless, a universal therapy of this genetic disease is not known yet [42,172,173].

However, mutations in the human *taz* gene (located on qX28), encoding the phospholipid-lysophospholipid transacylase tafazzin, are known to cause BTHS [42]. Currently, about 28 different missense mutations are described, resulting in replacement of single amino acids in the tafazzin sequence, consequently leading to a reduction of functional tafazzin [41,174]. A deficiency in functional tafazzin is biochemically characterized by a decrease in cardiolipin levels, resulting in an increase of monolysocardiolipin (MLCL) and an abnormal acyl chain profile in the remaining cardiolipin [174–176]. The reason is the crucial involvement of tafazzin in cardiolipin remodeling and maturing.

In eukaryotes, cardiolipin is synthesized exclusively in mitochondria [109]. In this process phosphatidic acid is converted into cytidine diphosphate-diacylglycerol (CDP-DAG). CDP-DAG is further processed by the phosphatidylglycerol phosphate (PGP) synthase, resulting in PGP formation [177], which is rapidly dephosphorylated to PG [42,178]. Finally, the cardiolipin synthase condenses PG and another CDP-DAG to nascent cardiolipin [109,179]. This immature cardiolipin, which is characterized by asymmetry and saturated acyl chains of variable length, is further remodeled for maturation [98,180]. Therefore, a phospholipase initially removes one acyl chain and MLCL is formed. In a second step, MLCL is reacylated by a transacylase or acyl transferase resulting in mature cardiolipin. Mature cardiolipin shows a high degree of symmetry of the acyl chains and contains only unsaturated acyl chains [98,181]. In mammals, three MLCL reacylation enzymes are known: MLCL acyltransferase-1 (MLCLAT1), acyl-CoA:lysocardiolipinacyltransferase-1 (ALCAT1) and tafazzin. Among those three, tafazzin is the only one being a transacylase, not requiring any acyl-CoA [182] and being conserved during evolution from yeast to higher eukaryotes [42]. As a mitochondrial phospholipid-lysophospholipid transacylase, tafazzin removes an acyl chain from another phospholipid (for example PG) and shuttles it to a MLCL, thereby producing mature cardiolipin [42,183,184]. This tafazzin-driven enzymatic reaction is unspecific and reversible [42].

Albeit much is known about the function of tafazzin, its precise localization in mammals is unfortunately not known. Clearly, tafazzin is a membrane-associated protein, and yeast tafazzin appears to be localized at the inner and outer mitochondrial



membrane within the inter-membrane space [174,185–187]. Even if it is still unclear how tafazzin attaches to membranes, two scenarios are discussed [51]: Possibly, tafazzin is membrane attached via a transmembrane helix at its N-terminus (Figure 25A). This helix is predicted in both yeast and human tafazzin. *Brandner et al.* suggest that this helix might not be transmembrane but only partially inserted into one leaflet of a bilayer [185]. On the other hand, a membrane anchor has been suggested in the middle of the acyltransferase domain (amino acid 215 to 232 in yeast) (Figure 25B). This anchor has been suggested to extend into, but not through, the lipid bilayer [174]. Orthologue regions can be found in human tafazzin (isoform 1, amino acid 201-218) [42].

Here, we analyzed whether the predicted N-terminal transmembrane helix [51,185] or the predicted membrane anchor [174] is responsible for membrane association of human tafazzin. Therefore, we first looked at the AlphaFold model and the sequence of tafazzin to discuss how accessible the two regions are. Based on our analyzes, we excluded the membrane anchor from further investigations, as it appears to be located in a very inaccessible region of the protein. Next, we generated a tafazzin construct lacking the predicted transmembrane helix and examined the membrane association of this construct and the wild type. Our results of the membrane association assay indicated that the helix is not solely responsible for the attachment of tafazzin to the membrane.

### **7.3. Results and Discussion**

Tafazzin is crucial for cardiolipin maturation and remodeling [42,183,184], and the membrane association of tafazzin is important for its enzymatic activity [174]. Two possible regions mediating membrane association were predicted for yeast tafazzin: a transmembrane helix at the N-terminus of tafazzin or a membrane anchor in the middle of the protein (amino acid 215 to 232 in yeast tafazzin) [174,185]. Thus far, for human tafazzin solely simulations are available, giving hints about its 3D structure, the phospholipid-binding cleft and its membrane association [51]. Yet, to study the impact of proper membrane association on certain diseases, it is crucial to identify the exact mode of membrane association of human tafazzin. Due to a high sequence similarity and since many regions are conserved between yeast and human tafazzin, a similar mode of membrane association is suggested for both enzymes [51].

### 7.3.1. The Predicted Membrane Anchor Presumably Lies in an Inaccessible Region

To test the putative mode of tafazzin membrane association, we first predicted the structure of human tafazzin using the AlphaFold server [188–190] (Figure 25). While the program does clearly not consider any constraints a biological membrane would introduce, an  $\alpha$ -helix is clearly predicted at the protein's N-terminus (Figure 25A), which could represent the transmembrane  $\alpha$ -helix anchoring tafazzin within a membrane. The region described by *Calypool et al.* as membrane anchor is, due to the AlphaFold model, predicted in the middle of the humans' enzyme's structure (Figure 25B) and hardly accessible or able to act as membrane anchor.

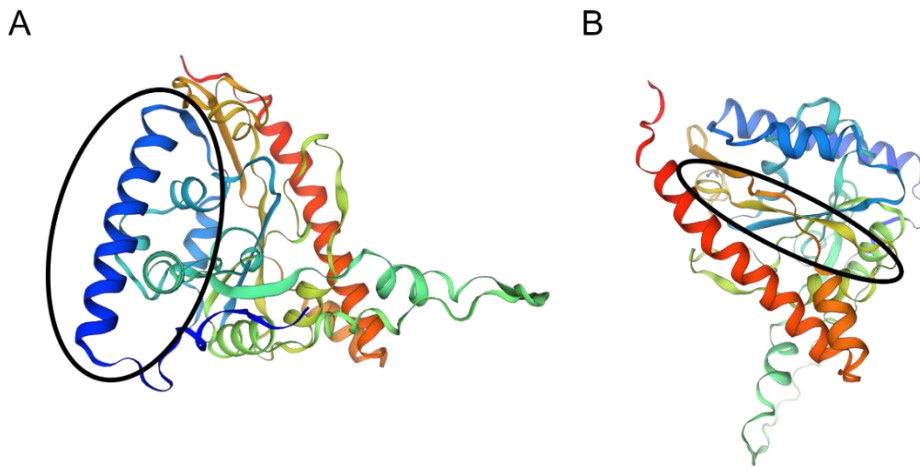


**Figure 25:** Two perspectives of the alphafold model of human tafazzin.

(A) surrounded by a black circle, the predicted transmembrane helix (16 TWTLASSVVMGLVGTYSFCWT 36).

(B) surrounded by the black circle, the predicted membrane anchor (201 AECHLNPIILPLWHVGMN 218).

(<https://swissmodel.expasy.org/repository/uniprot/Q16635?template=AlphaFold> [188–190]).

A suitable way to reveal which tafazzin domain might be responsible for membrane interaction/association is to analyze constructs lacking the suggested domains. Consequently, we used the gene coding for human tafazzin isoform 1 as a template and created a plasmid expressing a tafazzin variant, that lacks the transmembrane (TM) helix (amino acid (aa) 1 to 36). This tafazzin fragment is named in the following  $\Delta$ TM. Noteworthy, as can be seen in Figure 25A, removal of this (predicted)  $\alpha$ -helix is not expected to affect folding and the structure of the remaining protein. As the membrane anchoring region (Figure 25B, residues 201-218) is predicted in a region in the middle

of the protein no further analyzes of this region was done. An anchoring of the protein due to this region does not seem structurally possible.

### 7.3.2. The N-terminal Helix is not Alone Responsible for Membrane Association of Tafazzin

Tafazzin is a membrane-associated protein [51,174,185]. Whether the protein is peripheral or integral membrane anchored via an N-terminal transmembrane  $\alpha$ -helix [185] is not finally resolved yet. Peripheral membrane proteins interact with the polar headgroups of the lipids in the membrane, typically via ionic interactions. Plus, hydrophobic amino acid side chains additionally interact with the hydrophobic membrane core. These interactions can be disrupted or weakened by high concentrations of chaotropic salts as well as by changes in the pH, thus washing peripherally bound proteins from the membrane. In contrast, removing membrane integral proteins from membranes typically requires membrane disruption and protein solubilization by detergents.

We first checked whether the heterologous produced proteins can be extracted from the membranes. For this purpose, all membranes were incubated with buffer containing SDS [191], as shown in Figure 26. While in both cases upon addition of SDS some tafazzin was still present in the pellet fractions (indicating incomplete protein solubilization), a major fraction of both proteins clearly was extracted from membranes by SDS.

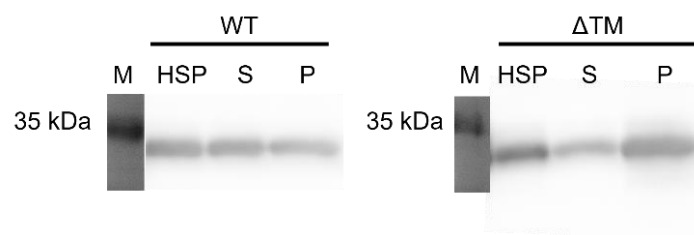


**Figure 26:** Western blot analysis of the wild type (wt) tafazzin and the  $\Delta$ TM construct.

M: marker, HSP: the pellet before SDS solubilization, S: the supernatant after SDS solubilization and P: the pellet after SDS solubilization. The proteins are found in every fraction.

To verify whether wild type (wt) tafazzin or the variant is peripherally bound to the membrane or a transmembrane protein, we prepared *E. coli* membranes containing the protein of interest and incubated them in various buffers containing high salt concentrations or increasing pH values.

The amount of solubilized protein in the supernatant or protein remaining in the membrane fraction after ultra-centrifugation was subsequently visualized via Western Blot analysis. Soluble proteins should already occur in the supernatant after centrifugation at physiological pH and low salt concentrations, whereas membrane-integral proteins are typically found in the supernatant exclusively when a detergent is used. In contrast, a peripherally membrane-attached protein might already be found in the supernatant at increasing salt concentrations or increasing pH values. This is due to the disturbance of electrostatic interactions between the aa and the membrane. Under most tested conditions, like physiological ones (buffer 1: Tris, EDTA pH 8; buffer 2: HEPES, pH 7.5,) or even high salt concentrations (buffer 4: HEPES + 2 M NaCl, buffer 5: HEPES + 2 M CaCl<sub>2</sub> and buffer 6: HEPES + 2 M NaSCN, Table 1), neither the wild type nor the  $\Delta$ TM construct were solubilized, indicating that both proteins remained membrane associated (Figure 27).

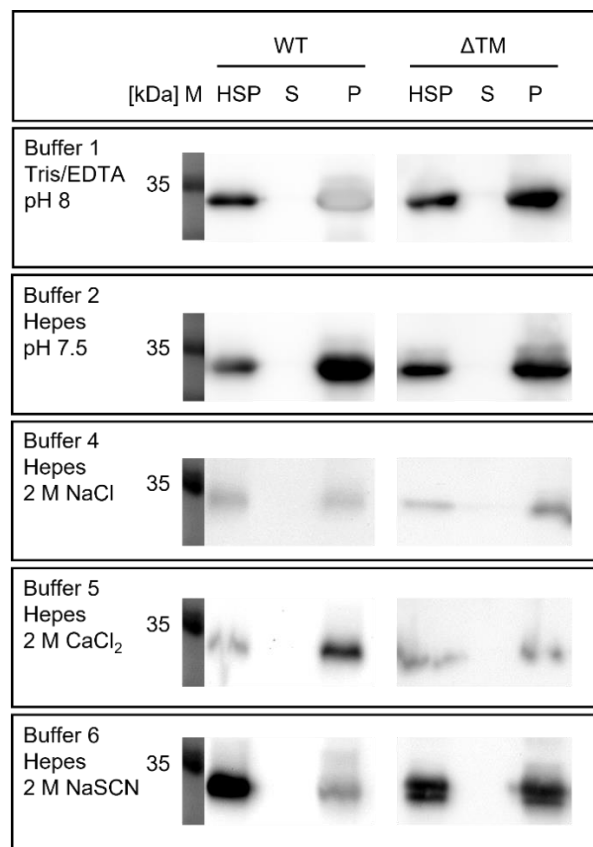


**Figure 27:** Western blot analysis of the wild type and the  $\Delta$ TM construct in buffer 1, 2, 4, 5 and 6 (Table 1).

None of the six buffers were able to solubilize the two proteins (M: marker; HSP: pellet before addition of specific buffer; S: supernatant; P: pellet). Buffer 1: 25 mM Tris, 2 mM EDTA, pH 8; buffer 2: 10 mM HEPES, pH 7.5; buffer 4: 50 mM HEPES, 2 M NaCl, pH 7.5; buffer 5: 50 mM HEPES, 2 M CaCl<sub>2</sub>, pH 7.5; buffer 6: 50 mM HEPES, 2 M NaSCN, pH 7.5.

To further analyze whether the helix is membrane integral or peripherally membrane associated, membrane association was next tested using buffers with increasing pH values (Figure 28). Wild type tafazzin was solubilized at pH 13, indicating that tafazzin is *de facto* a peripherally attached membrane protein.

Tafazzin  $\Delta$ TM is, besides at pH 13, also solubilized at pH 12, indicating a weakened membrane association. Thus, the predicted  $\alpha$ -helix at the N-terminus is (i) likely not “transmembrane” but only membrane associated and (ii) does not seem to be the only part of the protein responsible for membrane association. Based on these observations, it is likely that the N-terminal  $\alpha$ -helix is organized in a similar way as predicted by AlphaFold (Figure 25), and thus does not span the membrane but interacts partially with other parts of the protein, thereby anchoring tafazzin only peripherally to the membrane surface.

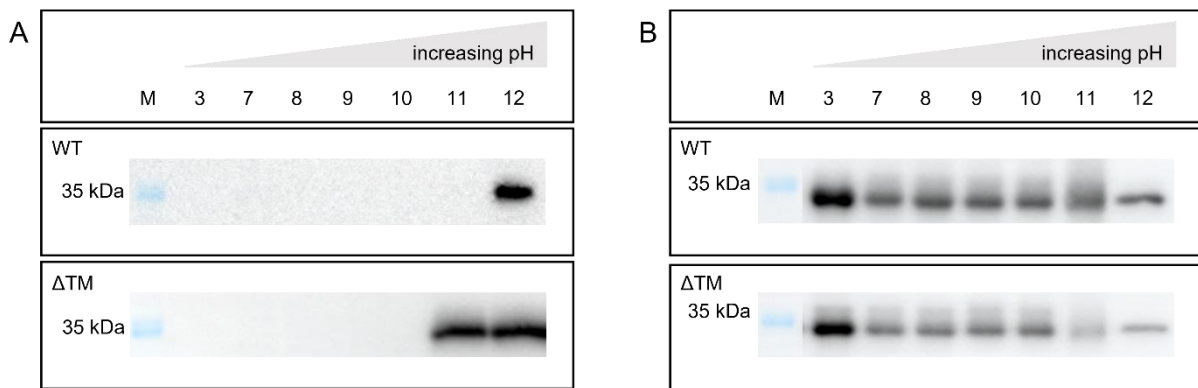


**Figure 28:** Western blots of the supernatant (A) and the pellet (B) of the membrane association assay.

Western blot of the wild type and the  $\Delta$ TM construct at different buffer conditions. M: marker; 3: 50 mM HEPES, pH 7.5; 7: 3 + 6 M Urea; 8: 10 mM Caps pH 10.5; 9: 10 mM Caps pH 11; 10: 10 mM Caps, pH 11.5; 11: 10 mM Caps, pH 12; 12: 0.1 M NaOH pH 13.

Based on our results, membrane attachment of human tafazzin is likely mediated by more than “just” the predicted N-terminal  $\alpha$ -helix. Yet the protein strongly associates with membranes still even upon deletion of the helix region. Thus, our observations indicate that the N-terminal  $\alpha$ -helix is central for membrane anchoring, assisted by further surface regions which together mediate membrane adhesion of human tafazzin.



## 8. References

- [1] Zalba S, ten Hagen TLM. Cell membrane modulation as adjuvant in cancer therapy. *Cancer Treat Rev* 2017;52:48–57. <https://doi.org/10.1016/j.ctrv.2016.10.008>.
- [2] Watson H. Biological membranes. *Essays Biochem* 2015;59:43–69. <https://doi.org/10.1042/bse0590043>.
- [3] Singer SJ, Nicolson GL. The Fluid Mosaic Model of the Structure of Cell Membranes. *Science* (80- ) 1972;175:720–31. <https://doi.org/10.1126/science.175.4023.720>.
- [4] Goñi FM. The basic structure and dynamics of cell membranes: An update of the Singer–Nicolson model. *Biochim Biophys Acta - Biomembr* 2014;1838:1467–76. <https://doi.org/10.1016/j.bbamem.2014.01.006>.
- [5] Nicolson GL. The Fluid–Mosaic Model of Membrane Structure: Still relevant to understanding the structure, function and dynamics of biological membranes after more than 40years. *Biochim Biophys Acta - Biomembr* 2014;1838:1451–66. <https://doi.org/10.1016/j.bbamem.2013.10.019>.
- [6] Fahy E, Subramaniam S, Brown HA, Glass CK, Merrill AH, Murphy RC, et al. A comprehensive classification system for lipids. *J Lipid Res* 2005;46:839–61. <https://doi.org/10.1194/jlr.E400004-JLR200>.
- [7] Ohvo-Rekilä H. Cholesterol interactions with phospholipids in membranes. *Prog Lipid Res* 2002;41:66–97. [https://doi.org/10.1016/S0163-7827\(01\)00020-0](https://doi.org/10.1016/S0163-7827(01)00020-0).
- [8] Berg JM, Tymoczko JL, Stryer L. *Stryer Biochemie*. 7th ed. Berlin, Heidelberg: Springer Berlin Heidelberg; 2013. <https://doi.org/10.1007/978-3-8274-2989-6>.
- [9] Goluszko P, Nowicki B. Membrane Cholesterol: a Crucial Molecule Affecting Interactions of Microbial Pathogens with Mammalian Cells. *Infect Immun* 2005;73:7791–6. <https://doi.org/10.1128/IAI.73.12.7791-7796.2005>.
- [10] Gruner SM. Intrinsic curvature hypothesis for biomembrane lipid composition: a role for nonbilayer lipids. *Proc Natl Acad Sci* 1985;82:3665–9. <https://doi.org/10.1073/pnas.82.11.3665>.
- [11] Seddon JM. Structure of the inverted hexagonal (HII) phase, and non-lamellar phase transitions of lipids. *Biochim Biophys Acta - Rev Biomembr* 1990;1031:1–69. [https://doi.org/10.1016/0304-4157\(90\)90002-T](https://doi.org/10.1016/0304-4157(90)90002-T).
- [12] Escribá P V., González-Ros JM, Goñi FM, Kinnunen PKJ, Vigh L, Sánchez-Magraner L, et al. Membranes: a meeting point for lipids, proteins and therapies. *J Cell Mol Med* 2008;12:829–75. <https://doi.org/10.1111/j.1582-4934.2008.00281.x>.
- [13] Janmey PA, Kinnunen PKJ. Biophysical properties of lipids and dynamic membranes. *Trends Cell Biol* 2006;16:538–46. <https://doi.org/10.1016/j.tcb.2006.08.009>.

- [14] White SH, Wimley WC. Membrane Protein Folding and Stability: Physical Principles. *Annu Rev Biophys Biomol Struct* 1999;28:319–65. <https://doi.org/10.1146/annurev.biophys.28.1.319>.
- [15] Bagatolli L, Parasassi T, Gratton E. Giant phospholipid vesicles: comparison among the whole lipid sample characteristics using different preparation methods. *Chem Phys Lipids* 2000;105:135–47. [https://doi.org/10.1016/S0009-3084\(00\)00118-3](https://doi.org/10.1016/S0009-3084(00)00118-3).
- [16] Koynova R, Caffrey M. Phases and phase transitions of the phosphatidylcholines. *Biochim Biophys Acta - Rev Biomembr* 1998;1376:91–145. [https://doi.org/10.1016/S0304-4157\(98\)00006-9](https://doi.org/10.1016/S0304-4157(98)00006-9).
- [17] Lewis RNAH, McElhaney RN. Membrane lipid phase transitions and phase organization studied by Fourier transform infrared spectroscopy. *Biochim Biophys Acta - Biomembr* 2013;1828:2347–58. <https://doi.org/10.1016/j.bbamem.2012.10.018>.
- [18] Eeman M, Deleu M. From biological membranes to biomimetic model membranes. *Biotechnol Agron Société Environ* 2010;14:719–36.
- [19] Subczynski WK, Wisniewska A. Physical properties of lipid bilayer membranes: relevance to membrane biological functions. *Acta Biochim Pol* 2000;47:613–25. [https://doi.org/10.18388/abp.2000\\_3983](https://doi.org/10.18388/abp.2000_3983).
- [20] Hao M, Mukherjee S, Sun Y, Maxfield FR. Effects of Cholesterol Depletion and Increased Lipid Unsaturation on the Properties of Endocytic Membranes. *J Biol Chem* 2004;279:14171–8. <https://doi.org/10.1074/jbc.M309793200>.
- [21] Quinn PJ, Wolf C. The liquid-ordered phase in membranes. *Biochim Biophys Acta - Biomembr* 2009;1788:33–46. <https://doi.org/10.1016/j.bbamem.2008.08.005>.
- [22] Barba-Bon A, Nilam M, Hennig A. Supramolecular Chemistry in the Biomembrane. *ChemBioChem* 2020;21:886–910. <https://doi.org/10.1002/cbic.201900646>.
- [23] Krylov A V., Pohl P, Zeidel ML, Hill WG. Water Permeability of Asymmetric Planar Lipid Bilayers. *J Gen Physiol* 2001;118:333–40. <https://doi.org/10.1085/jgp.118.4.333>.
- [24] Hill WG, Zeidel ML. Reconstituting the Barrier Properties of a Water-tight Epithelial Membrane by Design of Leaflet-specific Liposomes. *J Biol Chem* 2000;275:30176–85. <https://doi.org/10.1074/jbc.M003494200>.
- [25] Barák I, Muchová K. The Role of Lipid Domains in Bacterial Cell Processes. *Int J Mol Sci* 2013;14:4050–65. <https://doi.org/10.3390/ijms14024050>.
- [26] Symons JL, Cho K-J, Chang JT, Du G, Waxham MN, Hancock JF, et al. Lipidomic atlas of mammalian cell membranes reveals hierarchical variation induced by culture conditions, subcellular membranes, and cell lineages. *Soft Matter* 2021;17:288–97. <https://doi.org/10.1039/D0SM00404A>.



- [27] Shevchenko A, Simons K. Lipidomics: coming to grips with lipid diversity. *Nat Rev Mol Cell Biol* 2010;11:593–8. <https://doi.org/10.1038/nrm2934>.
- [28] Alberts B, Johnson A, Lewis J, Morgan D, Raff M, Roberts K, et al. *Molecular Biology of the cell*. 6th ed. 2015.
- [29] Kutschera U. Endosymbiosis, cell evolution, and speciation. *Theory Biosci* 2005;124:1–24. <https://doi.org/10.1016/j.thbio.2005.04.001>.
- [30] Ernster L, Schatz G. Mitochondria: a historical review. *J Cell Biol* 1981;91:227s-255s. <https://doi.org/10.1083/jcb.91.3.227s>.
- [31] Prasai K. Regulation of mitochondrial structure and function by protein import: A current review. *Pathophysiology* 2017;24:107–22. <https://doi.org/10.1016/j.pathophys.2017.03.001>.
- [32] McGeorge L, Kin A. Mitochondria : Structure , Function and Clinical Relevance. *Austin J Pharmacol Ther* 2017;5:3–5.
- [33] Horvath SE, Daum G. Lipids of mitochondria. *Prog Lipid Res* 2013;52:590–614. <https://doi.org/10.1016/j.plipres.2013.07.002>.
- [34] Kameoka S, Adachi Y, Okamoto K, Iijima M, Sesaki H. Phosphatidic Acid and Cardiolipin Coordinate Mitochondrial Dynamics. *Trends Cell Biol* 2018;28:67–76. <https://doi.org/10.1016/j.tcb.2017.08.011>.
- [35] Picard M, Taivassalo T, Gousspillou G, Hepple RT. Mitochondria: isolation, structure and function. *J Physiol* 2011;589:4413–21. <https://doi.org/10.1113/jphysiol.2011.212712>.
- [36] Palade GE. The fine structure of mitochondria. *Anat Rec* 1952;114:427–51. <https://doi.org/10.1002/ar.1091140304>.
- [37] Luévano-Martínez LA, Forni MF, dos Santos VT, Souza-Pinto NC, Kowaltowski AJ. Cardiolipin is a key determinant for mtDNA stability and segregation during mitochondrial stress. *Biochim Biophys Acta - Bioenerg* 2015;1847:587–98. <https://doi.org/10.1016/j.bbabi.2015.03.007>.
- [38] Houtkooper RH, Vaz FM. Cardiolipin, the heart of mitochondrial metabolism. *Cell Mol Life Sci* 2008;65:2493–506. <https://doi.org/10.1007/s00018-008-8030-5>.
- [39] Schlame M, Greenberg ML. Biosynthesis, remodeling and turnover of mitochondrial cardiolipin. *Biochim Biophys Acta - Mol Cell Biol Lipids* 2017;1862:3–7. <https://doi.org/10.1016/j.bbalip.2016.08.010>.
- [40] Planas-Iglesias J, Dwarakanath H, Mohammadyani D, Yanamala N, Kagan VE, Klein-Seetharaman J. Cardiolipin Interactions with Proteins. *Biophys J* 2015;109:1282–94. <https://doi.org/10.1016/j.bpj.2015.07.034>.
- [41] Ren M, Miller PC, Schlame M, Phoon CKL. A critical appraisal of the tafazzin knockdown mouse model of Barth syndrome: what have we learned about pathogenesis and potential treatments? *Am J Physiol Circ Physiol* 2019;317:H1183–93. <https://doi.org/10.1152/ajpheart.00504.2019>.

- [42] Saric A, Andreau K, Armand A-S, Møller IM, Petit PX. Barth Syndrome: From Mitochondrial Dysfunctions Associated with Aberrant Production of Reactive Oxygen Species to Pluripotent Stem Cell Studies. *Front Genet* 2016;6:1–26. <https://doi.org/10.3389/fgene.2015.00359>.
- [43] Seydel JK, Albores Velasco M, Coats EA, Cordes HP, Kunz B, Wiese M. The Importance of Drug-Membrane Interaction in Drug Research and Development. *Quant Struct Relationships* 1992;11:205–10. <https://doi.org/10.1002/qsar.19920110216>.
- [44] Seydel JK, Coats EA, Cordes HP, Wiese M. Drug Membrane Interaction and the Importance for Drug Transport, Distribution, Accumulation, Efficacy and Resistance. *Arch Pharm (Weinheim)* 1994;327:601–10. <https://doi.org/10.1002/ardp.19943271002>.
- [45] Lladó V, López DJ, Ibarguren M, Alonso M, Soriano JB, Escribá P V., et al. Regulation of the cancer cell membrane lipid composition by NaChOleate. *Biochim Biophys Acta - Biomembr* 2014;1838:1619–27. <https://doi.org/10.1016/j.bbamem.2014.01.027>.
- [46] Alves AC, Ribeiro D, Nunes C, Reis S. Biophysics in cancer: The relevance of drug-membrane interaction studies. *Biochim Biophys Acta - Biomembr* 2016;1858:2231–44. <https://doi.org/10.1016/j.bbamem.2016.06.025>.
- [47] Tiefenauer L, Demarche S. Challenges in the Development of Functional Assays of Membrane Proteins. *Materials (Basel)* 2012;5:2205–42. <https://doi.org/10.3390/ma5112205>.
- [48] Ugarte-Urbe B, Müller H-M, Otsuki M, Nickel W, García-Sáez AJ. Dynamin-related Protein 1 (Drp1) Promotes Structural Intermediates of Membrane Division. *J Biol Chem* 2014;289:30645–56. <https://doi.org/10.1074/jbc.M114.575779>.
- [49] Weinberger A, Tsai F-C, Koenderink GH, Schmidt TF, Itri R, Meier W, et al. Gel-Assisted Formation of Giant Unilamellar Vesicles. *Biophys J* 2013;105:154–64. <https://doi.org/10.1016/j.bpj.2013.05.024>.
- [50] Yeagle PL. *Laboratory Membrane Systems*. Membr. Cells, Elsevier; 2016, p. 95–114. <https://doi.org/10.1016/B978-0-12-800047-2.00006-1>.
- [51] Hijikata A, Yura K, Ohara O, Go M. Structural and functional analyses of Barth syndrome-causing mutations and alternative splicing in the tafazzin acyltransferase domain. *Meta Gene* 2015;4:92–106. <https://doi.org/10.1016/j.mgene.2015.04.001>.
- [52] Chung CT, Niemela SL, Miller RH. One-step preparation of competent *Escherichia coli*: transformation and storage of bacterial cells in the same solution. *Proc Natl Acad Sci* 1989;86:2172–5. <https://doi.org/10.1073/pnas.86.7.2172>.
- [53] Nweke CO, Ogbonna CJ. Statistical models for biphasic dose-response relationships (hormesis) in toxicological studies. *Ecotoxicol Environ Contam* 2017;12:39–55. <https://doi.org/10.5132/eec.2017.01.06>.

- [54] Sezonov G, Joseleau-Petit D, D'Ari R. Escherichia coli Physiology in Luria-Bertani Broth. *J Bacteriol* 2007;189:8746–9. <https://doi.org/10.1128/JB.01368-07>.
- [55] Gray WT, Govers SK, Xiang Y, Parry BR, Campos M, Kim S, et al. Nucleoid Size Scaling and Intracellular Organization of Translation across Bacteria. *Cell* 2019;177:1632-1648.e20. <https://doi.org/10.1016/j.cell.2019.05.017>.
- [56] Petrache HI, Dodd SW, Brown MF. Area per Lipid and Acyl Length Distributions in Fluid Phosphatidylcholines Determined by 2H NMR Spectroscopy. *Biophys J* 2000;79:3172–92. [https://doi.org/10.1016/S0006-3495\(00\)76551-9](https://doi.org/10.1016/S0006-3495(00)76551-9).
- [57] Laemmli UK. Cleavage of structural proteins during the assembly of the head of bacteriophage T4. *Nature* 1970;227:680–5. <https://doi.org/10.1038/227680a0>.
- [58] Parasassi T, De Stasio G, D'Ubaldo A, Gratton E. Phase fluctuation in phospholipid membranes revealed by Laurdan fluorescence. *Biophys J* 1990;57:1179–86. [https://doi.org/10.1016/S0006-3495\(90\)82637-0](https://doi.org/10.1016/S0006-3495(90)82637-0).
- [59] Fujita T, Winkler DA. Understanding the Roles of the “Two QSARs.” *J Chem Inf Model* 2016;56:269–74. <https://doi.org/10.1021/acs.jcim.5b00229>.
- [60] Ingram LO. Adaptation of membrane lipids to alcohols. *J Bacteriol* 1976;125:670–8. <https://doi.org/10.1128/jb.125.2.670-678.1976>.
- [61] Ingram LO, Vreeland NS. Differential effects of ethanol and hexanol on the Escherichia coli cell envelope. *J Bacteriol* 1980;144:481–8. <https://doi.org/10.1128/jb.144.2.481-488.1980>.
- [62] Gutknecht J, Tosteson DC. Ionic Permeability of Thin Lipid Membranes. *J Gen Physiol* 1970;55:359–74. <https://doi.org/10.1085/jgp.55.3.359>.
- [63] Silver S, Wendt L. Mechanism of Action of Phenethyl Alcohol: Breakdown of the Cellular Permeability Barrier. *J Bacteriol* 1967;93:560–6. <https://doi.org/10.1128/jb.93.2.560-566.1967>.
- [64] Zhu YJ, Zhou HT, Hu YH, Tang JY, Su MX, Guo YJ, et al. Antityrosinase and antimicrobial activities of 2-phenylethanol, 2-phenylacetaldehyde and 2-phenylacetic acid. *Food Chem* 2011;124:298–302. <https://doi.org/10.1016/j.foodchem.2010.06.036>.
- [65] Lilley BD, Brewer JH. The Selective Antibacterial Action of Phenylethyl Alcohol. *J Am Pharm Assoc (Scientific Ed)* 1953;42:6–8. <https://doi.org/10.1002/jps.3030420103>.
- [66] Anbazhagan V, Munz C, Tome L, Schneider D. Fluidizing the Membrane by a Local Anesthetic: Phenylethanol Affects Membrane Protein Oligomerization. *J Mol Biol* 2010;404:773–7. <https://doi.org/10.1016/j.jmb.2010.10.026>.
- [67] Stark D, Zala D, Münch T, Sonnleitner B, Marison IW, von Stockar U. Inhibition aspects of the bioconversion of l-phenylalanine to 2-phenylethanol by *Saccharomyces cerevisiae*. *Enzyme Microb Technol* 2003;32:212–23. [https://doi.org/10.1016/S0141-0229\(02\)00237-5](https://doi.org/10.1016/S0141-0229(02)00237-5).

- [68] Brossmer R, Bohn B, Schlicker H. Influence of 2-Phenylethanol and 1,1'-Dimethylphenylethanol on metabolic activity and cell membrane function in ehrlich ascites tumor cells 1973;35:191-4.
- [69] Prevost C, Moses V. Action of Phenethyl Alcohol on the Synthesis of Macromolecules in *Escherichia coli*. *J Bacteriol* 1966;91:1446-52. <https://doi.org/10.1128/jb.91.4.1446-1452.1966>.
- [70] Masker WE, Eberle H. Effect of Phenethyl Alcohol on Deoxyribonucleic Acid-Membrane Association in *Escherichia coli*. *J Bacteriol* 1972;109:1170-4. <https://doi.org/10.1128/jb.109.3.1170-1174.1972>.
- [71] Lucchini JJ, Bonnaveiro N, Cremieux A, Le Goffic F. Mechanism of bactericidal action of phenethyl alcohol in *Escherichia coli*. *Curr Microbiol* 1993;27:295-300. <https://doi.org/10.1007/BF01575995>.
- [72] Lovrien R, Hart G, Anderson KJ. Quantitative aspects of phenyl substituted alcohol and ether bacteriostatic interaction with *Escherichia coli* B/5. *Microbios* 1977;20:153-72.
- [73] Dieuleveux V, Lemarinier S, Guéguen M. Antimicrobial spectrum and target site of d-3-phenyllactic acid. *Int J Food Microbiol* 1998;40:177-83. [https://doi.org/10.1016/S0168-1605\(98\)00031-2](https://doi.org/10.1016/S0168-1605(98)00031-2).
- [74] Prema P, Smila D, Palavesam A, Immanuel G. Production and Characterization of an Antifungal Compound (3-Phenyllactic Acid) Produced by *Lactobacillus plantarum* Strain. *Food Bioprocess Technol* 2010;3:379-86. <https://doi.org/10.1007/s11947-008-0127-1>.
- [75] Lopez S, Bermudez B, Montserrat-de la Paz S, Jaramillo S, Varela LM, Ortega-Gomez A, et al. Membrane composition and dynamics: A target of bioactive virgin olive oil constituents. *Biochim Biophys Acta - Biomembr* 2014;1838:1638-56. <https://doi.org/10.1016/j.bbamem.2014.01.007>.
- [76] Sandler M, Ruthven CRJ, Goodwin BL, Lees A, Stern GM. Phenylacetic acid in human body fluids: high correlation between plasma and cerebrospinal fluid concentration values. *J Neurol Neurosurg Psychiatry* 1982;45:366-8. <https://doi.org/10.1136/jnnp.45.4.366>.
- [77] Sherwin C., Kennard K. Toxicity of phenylacetic acid. *J Inherit Metab Dis* 1919;40:259-.
- [78] Hudgins WR, Shack S, Myers CE, Samid D. Cytostatic activity of phenylacetate and derivatives against tumor cells. *Biochem Pharmacol* 1995;50:1273-9. [https://doi.org/10.1016/0006-2952\(95\)02013-3](https://doi.org/10.1016/0006-2952(95)02013-3).
- [79] Mu W, Yu S, Zhu L, Zhang T, Jiang B. Recent research on 3-phenyllactic acid, a broad-spectrum antimicrobial compound. *Appl Microbiol Biotechnol* 2012;95:1155-63. <https://doi.org/10.1007/s00253-012-4269-8>.
- [80] Dieuleveux V, Guéguen M. Antimicrobial Effects of d-3-Phenyllactic Acid on *Listeria monocytogenes* in TSB-YE Medium, Milk, and Cheese. *J Food Prot* 1998;61:1281-5. <https://doi.org/10.4315/0362-028X-61.10.1281>.

- [81] Mu W, Chen C, Li X, Zhang T, Jiang B. Optimization of culture medium for the production of phenyllactic acid by *Lactobacillus* sp. SK007. *Bioresour Technol* 2009;100:1366–70. <https://doi.org/10.1016/j.biortech.2008.08.010>.
- [82] Ning Y, Yan A, Yang K, Wang Z, Li X, Jia Y. Antibacterial activity of phenyllactic acid against *Listeria monocytogenes* and *Escherichia coli* by dual mechanisms. *Food Chem* 2017;228:533–40. <https://doi.org/10.1016/j.foodchem.2017.01.112>.
- [83] Hillenga DJ, Versantvoort H, van der Molen S, Driessen A, Konings WN. *Penicillium chrysogenum* Takes up the Penicillin G Precursor Phenylacetic Acid by Passive Diffusion. *Appl Environ Microbiol* 1995;61:2589–95. <https://doi.org/10.1128/aem.61.7.2589-2595.1995>.
- [84] Bittenbender WA., Degering EF. The effect of para-substituents on the bacteriostatic properties of phenylacetic acid. *J Am Pharm Assoc Am Pharm Assoc (Baltim)* 1972;28:514–9.
- [85] Giovannini C, Straface E, Modesti D, Coni E, Cantafora A, De Vincenzi M, et al. Tyrosol, the Major Olive Oil Biophenol, Protects Against Oxidized-LDL-Induced Injury in Caco-2 Cells. *J Nutr* 1999;129:1269–77. <https://doi.org/10.1093/jn/129.7.1269>.
- [86] Covas MI, Miró-Casas E, Fitó M, Farré-Albadalejo M, Gimeno E, Marrugat J, et al. Bioavailability of tyrosol, an antioxidant phenolic compound present in wine and olive oil, in humans. *Drugs Exp Clin Res* 2003;29:203–6.
- [87] Sardesai Y, Bhosle S. Tolerance of bacteria to organic solvents. *Res Microbiol* 2002;153:263–8. [https://doi.org/10.1016/S0923-2508\(02\)01319-0](https://doi.org/10.1016/S0923-2508(02)01319-0).
- [88] Bhal S. Log P – Making Sense of the Value. *Adv Chem Dev* 2007:1–4.
- [89] Paiva-Martins F, Gordon MH, Gameiro P. Activity and location of olive oil phenolic antioxidants in liposomes. *Chem Phys Lipids* 2003;124:23–36. [https://doi.org/10.1016/S0009-3084\(03\)00032-X](https://doi.org/10.1016/S0009-3084(03)00032-X).
- [90] Parasassi T, De Stasio G, Ravagnan G, Rusch RM, Gratton E. Quantitation of lipid phases in phospholipid vesicles by the generalized polarization of Laurdan fluorescence. *Biophys J* 1991;60:179–89. [https://doi.org/10.1016/S0006-3495\(91\)82041-0](https://doi.org/10.1016/S0006-3495(91)82041-0).
- [91] Parasassi T, Di Stefano M, Loiero M, Ravagnan G, Gratton E. Influence of cholesterol on phospholipid bilayers phase domains as detected by Laurdan fluorescence. *Biophys J* 1994;66:120–32. [https://doi.org/10.1016/S0006-3495\(94\)80763-5](https://doi.org/10.1016/S0006-3495(94)80763-5).
- [92] Levison ME, Levison JH. Pharmacokinetics and Pharmacodynamics of Antibacterial Agents. *Infect Dis Clin North Am* 2009;23:791–815. <https://doi.org/10.1016/j.idc.2009.06.008>.
- [93] Harayama T, Riezman H. Understanding the diversity of membrane lipid composition. *Nat Rev Mol Cell Biol* 2018;19:281–96. <https://doi.org/10.1038/nrm.2017.138>.
- [94] van Meer G, Voelker DR, Feigenson GW. Membrane lipids: where they are and how they behave. *Nat Rev Mol Cell Biol* 2008;9:112–24. <https://doi.org/10.1038/nrm2330>.

- [95] Moellering ER, Benning C. Galactoglycerolipid metabolism under stress: a time for remodeling. *Trends Plant Sci* 2011;16:98–107. <https://doi.org/10.1016/j.tplants.2010.11.004>.
- [96] Pangborn MC. Isolation and Purification of a Serologically Active Phospholipid from Beef Heart. *J Biol Chem* 1942;143:247–56. [https://doi.org/10.1016/S0021-9258\(18\)72683-5](https://doi.org/10.1016/S0021-9258(18)72683-5).
- [97] Dudek J. Role of Cardiolipin in Mitochondrial Signaling Pathways. *Front Cell Dev Biol* 2017;5:1–17. <https://doi.org/10.3389/fcell.2017.00090>.
- [98] Schlame M, Ren M, Xu Y, Greenberg ML, Haller I. Molecular symmetry in mitochondrial cardiolipins. *Chem Phys Lipids* 2005;138:38–49. <https://doi.org/10.1016/j.chemphyslip.2005.08.002>.
- [99] Stefanyk LE., Coverdale N, Roy BD., Peters SJ., LeBlanc PJ. Skeletal Muscle Type Comparison of Subsarcolemmal Mitochondrial Membrane Phospholipid Fatty Acid Composition in Rat. *J Membr Biol* 2010;234:207–15. <https://doi.org/10.1007/s00232-010-9247-4>.
- [100] de Kroon AIP., Dolis D, Mayer A, Lill R, de Kruijff B. Phospholipid composition of highly purified mitochondrial outer membranes of rat liver and *Neurospora crassa*. Is cardiolipin present in the mitochondrial outer membrane? *Biochim Biophys Acta - Biomembr* 1997;1325:108–16. [https://doi.org/10.1016/S0005-2736\(96\)00240-4](https://doi.org/10.1016/S0005-2736(96)00240-4).
- [101] Hallermayer G, Neupert W. Lipid Composition of Mitochondrial Outer and Inner Membranes of *Neurospora crassa*. *Biol Chem* 1974;355:279–88. <https://doi.org/10.1515/bchm2.1974.355.1.279>.
- [102] Kushwaha SC, Kates M, Kramer JKG, Subden RE. Lipid composition of *Neurospora crassa*. *Lipids* 1976;11:778–80. <https://doi.org/10.1007/BF02533055>.
- [103] Gryz, Perlińska-Lenart, Gawarecka, Jozwiak, Piłsyk, Lipko, et al. Poly-Saturated Dolichols from Filamentous Fungi Modulate Activity of Dolichol-Dependent Glycosyltransferase and Physical Properties of Membranes. *Int J Mol Sci* 2019;20:3043. <https://doi.org/10.3390/ijms20123043>.
- [104] Löser T, Joppe A, Hamann A, Osiewacz HD. Mitochondrial Phospholipid Homeostasis Is Regulated by the i-AAA Protease PaIAP and Affects Organismic Aging. *Cells* 2021;10:2775. <https://doi.org/10.3390/cells10102775>.
- [105] LeCocq J, Ballou CE. On the Structure of Cardiolipin \*. *Biochemistry* 1964;3:976–80. <https://doi.org/10.1021/bi00895a023>.
- [106] Kraffe E, Soudant P, Marty Y, Kervarec N, Jehan P. Evidence of a tetradocosahexaenoic cardiolipin in some marine bivalves. *Lipids* 2002;37:507–14. <https://doi.org/10.1007/s11745-002-0925-z>.
- [107] Oliver PM, Crooks JA, Leidl M, Yoon EJ, Saghatelian A, Weibel DB. Localization of Anionic Phospholipids in *Escherichia coli* Cells. *J Bacteriol* 2014;196:3386–98. <https://doi.org/10.1128/JB.01877-14>.

- [108] Huang KC, Mukhopadhyay R, Wingreen NS. A Curvature-Mediated Mechanism for Localization of Lipids to Bacterial Poles. *PLoS Comput Biol* 2006;2:e151. <https://doi.org/10.1371/journal.pcbi.0020151>.
- [109] Chicco AJ, Sparagna GC. Role of cardiolipin alterations in mitochondrial dysfunction and disease. *Am J Physiol Physiol* 2007;292:C33–44. <https://doi.org/10.1152/ajpcell.00243.2006>.
- [110] Beleznai Z, Jancsik V. Role of cardiolipin in the functioning of mitochondrial L-glycerol-3-phosphate dehydrogenase. *Biochem Biophys Res Commun* 1989;159:132–9. [https://doi.org/10.1016/0006-291X\(89\)92414-5](https://doi.org/10.1016/0006-291X(89)92414-5).
- [111] Bisaccia F, Palmieri F. Specific elution from hydroxylapatite of the mitochondrial phosphate carrier by cardiolipin. *Biochim Biophys Acta - Bioenerg* 1984;766:386–94. [https://doi.org/10.1016/0005-2728\(84\)90254-8](https://doi.org/10.1016/0005-2728(84)90254-8).
- [112] Müller M, Moser R, Cheneval D, Carafoli E. Cardiolipin is the membrane receptor for mitochondrial creatine phosphokinase. *J Biol Chem* 1985;260:3839–43. [https://doi.org/10.1016/S0021-9258\(19\)83700-6](https://doi.org/10.1016/S0021-9258(19)83700-6).
- [113] Kagan VE, Tyurina YY, Bayir H, Chu CT, Kapralov AA, Vlasova II, et al. The “pro-apoptotic genes” get out of mitochondria: Oxidative lipidomics and redox activity of cytochrome c/cardiolipin complexes. *Chem Biol Interact* 2006;163:15–28. <https://doi.org/10.1016/j.cbi.2006.04.019>.
- [114] Gonzalez F, Gottlieb E. Cardiolipin: Setting the beat of apoptosis. *Apoptosis* 2007;12:877–85. <https://doi.org/10.1007/s10495-007-0718-8>.
- [115] Wilson BA, Ramanathan A, Lopez CF. Cardiolipin-Dependent Properties of Model Mitochondrial Membranes from Molecular Simulations. *Biophys J* 2019;117:429–44. <https://doi.org/10.1016/j.bpj.2019.06.023>.
- [116] Zhang T, Muraih JK, Tishbi N, Herskowitz J, Victor RL, Silverman J, et al. Cardiolipin Prevents Membrane Translocation and Permeabilization by Daptomycin. *J Biol Chem* 2014;289:11584–91. <https://doi.org/10.1074/jbc.M114.554444>.
- [117] Leung CWT, Hong Y, Hanske J, Zhao E, Chen S, Pletneva E V., et al. Superior Fluorescent Probe for Detection of Cardiolipin. *Anal Chem* 2014;86:1263–8. <https://doi.org/10.1021/ac403616c>.
- [118] Pyshev K, Yesylevskyy S, Bogdanov M. TTape-Me dye is not selective to cardiolipin and binds to common anionic phospholipids nonspecifically. *Biophys J* 2021;120:3776–86. <https://doi.org/10.1016/j.bpj.2021.06.039>.
- [119] Maftah A, Petit JM, Julien R. Specific interaction of the new fluorescent dye 10-N-nonyl acridine orange with inner mitochondrial membrane. *FEBS Lett* 1990;260:236–40. [https://doi.org/10.1016/0014-5793\(90\)80112-V](https://doi.org/10.1016/0014-5793(90)80112-V).
- [120] Maftah A, Petit JM, Ratinaud M-H, Julien R. 10-N Nonyl-Acridine Orange: A fluorescent probe which stains mitochondria independently of their energetic state. *Biochem Biophys Res Commun* 1989;164:185–90. [https://doi.org/10.1016/0006-291X\(89\)91700-2](https://doi.org/10.1016/0006-291X(89)91700-2).

- [121] Septinus M, Berthold T, Naujok A, Zimmermann HW. Über hydrophobe Acridinfarbstoffe zur Fluorochromierung von Mitochondrien in lebenden Zellen. *Histochemistry* 1985;82:51–66. <https://doi.org/10.1007/BF00502091>.
- [122] Ratinaud MH, Leprat P, Julien R. In situ flow cytometric analysis of nonyl acridine orange-stained mitochondria from splenocytes. *Cytometry* 1988;9:206–12. <https://doi.org/10.1002/cyto.990090304>.
- [123] Petit J-M, Maftah A, Ratinaud M-H, Julien R. 10N-Nonyl acridine orange interacts with cardiolipin and allows the quantification of this phospholipid in isolated mitochondria. *Eur J Biochem* 1992;209:267–73. <https://doi.org/10.1111/j.1432-1033.1992.tb17285.x>.
- [124] Gallet PF, Maftah A, Petit J -M, Denis-Gay M, Julien R. Direct Cardiolipin Assay in Yeast Using the Red Fluorescence Emission of 10-N-Nonyl Acridine Orange. *Eur J Biochem* 1995;228:113–9. <https://doi.org/10.1111/j.1432-1033.1995.tb20238.x>.
- [125] Gohil VM, Gvozdencovic-Jeremic J, Schlame M, Greenberg ML. Binding of 10-N-nonyl acridine orange to cardiolipin-deficient yeast cells: Implications for assay of cardiolipin. *Anal Biochem* 2005;343:350–2. <https://doi.org/10.1016/j.ab.2005.04.039>.
- [126] Wang X, Guan Y. COVID-19 drug repurposing: A review of computational screening methods, clinical trials, and protein interaction assays. *Med Res Rev* 2021;41:5–28. <https://doi.org/10.1002/med.21728>.
- [127] Tahir ul Qamar M, Maryam A, Muneer I, Xing F, Ashfaq UA, Khan FA, et al. Computational screening of medicinal plant phytochemicals to discover potent pan-serotype inhibitors against dengue virus. *Sci Rep* 2019;9:1433. <https://doi.org/10.1038/s41598-018-38450-1>.
- [128] Rastelli G, Pellati F, Pinzi L, Gamberini MC. Repositioning Natural Products in Drug Discovery. *Molecules* 2020;25:1154. <https://doi.org/10.3390/molecules25051154>.
- [129] Gupta S, Parihar D, Shah M, Yadav S, Managori H, Bhowmick S, et al. Computational screening of promising beta-secretase 1 inhibitors through multi-step molecular docking and molecular dynamics simulations - Pharmacoinformatics approach. *J Mol Struct* 2020;1205:127660. <https://doi.org/10.1016/j.molstruc.2019.127660>.
- [130] Lee VS, Chong WL, Sukumaran SD, Nimmanpipug P, Letchumanan V, Goh BH, et al. Computational screening and identifying binding interaction of anti-viral and anti-malarial drugs: Toward the potential cure for SARS-CoV-2. *Prog Drug Discov Biomed Sci* 2020;3:1–9. <https://doi.org/10.36877/pddbs.a0000065>.
- [131] Panman W, Nutho B, Chamni S, Dokmaisrijan S, Kungwan N, Rungrotmongkol T. Computational screening of fatty acid synthase inhibitors against thioesterase domain. *J Biomol Struct Dyn* 2018;36:4114–25. <https://doi.org/10.1080/07391102.2017.1408496>.
- [132] Bereau T, Andrienko D, Kremer K. Research Update: Computational materials discovery in soft matter. *APL Mater* 2016;4:053101. <https://doi.org/10.1063/1.4943287>.



- [133] López Barreiro D, Minten IJ, Thies JC, Sagt CMJ. Structure–Property Relationships of Elastin-like Polypeptides: A Review of Experimental and Computational Studies. *ACS Biomater Sci Eng* 2021:acsbiomaterials.1c00145. <https://doi.org/10.1021/acsbiomaterials.1c00145>.
- [134] Poater A, Saliner AG, Solà M, Cavallo L, Worth AP. Computational methods to predict the reactivity of nanoparticles through structure–property relationships. *Expert Opin Drug Deliv* 2010;7:295–305. <https://doi.org/10.1517/17425240903508756>.
- [135] Durrant JD, McCammon JA. Molecular dynamics simulations and drug discovery. *BMC Biol* 2011;9:71. <https://doi.org/10.1186/1741-7007-9-71>.
- [136] Salo-Ahen OMH, Alanko I, Bhadane R, Bonvin AMJJ, Honorato RV, Hossain S, et al. Molecular Dynamics Simulations in Drug Discovery and Pharmaceutical Development. *Processes* 2020;9:71. <https://doi.org/10.3390/pr9010071>.
- [137] Veljkovic N, Glisic S, Perovic V, Veljkovic V. The role of long-range intermolecular interactions in discovery of new drugs. *Expert Opin Drug Discov* 2011;6:1263–70. <https://doi.org/10.1517/17460441.2012.638280>.
- [138] Naqvi AAT, Mohammad T, Hasan GM, Hassan MI. Advancements in Docking and Molecular Dynamics Simulations Towards Ligand-receptor Interactions and Structure-function Relationships. *Curr Top Med Chem* 2018;18:1755–68. <https://doi.org/10.2174/1568026618666181025114157>.
- [139] Hu J-P, Wu Z-X, Xie T, Liu X-Y, Yan X, Sun X, et al. Applications of Molecular Simulation in the Discovery of Antituberculosis Drugs: A Review. *Protein Pept Lett* 2019;26:648–63. <https://doi.org/10.2174/0929866526666190620145919>.
- [140] Kanekal KH, Bereau T. Resolution limit of data-driven coarse-grained models spanning chemical space. *J Chem Phys* 2019;151:164106. <https://doi.org/10.1063/1.5119101>.
- [141] Giulini M, Menichetti R, Shell MS, Potestio R. An Information-Theory-Based Approach for Optimal Model Reduction of Biomolecules. *J Chem Theory Comput* 2020;16:6795–813. <https://doi.org/10.1021/acs.jctc.0c00676>.
- [142] Hoffmann C, Menichetti R, Kanekal KH, Bereau T. Controlled exploration of chemical space by machine learning of coarse-grained representations. *Phys Rev E* 2019;100:033302. <https://doi.org/10.1103/PhysRevE.100.033302>.
- [143] Menichetti R, Kanekal KH, Bereau T. Drug–Membrane Permeability across Chemical Space. *ACS Cent Sci* 2019;5:290–8. <https://doi.org/10.1021/acscentsci.8b00718>.
- [144] Menichetti R, Kanekal KH, Kremer K, Bereau T. In silico screening of drug-membrane thermodynamics reveals linear relations between bulk partitioning and the potential of mean force. *J Chem Phys* 2017;147:125101. <https://doi.org/10.1063/1.4987012>.
- [145] Mohr B, Shmilovich K, Kleinwächter I, Schneider D, Ferguson AL, Bereau T. Data-driven discovery of cardiolipin-selective smallmolecules by computational active learning 2021.

- [146] Mileykovskaya E, Dowhan W, Birke RL, Zheng D, Lutterodt L, Haines TH. Cardiolipin binds nonyl acridine orange by aggregating the dye at exposed hydrophobic domains on bilayer surfaces. *FEBS Lett* 2001;507:187–90. [https://doi.org/10.1016/S0014-5793\(01\)02948-9](https://doi.org/10.1016/S0014-5793(01)02948-9).
- [147] Kiss R, Sandor M, Szalai FA. <http://McuLe.com>: a public web service for drug discovery. *J Cheminform* 2012;4:P17. <https://doi.org/10.1186/1758-2946-4-S1-P17>.
- [148] Tanimoto TT. An elementary mathematical theory of classification and prediction. International Business Machines Corp; 1985.
- [149] Jaccard P. The Distribution of the Flora in the Alpine Zone. *New Phytol* 1912;11:37–50. <https://doi.org/10.1111/j.1469-8137.1912.tb05611.x>.
- [150] Nekoei A-R, Vatanparast M.  $\pi$ -Hydrogen bonding and aromaticity: a systematic interplay study. *Phys Chem Chem Phys* 2019;21:623–30. <https://doi.org/10.1039/C8CP07003B>.
- [151] Landrum G. RDKit: A software suite for cheminformatics, computational chemistry, and predictive modeling n.d. [https://www.rdkit.org/rdkit\\_overview.pdf](https://www.rdkit.org/rdkit_overview.pdf) (accessed July 14, 2021).
- [152] Kleinwächter IS, Pannwitt S, Centi A, Hellmann N, Thines E, Bereau T, et al. The Bacteriostatic Activity of 2-Phenylethanol Derivatives Correlates with Membrane Binding Affinity. *Membranes (Basel)* 2021;11:254. <https://doi.org/10.3390/membranes11040254>.
- [153] Seelig J. Thermodynamics of lipid–peptide interactions. *Biochim Biophys Acta - Biomembr* 2004;1666:40–50. <https://doi.org/10.1016/j.bbamem.2004.08.004>.
- [154] Gredilla R, Grief J, Osiewacz HD. Mitochondrial free radical generation and lifespan control in the fungal aging model *Podospora anserina*. *Exp Gerontol* 2006;41:439–47. <https://doi.org/10.1016/j.exger.2006.01.010>.
- [155] Westermann B. Mitochondrial dynamics in model organisms: What yeasts, worms and flies have taught us about fusion and fission of mitochondria. *Semin Cell Dev Biol* 2010;21:542–9. <https://doi.org/10.1016/j.semcdb.2009.12.003>.
- [156] Youle RJ, van der Bliek AM. Mitochondrial Fission, Fusion, and Stress. *Science (80- )* 2012;337:1062–5. <https://doi.org/10.1126/science.1219855>.
- [157] Bustillo-Zabalbeitia I, Montessuit S, Raemy E, Basañez G, Terrones O, Martinou J-C. Specific Interaction with Cardiolipin Triggers Functional Activation of Dynamin-Related Protein 1. *PLoS One* 2014;9:e102738. <https://doi.org/10.1371/journal.pone.0102738>.
- [158] Daumke O, Praefcke GJK. Invited review: Mechanisms of GTP hydrolysis and conformational transitions in the dynamin superfamily. *Biopolymers* 2016;105:580–93. <https://doi.org/10.1002/bip.22855>.
- [159] Praefcke GJK, McMahon HT. The dynamin superfamily: universal membrane tubulation and fission molecules? *Nat Rev Mol Cell Biol* 2004;5:133–47. <https://doi.org/10.1038/nrm1313>.

- [160] Francy CA, Clinton RW, Fröhlich C, Murphy C, Mears JA. Cryo-EM Studies of Drp1 Reveal Cardiolipin Interactions that Activate the Helical Oligomer. *Sci Rep* 2017;7:10744. <https://doi.org/10.1038/s41598-017-11008-3>.
- [161] Frank S, Gaume B, Bergmann-Leitner ES, Leitner WW, Robert EG, Catez F, et al. The Role of Dynamin-Related Protein 1, a Mediator of Mitochondrial Fission, in Apoptosis. *Dev Cell* 2001;1:515–25. [https://doi.org/10.1016/S1534-5807\(01\)00055-7](https://doi.org/10.1016/S1534-5807(01)00055-7).
- [162] Macdonald PJ, Stepanyants N, Mehrotra N, Mears JA, Qi X, Sesaki H, et al. A dimeric equilibrium intermediate nucleates Drp1 reassembly on mitochondrial membranes for fission. *Mol Biol Cell* 2014;25:1905–15. <https://doi.org/10.1091/mbc.e14-02-0728>.
- [163] Pitts KR, McNiven MA, Yoon Y. Mitochondria-specific Function of the Dynamin Family Protein DLP1 Is Mediated by Its C-terminal Domains. *J Biol Chem* 2004;279:50286–94. <https://doi.org/10.1074/jbc.M405531200>.
- [164] Kalia R, Wang RY-R, Yusuf A, Thomas P V., Agard DA, Shaw JM, et al. Structural basis of mitochondrial receptor binding and constriction by DRP1. *Nature* 2018;558:401–5. <https://doi.org/10.1038/s41586-018-0211-2>.
- [165] Fröhlich C, Grabiger S, Schwefel D, Faelber K, Rosenbaum E, Mears J, et al. Structural insights into oligomerization and mitochondrial remodelling of dynamin 1-like protein. *EMBO J* 2013;32:1280–92. <https://doi.org/10.1038/emboj.2013.74>.
- [166] Kaewsuya P, Danielson ND, Ekhterae D. Fluorescent determination of cardiolipin using 10-N-nonyl acridine orange. *Anal Bioanal Chem* 2007;387:2775–82. <https://doi.org/10.1007/s00216-007-1135-0>.
- [167] Osman C, Voelker DR, Langer T. Making heads or tails of phospholipids in mitochondria. *J Cell Biol* 2011;192:7–16. <https://doi.org/10.1083/jcb.201006159>.
- [168] Sakihara T, Takiguchi N, Uzawa H, Serizawa R, Kobayashi T. Erylysin A inhibits cytokinesis in *Escherichia coli* by binding with cardiolipin. *J Biochem* 2021;170:369–77. <https://doi.org/10.1093/jb/mvab052>.
- [169] Scheu K, Gill R, Saberi S, Meyer P, Emberly E. Localization of aggregating proteins in bacteria depends on the rate of addition. *Front Microbiol* 2014;5:1–5. <https://doi.org/10.3389/fmicb.2014.00418>.
- [170] Cho B, Choi SY, Cho HM, Kim HJ, Sun W. Physiological and Pathological Significance of Dynamin-Related Protein 1 (Drp1)-Dependent Mitochondrial Fission in the Nervous System. *Exp Neurobiol* 2013;22:149–57. <https://doi.org/10.5607/en.2013.22.3.149>.
- [171] Barák I, Muchová K. The role of lipid domains in bacterial cell processes. *Int J Mol Sci* 2013;14:4050–65. <https://doi.org/10.3390/ijms14024050>.
- [172] Claypool SM, Whited K, Srijumngong S, Han X, Koehler CM. Barth syndrome mutations that cause tafazzin complex lability. *J Cell Biol* 2011;192:447–62. <https://doi.org/10.1083/jcb.201008177>.

- [173] Barth PG, Scholte HR, Berden JA, Van Der Klei-Van Moorsel JM, Luyt-Houwen IEM, Van'T Veer-Korthof ET, et al. An X-linked mitochondrial disease affecting cardiac muscle, skeletal muscle and neutrophil leucocytes. *J Neurol Sci* 1983;62:327–55. [https://doi.org/10.1016/0022-510X\(83\)90209-5](https://doi.org/10.1016/0022-510X(83)90209-5).
- [174] Claypool SM, McCaffery JM, Koehler CM. Mitochondrial mislocalization and altered assembly of a cluster of Barth syndrome mutant tafazzins. *J Cell Biol* 2006;174:379–90. <https://doi.org/10.1083/jcb.200605043>.
- [175] Houtkooper RH, Turkenburg M, Poll-The BT, Karall D, Pérez-Cerdá C, Morrone A, et al. The enigmatic role of tafazzin in cardiolipin metabolism. *Biochim Biophys Acta - Biomembr* 2009;1788:2003–14. <https://doi.org/10.1016/j.bbamem.2009.07.009>.
- [176] Valianpour F, Mitsakos V, Schlemmer D, Towbin JA, Taylor JM, Ekert PG, et al. Monolysocardiolipins accumulate in Barth syndrome but do not lead to enhanced apoptosis. *J Lipid Res* 2005;46:1182–95. <https://doi.org/10.1194/jlr.M500056-JLR200>.
- [177] Chang S-C, Heacock PN, Clancey CJ, Dowhan W. The PEL1 Gene (Renamed PGS1) Encodes the Phosphatidylglycero-phosphate Synthase of *Saccharomyces cerevisiae*. *J Biol Chem* 1998;273:9829–36. <https://doi.org/10.1074/jbc.273.16.9829>.
- [178] Zhang J, Guan Z, Murphy AN, Wiley SE, Perkins GA, Worby CA, et al. Mitochondrial Phosphatase PTPMT1 Is Essential for Cardiolipin Biosynthesis. *Cell Metab* 2011;13:690–700. <https://doi.org/10.1016/j.cmet.2011.04.007>.
- [179] Schlame M, Haldar D. Cardiolipin is synthesized on the matrix side of the inner membrane in rat liver mitochondria. *J Biol Chem* 1993;268:74–9. [https://doi.org/10.1016/S0021-9258\(18\)54116-8](https://doi.org/10.1016/S0021-9258(18)54116-8).
- [180] Schlame M, Ren M. Barth syndrome, a human disorder of cardiolipin metabolism. *FEBS Lett* 2006;580:5450–5. <https://doi.org/10.1016/j.febslet.2006.07.022>.
- [181] Claypool SM, Koehler CM. The complexity of cardiolipin in health and disease. *Trends Biochem Sci* 2012;37:32–41. <https://doi.org/10.1016/j.tibs.2011.09.003>.
- [182] Gonzalez F, D'Aurelio M, Boutant M, Moustapha A, Puech J-P, Landes T, et al. Barth syndrome: Cellular compensation of mitochondrial dysfunction and apoptosis inhibition due to changes in cardiolipin remodeling linked to tafazzin (TAZ) gene mutation. *Biochim Biophys Acta - Mol Basis Dis* 2013;1832:1194–206. <https://doi.org/10.1016/j.bbadis.2013.03.005>.
- [183] Xu Y, Malhotra A, Ren M, Schlame M. The Enzymatic Function of Tafazzin. *J Biol Chem* 2006;281:39217–24. <https://doi.org/10.1074/jbc.M606100200>.
- [184] Xu Y, Kelley RI, Blanck TJJ, Schlame M. Remodeling of Cardiolipin by Phospholipid Transacylation. *J Biol Chem* 2003;278:51380–5. <https://doi.org/10.1074/jbc.M307382200>.
- [185] Brandner K, Mick DU., Frazier AE., Taylor RD., Meisinger C, Rehling P. Taz1, an Outer Mitochondrial Membrane Protein, Affects Stability and Assembly of Inner Membrane Protein Complexes: Implications for Barth Syndrome. *Mol Biol Cell*

- 2005;16:5202–14. <https://doi.org/10.1091/mbc.E05-03-0256>.
- [186] Gebert N, Joshi AS, Kutik S, Becker T, McKenzie M, Guan XL, et al. Mitochondrial Cardiolipin Involved in Outer-Membrane Protein Biogenesis: Implications for Barth Syndrome. *Curr Biol* 2009;19:2133–9. <https://doi.org/10.1016/j.cub.2009.10.074>.
- [187] Xu Y, Malhotra A, Claypool SM, Ren M, Schlame M. Tafazzins from *Drosophila* and mammalian cells assemble in large protein complexes with a short half-life. *Mitochondrion* 2015;21:27–32. <https://doi.org/10.1016/j.mito.2015.01.002>.
- [188] Guex N, Peitsch MC., Schwede T. Automated comparative protein structure modeling with SWISS-MODEL and Swiss-PdbViewer: A historical perspective. *Electrophoresis* 2009;30:S162–73. <https://doi.org/10.1002/elps.200900140>.
- [189] Waterhouse A, Bertoni M, Bienert S, Studer G, Tauriello G, Gumienny R, et al. SWISS-MODEL: homology modelling of protein structures and complexes. *Nucleic Acids Res* 2018;46:W296–303. <https://doi.org/10.1093/nar/gky427>.
- [190] Bienert S, Waterhouse A, de Beer TAP, Tauriello G, Studer G, Bordoli L, et al. The SWISS-MODEL Repository—new features and functionality. *Nucleic Acids Res* 2017;45:D313–9. <https://doi.org/10.1093/nar/gkw1132>.
- [191] le Maire M, Champeil P, Møller J V. Interaction of membrane proteins and lipids with solubilizing detergents. *Biochim Biophys Acta - Biomembr* 2000;1508:86–111. [https://doi.org/10.1016/S0304-4157\(00\)00010-1](https://doi.org/10.1016/S0304-4157(00)00010-1).
- [192] Centi A, Dutta A, Parekh SH, Bereau T. Inserting Small Molecules across Membrane Mixtures: Insight from the Potential of Mean Force. *Biophys J* 2020;118:1321–32. <https://doi.org/10.1016/j.bpj.2020.01.039>.
- [193] Hoffmann C, Centi A, Menichetti R, Bereau T. Molecular dynamics trajectories for 630 coarse-grained drug-membrane permeations. *Sci Data* 2020;7:51. <https://doi.org/10.1038/s41597-020-0391-0>.
- [194] Hess B, Kutzner C, van der Spoel D, Lindahl E. GROMACS 4: Algorithms for Highly Efficient, Load-Balanced, and Scalable Molecular Simulation. *J Chem Theory Comput* 2008;4:435–47. <https://doi.org/10.1021/ct700301q>.
- [195] de Jong DH, Singh G, Bennett WFD, Arnarez C, Wassenaar TA, Schäfer L V., et al. Improved Parameters for the Martini Coarse-Grained Protein Force Field. *J Chem Theory Comput* 2013;9:687–97. <https://doi.org/10.1021/ct300646g>.
- [196] Bereau T, Kremer K. Automated Parametrization of the Coarse-Grained Martini Force Field for Small Organic Molecules. *J Chem Theory Comput* 2015;11:2783–91. <https://doi.org/10.1021/acs.jctc.5b00056>.
- [197] Marrink SJ, Risselada HJ, Yefimov S, Tieleman DP, de Vries AH. The MARTINI Force Field: Coarse Grained Model for Biomolecular Simulations. *J Phys Chem B* 2007;111:7812–24. <https://doi.org/10.1021/jp071097f>.
- [198] Marrink Lab Univ. of Groningen. Martini: General Purpose Coarse-Grained Force Field 2021. <http://cgmartini.nl> (accessed July 14, 2021).
- [199] Periolo X, Marrink S-J. The Martini Coarse-Grained Force Field. *Methods Mol. Biol.*, 2013, p. 533–65. [https://doi.org/10.1007/978-1-62703-017-5\\_20](https://doi.org/10.1007/978-1-62703-017-5_20).



- [200] Dahlberg M, Maliniak A. Molecular Dynamics Simulations of Cardiolipin Bilayers. *J Phys Chem B* 2008;112:11655–63. <https://doi.org/10.1021/jp803414g>.
- [201] Olofsson G, Sparr E. Ionization Constants pKa of Cardiolipin. *PLoS One* 2013;8:e73040. <https://doi.org/10.1371/journal.pone.0073040>.
- [202] Sathappa M, Alder NN. The ionization properties of cardiolipin and its variants in model bilayers. *Biochim Biophys Acta - Biomembr* 2016;1858:1362–72. <https://doi.org/10.1016/j.bbamem.2016.03.007>.
- [203] Serpas L, Milorey B, Pandiscia LA, Addison AW, Schweitzer-Stenner R. Autoxidation of Reduced Horse Heart Cytochrome c Catalyzed by Cardiolipin-Containing Membranes. *J Phys Chem B* 2016;120:12219–31. <https://doi.org/10.1021/acs.jpcc.6b05620>.
- [204] Jo S, Cheng X, Lee J, Kim S, Park S, Patel DS, et al. CHARMM-GUI 10 years for biomolecular modeling and simulation. *J Comput Chem* 2017;38:1114–24. <https://doi.org/10.1002/jcc.24660>.
- [205] Yesylevskyy SO, Schäfer L V., Sengupta D, Marrink SJ. Polarizable Water Model for the Coarse-Grained MARTINI Force Field. *PLoS Comput Biol* 2010;6:e1000810. <https://doi.org/10.1371/journal.pcbi.1000810>.
- [206] Abraham MJ, Murtola T, Schulz R, Páll S, Smith JC, Hess B, et al. GROMACS: High performance molecular simulations through multi-level parallelism from laptops to supercomputers. *SoftwareX* 2015;1–2:19–25. <https://doi.org/10.1016/j.softx.2015.06.001>.
- [207] Bussi G, Donadio D, Parrinello M. Canonical sampling through velocity rescaling. *J Chem Phys* 2007;126:014101. <https://doi.org/10.1063/1.2408420>.
- [208] Parrinello M, Rahman A. Polymorphic transitions in single crystals: A new molecular dynamics method. *J Appl Phys* 1981;52:7182–90. <https://doi.org/10.1063/1.328693>.
- [209] Darden T, York D, Pedersen L. Particle mesh Ewald: An  $N \cdot \log(N)$  method for Ewald sums in large systems. *J Chem Phys* 1993;98:10089–92. <https://doi.org/10.1063/1.464397>.
- [210] de Jong DH, Baoukina S, Ingólfsson HI, Marrink SJ. Martini straight: Boosting performance using a shorter cutoff and GPUs. *Comput Phys Commun* 2016;199:1–7. <https://doi.org/10.1016/j.cpc.2015.09.014>.
- [211] Shirts MR, Mobley DL, Chodera JD. Chapter 4 Alchemical Free Energy Calculations: Ready for Prime Time? *Annu. Rep. Comput. Chem.*, vol. 3, 2007, p. 41–59. [https://doi.org/10.1016/S1574-1400\(07\)03004-6](https://doi.org/10.1016/S1574-1400(07)03004-6).
- [212] Straatsma TP. Free Energy by Molecular Simulation, 2007, p. 81–127. <https://doi.org/10.1002/9780470125861.ch2>.
- [213] Kollman P. Free energy calculations: Applications to chemical and biochemical phenomena. *Chem Rev* 1993;93:2395–417. <https://doi.org/10.1021/cr00023a004>.

- [214] Chen W, Deng Y, Russell E, Wu Y, Abel R, Wang L. Accurate Calculation of Relative Binding Free Energies between Ligands with Different Net Charges. *J Chem Theory Comput* 2018;14:6346–58. <https://doi.org/10.1021/acs.jctc.8b00825>.
- [215] Pohorille A, Jarzynski C, Chipot C. Good Practices in Free-Energy Calculations. *J Phys Chem B* 2010;114:10235–53. <https://doi.org/10.1021/jp102971x>.
- [216] Klimovich P V., Shirts MR, Mobley DL. Guidelines for the analysis of free energy calculations. *J Comput Aided Mol Des* 2015;29:397–411. <https://doi.org/10.1007/s10822-015-9840-9>.
- [217] Shirts MR, Chodera JD. Statistically optimal analysis of samples from multiple equilibrium states. *J Chem Phys* 2008;129:124105. <https://doi.org/10.1063/1.2978177>.
- [218] Torrie GM, Valleau J. Nonphysical sampling distributions in Monte Carlo free-energy estimation: Umbrella sampling. *J Comput Phys* 1977;23:187–99. [https://doi.org/10.1016/0021-9991\(77\)90121-8](https://doi.org/10.1016/0021-9991(77)90121-8).
- [219] Kästner J. Umbrella sampling. *Wiley Interdiscip Rev Comput Mol Sci* 2011;1:932–42. <https://doi.org/10.1002/wcms.66>.
- [220] Kumar S, Rosenberg JM, Bouzida D, Swendsen RH, Kollman PA. THE weighted histogram analysis method for free-energy calculations on biomolecules. I. The method. *J Comput Chem* 1992;13:1011–21. <https://doi.org/10.1002/jcc.540130812>.
- [221] Berau T, Swendsen RH. Optimized convergence for multiple histogram analysis. *J Comput Phys* 2009;228:6119–29. <https://doi.org/10.1016/j.jcp.2009.05.011>.
- [222] Hub JS, de Groot BL, van der Spoel D. g\_wham—A Free Weighted Histogram Analysis Implementation Including Robust Error and Autocorrelation Estimates. *J Chem Theory Comput* 2010;6:3713–20. <https://doi.org/10.1021/ct100494z>.
- [223] Liao TF, Mooney CZ, Duval RD, Eliason SR. Bootstrapping: A Nonparametric Approach to Statistical Inference. *Contemp Sociol* 1995;24:269. <https://doi.org/10.2307/2076915>.
- [224] Rogers D, Hahn M. Extended-Connectivity Fingerprints. *J Chem Inf Model* 2010;50:742–54. <https://doi.org/10.1021/ci100050t>.
- [225] Baldi P, Nasr R. When is Chemical Similarity Significant? The Statistical Distribution of Chemical Similarity Scores and Its Extreme Values. *J Chem Inf Model* 2010;50:1205–22. <https://doi.org/10.1021/ci100010v>.
- [226] Bajusz D, Rácz A, Héberger K. Why is Tanimoto index an appropriate choice for fingerprint-based similarity calculations? *J Cheminform* 2015;7:20. <https://doi.org/10.1186/s13321-015-0069-3>.
- [227] Rizet G. [Impossibility of obtaining uninterrupted and unlimited multiplication of the ascomycete *Podospora anserina*]. *C R Hebd Seances Acad Sci* 1953;237:838–40.



- [228] Osiewacz HD, Hamann A, Zintel S. Assessing Organismal Aging in the Filamentous Fungus *Podospora anserina*. *Methods Mol. Biol.*, vol. 965, 2013, p. 439–62. [https://doi.org/10.1007/978-1-62703-239-1\\_29](https://doi.org/10.1007/978-1-62703-239-1_29).
- [229] Warnsmann V, Hainbuch S, Osiewacz HD. Quercetin-Induced Lifespan Extension in *Podospora anserina* Requires Methylation of the Flavonoid by the O-Methyltransferase PaMTH1. *Front Genet* 2018;9:1–14. <https://doi.org/10.3389/fgene.2018.00160>.



## 9. List of Abbreviations

%	Percent
°C	Degree Celsius
μL	Microliter
μM	Micromolar
2-PeOH	2-phenylethanol
ADP	Adenosine diphosphate
ALCAT1	Acyl-CoA: lysocardiolipinacyltransferase-1
AOX	Alternative oxidase
APS	Ammonium persulfate
ATP	Adenosine triphosphate
BSA	Bovine serum albumin
BSE	Bundle signaling element
BTHS	Barth syndrome
CDP-DAG	Diphosphate-diacylglycerol
CG	Coarse graining
CL	Cardiolipin
CLiB	Cardiolipin-binder
CoA	Coenzyme A
COX	Cytochrome <i>c</i> oxidase
DDT	Dichlorodiphenyltrichloroethane
DLiPC	Di-linoleoyl-phosphatidyl-choline
DMSO	Dimethyl sulfoxide
DNA	Deoxyribonucleic acid
DOPC	1,2-dioleoyl-sn-glycero-3-phosphocholine
DOPG	1,2-dioleoyl-sn-glycero-3-phosphoglycerol
DRP1	Dynamin-related protein 1
<i>E. coli</i>	<i>Escherichia coli</i>
e. g.	<i>Exempli gratia</i>
EDTA	Ethylenediaminetetraacetic acid, disodium salt
EPL	<i>E. coli</i> total lipid extract
eYFP	Enhanced yellow fluorescent protein

FCFP	Feature-based circular fingerprints
g	Gram
GP	Generalized polarization
GTP	Guanosine-5'-triphosphate
GUV	Giant unilamellar vesicle
HEPES	4-(2-hydroxyethyl)-1-piperazineethanesulfonic acid
His-Tag	Histidine tag
i.e.	<i>Id est</i>
IPTG	Isopropyl $\beta$ -D-thiogalactopyranoside
K	Kelvin
kDa	Kilo dalton
L	Liter
LB	Lysogeny broth
L <sub>d</sub>	Liquid disordered
LJ	Lennard-Jones potential
logP	Partition coefficient
LUV	Large unilamellar vesicle
MD	Molecular dynamics
MIC <sub>50</sub>	Minimal inhibitory concentration 50
mL	milliliter
MLCL	Monolyso cardiolipin
MLCLAT1	MLCL acyltransferase-1
NAO	10- <i>N</i> -nonyl-acridine-orange
Ni-NTA	Nickel-Nitrilotriacetic acid
ns	Nanoseconds
OCR	Oxygen consumption rates
OD	Optical density
P <sub><math>\beta</math></sub>	Ripple phase
<i>P. anserina</i>	<i>Podospora Anserina</i>
PA	Phosphatidic acid
PC	Phosphatidylcholine
PCR	Polymerase chain reaction
PDB	Protein data bank

PE	Phosphatidylethanolamine
PG	Phosphatidylglycerol
PGP	Phosphatidylglycerol phosphate
pH	<i>Potential hydrogenii</i>
PI	Phosphatidylinositol
PMF	Potential of mean force
POPG	1-palmitoyl-2-oleoyl-sn-glycero-3-phosphoglycerol
PS	Phosphatidylserine
psi	Pound-force per square inch
PVA	Poly(vinyl alcohol)
RNA	Ribonucleic acid
ROS	Reactive oxygen species
rpm	Revolutions per minute
SD	Standard deviation
SDM	Site directed mutagenesis
SDS	Sodium dodecyl sulfate
SDS-PAGE	Sodium dodecyl sulfate polyacrylamide gel electrophoresis
SEM	Standard error of the mean
SM	Small molecule
S <sub>o</sub>	Solid ordered
TAE	Tris acetate EDTA
TB	Terrific broth
TBST	Tris-buffered saline with Tween20
TEMED	Tetramethylethylenediamine
T <sub>m</sub>	Transition temperature
TOCL	Tetra oleoyl-cardiolipin
TRIS	Tris(hydroxymethyl)aminoethane
TSB	Tryptic soy broth
TTAPE-Me	1,1,2,2-tetrakis[4-(2-trimethylammonioethoxy)-phenylethene
UV	Ultraviolet
Vis	Visible
vs	Versus
wt	Wild type



## 10. List of Figures

<b>Figure 1:</b> Structure of the most common eukaryotic lipid classes. _____	16
<b>Figure 2:</b> Lipid shapes and lipid self-assemblies. _____	17
<b>Figure 3:</b> Acyl chain configurations and membrane phases. _____	18
<b>Figure 4:</b> Schematic structure of a mitochondrion. _____	20
<b>Figure 5:</b> Structure of cardiolipin. _____	22
<b>Figure 6:</b> Chemical structures of 2-phenylethanol (2-PEtOH) and derivatives. ____	52
<b>Figure 7:</b> Number–density profiles, compound orientation relative to the membrane normal and simulation snapshots. _____	55
<b>Figure 8:</b> 2-PEtOH and derivatives affect the structure of the model membranes. _____	57
<b>Figure 9:</b> Determination of MIC <sub>50</sub> values. _____	58
<b>Figure 10:</b> The logP values of 2-PEtOH linearly correlate with the log(1/MIC <sub>50</sub> ) values. _____	60
<b>Figure 11:</b> Molecular structures of (A) cardiolipin, (B) PG and (C) NAO. _____	65
<b>Figure 12:</b> Results of the computational investigation. _____	70
<b>Figure 13:</b> Structures of the 22 molecules further analyzed. _____	73
<b>Figure 14:</b> $\Delta$ GP values of the preselected 22 SMs in various model membrane systems. _____	76
<b>Figure 15:</b> $\Delta$ GP values in presence of the three most promising cardiolipin-binders determined in cardiolipin- or PG-containing model membranes. _____	78
<b>Figure 16:</b> Ratio between the $\Delta$ GP values in DOPC/DOPG and DOPC/cardiolipin containing liposomes. _____	78
<b>Figure 17:</b> Specificity of SM <sub>19</sub> -binding to cardiolipin-containing PC membranes. _	79
<b>Figure 18:</b> Membrane incorporation of SM <sub>19</sub> in cardiolipin-containing <i>E. coli</i> bacteria. _____	80
<b>Figure 19:</b> Oxygen consumption measured with mitochondria isolated from 6 days old wild-type and $\Delta$ PaCrd1 isolates. _____	82
<b>Figure 20:</b> Scheme and structure of human DRP1 isoform 3 and our construct. _	88
<b>Figure 21:</b> Fluorescence microscopy picture of <i>E. coli</i> MC4100/eYFP-stalk. _____	89
<b>Figure 22:</b> SDS-PAGE analysis of the sedimentation assay before (A) and after high-speed centrifugation (B and C). _____	90
<b>Figure 23:</b> DOPC/cardiolipin (CL) or DOPC/DOPG GUVs incubated with eYFP-stalk. _____	92

**Figure 24:** Structural change of GUVs after adding eYFP-stalk. \_\_\_\_\_ 93

**Figure 25:** Two perspectives of the alphafold model of human tafazzin. \_\_\_\_\_ 98

**Figure 26:** Western blot analysis of the wild type (wt) tafazzin and the  $\Delta$ TM construct.  
\_\_\_\_\_ 99

**Figure 27:** Western blot analysis of the wild type and the  $\Delta$ TM construct in buffer 1, 2, 4, 5 and 6 (Table 1). \_\_\_\_\_ 100

**Figure 28:** Western blots of the supernatant (A) and the pellet (B) of the membrane association assay. \_\_\_\_\_ 101

**Figure 29:** The computational workflow. \_\_\_\_\_ 138



---

## 11. List of Tables

<b>Table 1:</b> Composition of buffers and solutions. _____	27
<b>Table 2:</b> Used kits. _____	30
<b>Table 3:</b> Used marker. _____	31
<b>Table 4:</b> Used media. _____	31
<b>Table 5:</b> Used bacteria strains. _____	32
<b>Table 6:</b> Used and generated plasmids. _____	32
<b>Table 7:</b> Used instruments. _____	33
<b>Table 8:</b> Used software programs _____	34
<b>Table 9:</b> PCR reaction mixture. _____	35
<b>Table 10:</b> Programs used for polymerase chain reaction (PCR) and site-directed mutagenesis (SDM) _____	36
<b>Table 11:</b> Primers used for DRP1 construct design _____	38
<b>Table 12:</b> Primers used for tafazzin construct design _____	39
<b>Table 13:</b> Composition of the separation and stacking gels _____	43
<b>Table 14:</b> Instrument and methods used for Laurdan fluorescence spectroscopy. _	46
<b>Table 15:</b> Author contributions to “The Bacteriostatic Activity of 2-Phenylethanol Derivatives Correlates with Membrane Binding Affinity” _____	49
<b>Table 16.</b> LogP and MIC <sub>50</sub> values of 2-PEtOH and derivatives. _____	54
<b>Table 17:</b> Author contributions to CLiB – a novel cardiolipin-binder isolated via data-driven and in vitro screening. _____	61
<b>Table 18:</b> Descriptors used to select the 22 molecules for experimental validation. _____	72
<b>Table 19:</b> Systematic names of the 22 small molecules. _____	74



## 12. Author Affiliations

[Redacted]

[Redacted]  
[Redacted]  
[Redacted]

[Redacted]

[Redacted]  
[Redacted]

[Redacted]

[Redacted]

[Redacted]

[Redacted]  
[Redacted]

[Redacted]

[Redacted]  
[Redacted]



## 13. Appendix

### 13.1. Methods

#### 13.1.1. Addition Chapter 4: [REDACTED]

This work was done by [REDACTED]. The chapter is an unchanged section of my 2020 in MDPI membranes published article “The Bacteriostatic Activity of 2-Phenylethanol Derivatives Correlates with Membrane Binding Affinity”. The entire article can be found in Appendix 13.2.

#### *Computer simulations*

We followed previously established simulation protocols that were described in detail elsewhere [192,193]. Coarse-grained simulations were performed using Gromacs 4.6 [194] and the Martini force field [195]. Small molecules were parametrized using the auto-martini scheme [196] and inserted into a symmetric di-linoleoyl-phosphatidylcholine (DLiPC) bilayer consisting of 64 lipids per leaflet and solvated in water. We ran simulations in the *NPT* ensemble at 300 K and 1 bar. Each simulation included a sequence of minimization, heat-up, and equilibration runs prior to the production one, the latter being simulated for  $10^5 \tau$  using a time step of  $\delta t = 0.02 \tau$ , where  $\tau$  (1 ps) refers to the model’s natural unit of time.

#### 13.1.2. Addition Chapter 5: [REDACTED]

This work was done by [REDACTED].

#### *Molecular representations*

Coarse-grained (CG) representations of each lipid from the Martini 2 force field were used [197,198]. The bead types defined in the Martini force field link to specific physicochemical interaction types, considering four main types of interactions: polar (**P**), nonpolar (**N**), apolar (**C**), and charged (**Q**). Within a main type, subtypes are distinguished either for hydrogen-bonding capability (**d**  $\equiv$  donor, **a**  $\equiv$  acceptor, **da**  $\equiv$  both, **o**  $\equiv$  none) or by a number indicating the degree of hydrophobicity (from **1**  $\equiv$  strongly hydrophobic to **5**  $\equiv$  weakly hydrophobic) [199]. cardiolipin was modelled from di-anionic tetraoleoyl-cardiolipin (TOCL) [200]. We chose the cardiolipin

representation carrying two negative charges, following evidence of cardiolipin likely being fully ionized at physiological conditions [201–203]. While bilayers consisting of only one lipid type are not found in nature, we used homogeneous membranes as proxy systems to isolate the contributions of individual lipid types to the investigated interactions. The CG force field of PG represents 1-palmitoyl-2-oleoyl-sn-glycero-3-phosphoglycerol (POPG). Homogeneous bilayers for each lipid were created using the CHARMM-GUI Martini Maker [204] with the Martini [197] force field version 2.0, 06/2015. We solvated the membranes with the Martini polarizable water [205]. The net charges of the systems were brought to zero by adding the appropriate number of negatively charged counter ions per head group (one ion for PG, two for cardiolipin). This led to the cardiolipin simulation system containing 98 lipid representations (49 per membrane leaflet), 3609 water particles, and 196 counter ions. The PG system contained 118 lipids, 1957 water particles and 118 counter ions. The CG force field of NAO was generated using the auto-martini algorithm [196] and then manually refined to balance the overestimated hydrophobicity of the aromatic groups. Subsequently, new chemical interactions were introduced by systematically changing individual bead types and monitoring the resulting change in free energy (Figure 29A). Additional details of the CG force field and the simulation systems can be found in the corresponding paragraphs in the supplements.

### *Molecular Dynamics (MD) Simulations*

MD simulations were performed in Gromacs 5.1 [206]. The integration time step was  $\delta t = 0.02\tau$ , where  $\tau$  is the time constant defined as  $\tau = L\sqrt{M/E}$  with the units of length  $L$ , mass  $M$  and energy  $E$ . Temperature and pressure of the system ( $T = 300\text{ K}$  and  $P = 1\text{ bar}$ ) were controlled by means of a velocity rescaling thermostat [207] and a Parrinello- Rahman barostat [208], with coupling constants  $\tau_T = \tau$  and  $\tau_P = 12\tau$ . Long-range electrostatic interactions were calculated using Particle-mesh Ewald summation [209]. Other parameters, such as cut-off range and dielectric constant, follow recommendations for the Martini force field [210]. The small molecule was inserted at the appropriate position in the system, either at the membrane-water interface or in the water phase (see Figure 29B). The whole system was subsequently minimized and equilibrated for 8 ns. The free energy calculations were performed in a production run for 40 ns following the protocol described below.

### *Free-Energy Calculations*

A change in free energy  $\Delta G$  between two states of a system indicates whether the transitioning process between those states is thermodynamically favorable ( $\Delta G < 0$ ) or not ( $\Delta G > 0$ ). We compared the difference in partitioning free energies of different NAO-derived CG candidates into a cardiolipin membrane and a PG membrane at the interface region (Figure 29B). Thereby, we identified which types of physicochemical interaction introduced into the CG candidate structures positively influence cardiolipin selectivity. This is measured as the difference in partitioning free energy of a candidate compound between the two different lipid membranes,  $\Delta\Delta G_{PG \rightarrow CL}$  (Figure 29B (c)).

The free energy change was calculated by two different methods; by the transformation of a parameter of the potential energy function (alchemical transformations [211–217]) or as a potential of mean force (PMF) along a reaction coordinate defined on atomic coordinates shown as red, blue, and yellow curves in Figure 29B [218–223]. The details of the two free-energy methods can be found in the corresponding paragraphs in the supplements.

We used the less computationally expensive alchemical transformation approach for an initial screening, the promising compounds were validated using umbrella sampling.

### *Alchemical transformations*

Alchemical transformations [211–213] allow us to estimate the free-energy difference of physical processes by transforming an initial state A of a molecular system to an end state B via a succession of intermediate steps. This facilitates the calculation of free energy differences between states not necessarily connected by actual chemical or physical processes. Using this method, we could determine the influence of introducing different chemical interactions by turning individual CG beads from one bead type into another. State A is the free energy calculated for the CG representation of the original NAO molecule; state B is the corresponding free energy for a modified version of NAO. The transformation free energy was calculated by defining a thermodynamic path between the states and integrating over the ensemble average of the potential energy changes relative to a coupling parameter  $\lambda$  along this path (Equation 5).

$$U(\lambda) = U_X + \lambda(U_Y - U_X) \quad (5)$$

$$\Delta G_{X \rightarrow Y} = \int_0^1 d\lambda \left\langle \frac{\delta U(\lambda)}{\delta \lambda} \right\rangle_{\lambda} \quad (6)$$

To investigate the influence of van der Waals interactions modeled by the Lennard-Jones potential (LJ), 20 intermediate steps between state A and state B were calculated with successively increasing values for  $\lambda \in [0, 1]$ . The influence of electrostatic interactions was evaluated by introducing additional charged particles or moving the position of existing charges involved. The interactions of charged beads were transformed first through 18 LJ steps followed by 18 Coulomb steps, adding up to 36 intermediate steps. The net charge of the system was kept at zero by simultaneously transforming the appropriate number of ions in the solution into water particles [214,215]. The individual free energy contributions of the intermediate steps were integrated into the overall free energy change  $\Delta G$  between states X and Y using the MBAR method [216,217], which also gives the statistical uncertainty of the calculated free energy.

We calculated the transfer free energy  $\Delta G_{W \rightarrow I}$  of a candidate compound from bulk water to the membrane interface to determine whether this compound freely partitions into the membrane. This partitioning free energy  $\Delta G_{W \rightarrow I}$  comprises the transformation free energy (Equation 6)  $\Delta G_{X \rightarrow Y}^I$  of this compound at the interface region and the transformation free energy  $\Delta G_{X \rightarrow Y}^W$  of the same compound in the bulk water phase, following Equation 7:

$$\Delta G_{W \rightarrow I} = \Delta G_{X \rightarrow Y}^I - \Delta G_{X \rightarrow Y}^W = (\Delta G_Y^I - \Delta G_X^I) - (\Delta G_Y^W - \Delta G_X^W) \quad (7)$$

This necessitated three individual series of calculations for each NAO variant, one at the interface of each membrane and one in bulk water (Figure 29B (a)). To keep the small molecules in the interface region of the membrane-containing systems, a small constraint force of 500 kJ·mol<sup>-1</sup>nm<sup>-2</sup> was applied.

To evaluate the selectivity of the modified NAO structures for cardiolipin over PG, we used the free energy difference  $\Delta \Delta G_{PG \rightarrow CL}$  (Equation 8) between the partitioning free energies of the candidate compounds into each membrane

$$\Delta \Delta G_{PG \rightarrow CL} = \Delta G_{W \rightarrow I}^{CL} - \Delta G_{W \rightarrow I}^{PG} \quad (8)$$

$\Delta \Delta G < 0$  indicated that the modified NAO representation binds more selectively to cardiolipin than to PG (Figure 29B (c)).



### *Umbrella Sampling*

Umbrella sampling [218,219] is a free-energy technique that allows the calculation of the potential of mean force (PMF) from moving a molecule along defined reaction coordinates (Figure 29B, colored curves). We applied it to a selection of the modified candidate structures to show the difference in partitioning free energy between NAO representations with replaced bead types (Figure 29B (b)).

The reaction coordinate was the normal of the membrane midplane and the PMF describes how the free energy of a compound changes as a function of the normal distance  $z$  between its center of mass and the membrane midplane. The reaction coordinate was split into 24 individual sampling windows and the molecule was kept close to the center  $z_i$  of each window  $i$  along the reaction coordinate  $z$  by a biasing potential of  $1000 \text{ kJ}\cdot\text{mol}^{-1}\text{nm}^{-2}$ . Unbiased potentials of mean force were extracted from the biased Umbrella simulations by means of the weighted histogram analysis method [220–222] and the corresponding errors via bootstrapping [223].

### *Virtual Screening*

Molecules were selected from the MCULE database of purchasable, in-stock compounds (<https://mcule.com/>, version 18-08-17 [147], (Figure 29 and Figure 12)). This was done using Morgan circular fingerprints [224] implemented in the RDKit [151] with feature-based atom invariants and a bit vector length of 2084 bits. The interaction radius was set to two, considering the two nearest neighbors of each atom, the setting best suited for comparing diverse structures for similarity [201]. The chemical features defined in the RDKit for feature-based circular fingerprints (FCFP) are hydrogen bond donor and acceptor sites, aromaticity, the presence of a halogen and acidic or basic properties. The resulting FCFP representations of the molecules were used to calculate the Tanimoto similarity coefficient [225,226] to the FCFP representation of NAO. The similarity score reads as follows: 0.0  $\equiv$  no similarity at all to 1.0  $\equiv$  identity.

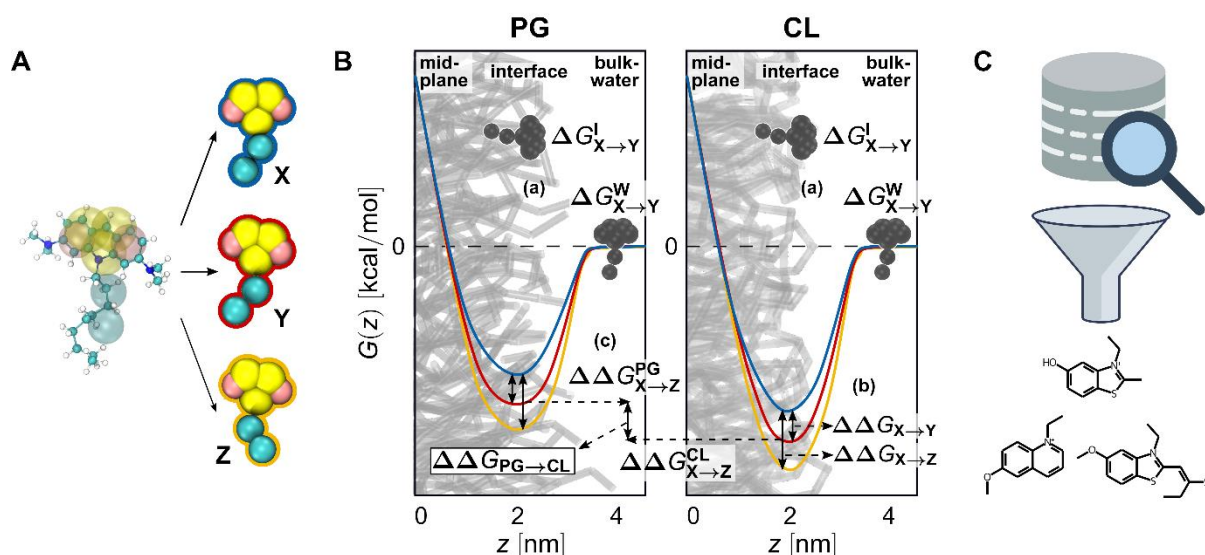


**Figure 29:** The computational workflow.

(A) Introduction of new chemical interactions by systematically changing of individual bead types. (B) The different areas of a membrane system where free energies are calculated. The black compounds indicate the two regions for the alchemical transformations, the PMFs show the free energy change of a molecule moving along the membrane normal  $z$ . The deeper the minimum of the PMF at the interface, the more selective the candidate is for the lipid headgroup. (C) Screening of a database of small molecules for candidates conforming to our identified design rules. The structures were drawn using RDKit [151], the images were obtained from Flaticon.com.

### 13.1.3. Addition Chapter 5:

#### *Generation and cultivation of *P. anserina* strains*

The wild-type strain “s” [227] and the  $\Delta PaCrd1$ -mutant [104] of *P. anserina* was used in this study. The  $\Delta PaCrd1$ -mutant lacking the gene encoding PaCRD1 (UniProt B2AX19) was generated as described in [104]. Monokaryotic ascospores were allowed to germinate at BMM medium containing 80 mM ammonium acetate for 2 days at 27 °C in the dark. For mitochondria isolation, monokaryotic strains of wild-type and  $\Delta PaCrd1$  were grown on cellophane foil covered solid M2 agar under constant light for 2 days at 27 °C. After 2 days, grown mycelia were transferred to CM for 2 days at 27 °C with shaking [228].

*Isolation of mitochondria from P. anserina*

Isolation of mitochondria was performed as described in [228]. Briefly, grown mycelia of 6 days old strains were disrupted in isotonic mitochondria buffer with 0.2 % (w/v) of bovine serum albumin (BSA) (Sigma-Aldrich, St. Louis, Missouri, USA, A6003). The homogenate was filtered through nettle cloth and centrifuged at 600 g for 10 minutes at 4 °C. Subsequently, the supernatant was filtered through glass wool and centrifuged at 12,000 g for 20 minutes at 4 °C. The pellet was resuspended in isotonic mitochondrial buffer without BSA and centrifuged at 15,000 g for 20 minutes at 4 °C. The mitochondria were enriched in the exterior circle of the pellet. The interior part (consisting of vacuoles) was removed, and the mitochondria were resuspended in isotonic mitochondrial buffer without BSA. The freshly isolated mitochondria were immediately used for respirometry.

*Respirometry of P. anserina mitochondria*

For measurement of the mitochondrial oxygen consumption rate, 150 µg of freshly isolated mitochondria was used and measured by high-resolution respirometry at 27 °C (Oxygraph-2k series C and G, OROBOROS Instruments, Innsbruck, Austria). Mitochondria were injected into a chamber with 2 ml of air-saturated buffer (0.3 M sucrose, 10 mM KH<sub>2</sub>PO<sub>4</sub>, 5 mM MgCl<sub>2</sub>, 1 mM EGTA, 10 mM KCl and 0.1 % BSA; pH 7.2) in presence vs. absence of 1 µM SM<sub>19</sub>. To stimulate complex I-dependent phosphorylating respiration in the presence of ADP, 10 mM pyruvate (Sigma-Aldrich, P2256), 2 mM malate (Sigma-Aldrich, M1000) and 1.5 mM ADP (Sigma-Aldrich, A5285) was added [229]. When oxygen consumption reached a constant level, 1 mM potassium cyanide (KCN, inhibitor of cytochrome *c* oxidase (COX)) and 1 mM salicylhydroxamic acid (SHAM, inhibitor of the alternative oxidase (AOX)) were added to completely block respiration. Wild-type and  $\Delta PaCrd1$  mitochondria were analyzed in presence of absence of 1 µM SM<sub>19</sub>. For analyzing the data, the manufacturer's software DatLab 6 was used.

## 13.2. Full Article of Chapter 4

The format of the article was adapted to the style of this thesis. No content was changed.

Copyright: © 2021 by the authors. Licensee MDPI, Basel, Switzerland. This article is an open access article distributed under the terms and conditions of the Creative Commons Attribution (CC BY) license (<https://creativecommons.org/licenses/by/4.0/>)

### **The Bacteriostatic Activity of 2-Phenylethanol Derivatives Correlates with Membrane Binding Affinity**

Isabel S. Kleinwächter<sup>1</sup>, Stefanie Pannwitt<sup>1</sup>, Alessia Centi<sup>2</sup>, Nadja Hellmann<sup>1</sup>, Eckhard Thines<sup>3</sup> Tristan Bereau<sup>4,2</sup> and Dirk Schneider<sup>1,2</sup>

<sup>1</sup>Department of Chemistry, Biochemistry, Johannes Gutenberg University Mainz, Hanns-Dieter-Hüsch-Weg 17, 55128 Mainz, Germany; kisabels@uni-mainz.de (I.S.K.); Stefanie.Pannwitt@gmx.de (S.P.); nhellmann@uni-mainz.de (N.H.)

<sup>2</sup>Max Planck Institute for Polymer Research, 55128 Mainz, Germany; centia@mpip-mainz.mpg.de (A.C.)

<sup>3</sup>Institute of Molecular Physiology, Johannes Gutenberg University, Hanns-Dieter-Hüsch-Weg 17, 55128 Mainz, Germany; thines@uni-mainz.de

<sup>4</sup>Van 't Hoff Institute for Molecular Sciences and Informatics Institute, University of Amsterdam, 1098 XH Amsterdam, The Netherlands; t.bereau@uva.nl

**Received:** 09. March 2021; **Accepted:** 26. March 2021; **Published:** 31. March 2021

**Edited by:** Luis Octavio Regasini

### **Abstract**

The hydrophobic tails of aliphatic primary alcohols do insert into the hydrophobic core of a lipid bilayer. Thereby, they disrupt hydrophobic interactions between the lipid molecules, resulting in a decreased lipid order, i.e., an increased membrane fluidity. While aromatic alcohols, such as 2-phenylethanol, also insert into lipid bilayers and disturb the membrane organization, the impact of aromatic alcohols on the structure of biological membranes, as well as the potential physiological implication of membrane incorporation has only been studied to a limited extent. Although diverse targets are discussed to be causing the bacteriostatic and bactericidal activity of 2-phenylethanol, it is clear that 2-phenylethanol severely affects the structure of biomembranes, which has been linked to its bacteriostatic activity. Yet, in fungi some

2-phenylethanol derivatives are also produced, some of which appear to also have bacteriostatic activities. We showed that the 2-phenylethanol derivatives phenylacetic acid, phenyllactic acid, and methyl phenylacetate, but not Tyrosol, were fully incorporated into model membranes and affected the membrane organization. Furthermore, we observed that the propensity of the herein-analyzed molecules to partition into biomembranes positively correlated with their respective bacteriostatic activity, which clearly linked the bacteriotoxic activity of the substances to biomembranes.

**Keywords:** 2-phenylethanol; phenylacetic acid; phenyllactic acid; methyl phenylacetate; Tyrosol; biomembranes; membrane interaction; bacteriotoxic

## 1. Introduction

Due to their amphipathic properties, alcohols affect numerous biological processes, many of which are related to cellular membranes. The hydrophobic tails of alcohols insert into the hydrophobic core region of a lipid bilayer and disrupt hydrophobic interactions between the lipid molecules, resulting in a decreased lipid order, i.e., an increased membrane fluidity [1,2]. The exact impact of alcohol on the structure of a lipid bilayer depends on the length and overall hydrophobicity of the alcohol alkyl chain, and it is predicted that the effect of alcohols on membranes increases with increasing alkyl chain lengths [3]. Thus far, the impact of alcohols on biomembranes has been studied to a great extent using, aliphatic primary alcohols, albeit aromatic alcohols, such as 2-phenylethanol (2-PEtOH), also insert into lipid bilayers and disturb the membrane organization [4].

2-PEtOH, a compound also known as phenylethyl alcohol or benzylcarbiol, is a colorless liquid with a rose-like odor. 2-PEtOH occurs widely in nature and is—besides in rose extracts—a major component in a variety of plant extracts from carnations, hyacinths, jasminum, geranium species, and others [5]. 2-PEtOH has been shown to affect cell proliferation in bacteria, yeast, plants, fungi, and mammalian cells, albeit its exact mode of action is still under debate [6–9]. Due to its bactericidal effect, 2-PEtOH is frequently used in concentrations of up to 100 mM to protect pharmaceuticals, cosmetics, and other personal care products from spoilage. However, 2-PEtOH is already bacteriostatic at vastly lower concentrations, starting at concentrations as low as 8 mM with explicit effects at 12–16 mM [7].

2-PEtOH appears to affect DNA, RNA, and protein synthesis in bacteria [10–12]. Additionally, it has been suggested that the bactericidal activity of 2-PEtOH in fact depends on its conversion into phenylacetaldehyde, which is way more toxic to bacteria than 2-PEtOH [12]. Yet, while diverse targets are discussed to be causing the bacteriostatic activity of 2-PEtOH, it is clear that 2-PEtOH partitions into bacterial membranes and severely affects the structure of biomembranes [4,7,13]. As observed with other alcohols, the interaction of 2-PEtOH with the model as well as with biological membranes results in a drastic change of the lipid acyl-chain order [14–16]. This 2-PEtOH-induced change in the lipid order significantly affects the dimerization of transmembrane helices in the model, as well as in cellular membranes [14]. Thus, 2-PEtOH-induced lipid disordering might crucially affect the structure of transmembrane proteins in general, and this effect on the structure of biological membranes might be the first and ultimate line of the 2-PEtOH bacteriostatic activity. Further, 2-PEtOH is also produced by some fungi, which can significantly retard their growth and development [6,9]. Yet, fungi also produce some 2-PEtOH-derivatives, such as Tyrosol, phenyllactic acid, and phenylacetic acid (Figure 1), some of which appear to also have bacteriostatic activities. Already decades ago, a correlation between the bacteriostatic activity of phenyl-substituted alcohols (other than analyzed here) and their partitioning between an aqueous phase and an organic layer was described, and it was suggested that the compounds acted on cellular membranes [13]. Thus, it is reasonable to assume that the 2-PEtOH derivatives also act on cellular membranes and affect cell viability.

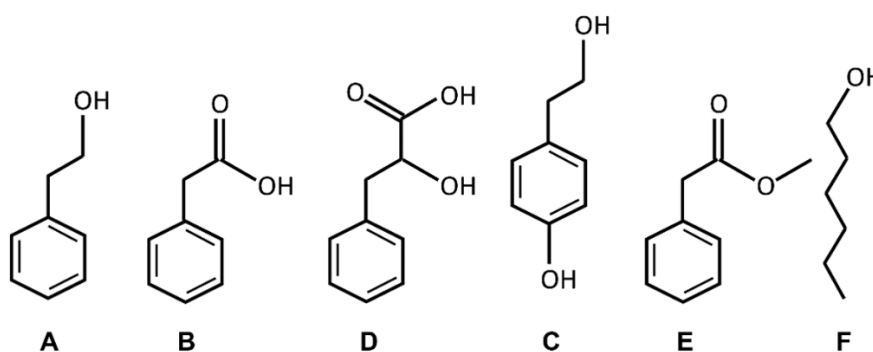


**Figure 1.** Chemical structures of 2-phenylethanol (2-PEtOH) and derivatives.

2-phenylethanol (A), phenylacetic acid (B), phenyllactic acid (C), Tyrosol (D), methyl phenylacetate (E), and 1-hexanol (F). The structures were drawn with ChemSketch V5.

Similar to 2-PEtOH, phenyllactic acid, the metabolite of phenylethylamine that occurs in the phenylalanine metabolism [17–19], also appears to have antimicrobial properties, targeting fungi and bacteria [14,15,20–22]. Just as for 2-PEtOH, also for phenyllactic acid, diverse modes of actions are discussed, and the compound appears to affect the integrity of the bacterial cell wall [14,20], and/or it might intercalate into the DNA and hinder DNA replication [23].

Yet, just as 2-PEtOH, it has been suggested that phenylacetic acid does also act at the cell membrane, albeit not knowing the mode of action [17]. Clearly, phenylacetic acid can passively cross liposomal membranes in vitro [24], and a correlation between the membrane partition coefficients of some of its para-substituents and their bacteriostatic properties is described [25], and phenyllactic acid potentially makes the outer membrane of *Escherichia coli* more permeable, without disrupting it [23]. In contrast to 2-PEtOH and phenylacetic acid, membrane interaction of methyl phenylacetate, the methyl ester of phenylacetic acid, which is produced by several plants, has not been analyzed yet.

Tyrosol belongs to the most widely distributed compounds in plants [16]. It is the major phenolic compound found in olive oil, red wine and white wine [26,27].

While membrane interaction of 2-PEtOH has been studied to some extent and the bacteriostatic activity of 2-PEtOH has been linked to its membrane activity, the interaction of 2-PEtOH derivatives with model and biomembranes has only marginally been studied, if at all. Given that most compounds have an amphipathic nature, membrane interaction is expected, and it is well possible that membrane interactions affect bacterial homeostasis. In the present study, we showed that the 2-PEtOH derivatives phenylacetic acid, phenyllactic acid, and methyl phenylacetate (Figure 1) were incorporated into the model membranes and affected the membrane structure. The higher the overall hydrophobicity of a 2-PEtOH derivative, the higher its fluidizing impact on a membrane. Furthermore, we observed a positive correlation between membrane partitioning and the bacteriostaticity of the here analyzed 2-PEtOH derivatives.

## 2. Materials and Methods

### 2.1. Lipids and Chemicals

*E. coli* total lipid extract (EPL) was purchased from Avanti Polar Lipids (Alabaster, AL, USA). Laurdan (6-dodecanoyl-2-dimethylamino) was purchased from Sigma-Aldrich (Munich, Germany).

2-PEtOH, phenylacetic acid, phenyllactic acid, Tyrosol, 1-hexanol, and methyl phenylacetate were all purchased from Sigma-Aldrich (Munich, Germany). All structures were drawn with the program ChemSketch V5 (Freeware from ACD/Labs, Toronto, Ontario, Canada). The partition coefficient (logP value) was calculated using Molinspiration v2016.10 ([www.molinspiration.com](http://www.molinspiration.com), accessed on 21. June 2018.).

It can be expected that the effect of a given compound on a membrane correlates with its tendency to incorporate into the membrane, represented by the corresponding partitioning coefficient P. This type of correlation is probed as [28]

$$\log \frac{1}{C} = a \times \log P + b \quad (1)$$

if only logP is considered as the predictor for the activity of the substance, with a and b being constants and C the concentration relevant for the effect to be tested, here: Minimal inhibitory concentration 50 (MIC<sub>50</sub>; see [28] for a recent discussion of the approach).

### 2.2. Laurdan Fluorescence Spectroscopy and Generalized Polarization (GP) Values

For liposome preparation, 25  $\mu$ L EPL (10 mM in chloroform and methanol, 2:1) was mixed with Laurdan (dissolved in methanol) in a 500:1 molar ratio. The solvents were removed under a nitrogen stream, and the remaining traces of the solvent were removed by overnight vacuum desiccation. The next day, 250  $\mu$ L of the substances dissolved in 10 mM 4-(2-hydroxyethyl)-1-piperazineethanesulfonic acid (HEPES)-buffer (pH 7.4, 150 mM NaCl) at the desired concentrations were added and the lipid film was rehydrated, resulting in a solution with 1 mM lipid.

The mixture was vortexed and subsequently incubated for 30 minutes at 37 °C and 1000 rpm on a Thermoblock mixer comfort from Eppendorf. To prepare large unilamellar liposomes (LUVs), five freeze-thaw cycles were performed. The liposomes were again incubated for 30 minutes at 37 °C and 1000 rpm on a Thermoblock mixer



comfort from Eppendorf (Hamburg, Germany). Laurdan spectra were recorded at 25 °C using a Fluoro-Max-4 fluorescence spectrometer (Horiba (Bensheim, Germany)). The excitation and emission slits were set to 2 nm, and the spectra were recorded between 400 and 550 nm with excitation at 350 nm. Each tested substance was measured at least three times at each concentration using freshly prepared liposomes. The generalized polarization (GP) values were calculated from the fluorescence emission spectra using the following equation [29].

$$GP = \frac{I_{440} - I_{490}}{I_{440} + I_{490}} \quad (2)$$

$I_{440}$  and  $I_{490}$  are the emission intensities at 440 and 490 nm [29]. The range of concentrations employed was limited by the solubility of the tested substances in an aqueous buffer. Tyrosol and 2-phenylethanol were measured up to 100 mM, phenylacetic acid and phenyllactic acid up to 80 mM, 1-hexanol up to 70 mM, and methyl phenylacetate up to 15 mM.

### 2.3. Growth Assay and Determination of Minimal Inhibitory Concentrations 50 (MIC<sub>50</sub>) *Escherichia*

*Escherichia coli* strain MC4100 was grown in a terrific broth (TB)-medium buffered with 10 % K<sub>2</sub>HPO<sub>4</sub>/KH<sub>2</sub>PO<sub>4</sub> (0.17 M/0.72 M). 20 mL TB medium with 1:1000 streptomycin (50 mg/mL) was prepared, and the tested substance was dissolved in the medium at the given concentration. From an overnight culture, *E. coli* MC4100 was diluted in fresh medium to an OD<sub>600</sub> of 0.2. The cultures were incubated at 37 °C and 200 rpm for four hours, the OD<sub>600</sub> of a 5fold diluted sample was measured, and the real value was calculated. The highest tested concentration was defined by the solubility of the tested substances in TB medium or was the concentration where the *E. coli* were not able to grow anymore. A dose-response curve was fit to the data with a modified Hill equation using OriginPro 8.6 (Northampton, MA, US),

$$y = c + \frac{d-c}{1 + \left(\frac{x}{e}\right)^b} \quad (3)$$

[30], with the concentration of the substance  $x$  and the parameter  $e$  reflecting the MIC<sub>50</sub> for each tested substance (Figure 4). In order to get an idea about the concentration of the substance incorporated into the *E. coli* membrane, we calculated the overall surface area presented by the bacteria and, based on the partition

coefficient, calculated the concentration of the lipids required to obtain the corresponding area/ml as liposomes. According to [31], an OD of 0.2 corresponds to about  $2 \times 10^8$  *E. coli* cells/ml. The surface area of an *E. coli* cell is about  $3 \mu\text{m}^2$  [32], corresponding to about  $4.2 \times 10^6$  lipid molecules, assuming  $0.7 \text{ nm}^2/\text{lipid}$  [33]. Thus, the concentration of the lipids necessary to create the corresponding area of a lipid bilayer is about  $3 \mu\text{M}$ .

#### 2.4. Computer Simulations

We followed previously established simulation protocols that were described in detail elsewhere [34,35]. Coarse-grained simulations were performed using Gromacs 4.6 [36] and the Martini force field [37]. Small molecules were parametrized using the auto-martini scheme [38] and inserted into a symmetric di-linoleoyl-phosphatidyl-choline (DLiPC) bilayer consisting of 64 lipids per leaflet and solvated in water. We ran simulations in the *NPT* ensemble at 300 K and 1 bar. Each simulation included a sequence of minimization, heat-up, and equilibration runs prior to the production one, the latter being simulated for  $10^5 \tau$  using a time step of  $\delta t = 0.02 \tau$ , where  $\tau$  (1 ps) refers to the model's natural unit of time.

### 3. Results and Discussion

The impact of 2-PEtOH on the structure and the stability of the model, as well as biological membranes, were studied in the past [6–8,14–16]. Nevertheless, plants, some fungi, as well as some bacteria produce and secrete the 2-PEtOH derivatives phenylacetic acid permeabilizes the outer membrane of bacteria (by a yet unknown mechanism) [23], the membrane activity of the 2-PEtOH derivatives is largely unexplored. All molecules are amphiphilic and have a polar region with hydroxyl or carboxyl groups and a nonpolar phenyl ring. An exception is Tyrosol, which has an extra hydroxyl group at the phenyl ring that renders the molecule non-amphiphilic [16]. Furthermore, in the present study, we additionally analyzed methyl phenylacetate, the methyl ester of phenylacetic acid produced in some plants, as it allows separating effects of the polar group from effects potentially caused by the negative charge of the carboxylate group. Furthermore, 1-hexanol, whose membrane interaction is well studied [1,2], was used as a non-aromatic control.

### 3.1. Membrane Partitioning and the Impact of 2-PEtOH Derivatives on the Membrane Structure

To estimate the membrane-binding affinity of the here-analyzed substances, we first calculated logP values (Table 1), which provide information as to the partitioning of the substances between water and octanol (which is typically used as a mimic of the hydrophobic membrane core). This calculation is based on the hydrophobicity and polarity of a substance, and the less hydrophobic a molecule, the lower the logP value. [39].

**Table 1.** LogP and MIC<sub>50</sub> values of 2-PEtOH and derivatives.

<b>Substance</b>	<b>logP</b>	<b>MIC<sub>50</sub></b>
phenyllactic acid	0.72	44.97
Tyrosol	1.00	29.74
phenylacetic acid	1.36	20.28
2-phenylethanol	1.49	14.89
methyl phenylacetate	1.98	6.30
1-hexanol	2.13	7.05

The partition coefficient (logP) values of the substances, which provide information as to membrane partitioning of a molecule, were calculated with the online Molinspiration software v2016.10. The higher the value, the more hydrophobic the molecule and the higher will be the fraction of the membrane incorporated substance. The minimal inhibitory (MIC<sub>50</sub>) value provides information as to the bacteriostatic potential of a molecule (compare Figure 4). The higher this value, the less bacteriostatic a substance.

Phenyllactic acid has the lowest logP value and, thus, is the least hydrophobic molecule analyzed here, and 1-hexanol is the most hydrophobic molecule with the highest logP value of our studied substances.

Based on the definition of the logP, it is evident that a substance with a negative logP has a higher affinity to the aqueous phase, and a positive logP denotes a higher concentration in the lipid phase. Thus, based on this analysis, we expected all our tested substances to incorporate into the membrane (the lipid phase) as all the calculated values are positive [40]. Indeed, computer simulations clearly indicated that all substances incorporated around the lipid head groups (Figure 2). The ring lies deeper in the membrane than the side chain for all substances except Tyrosol. In fact, the angle distribution shown below (Figure 2) indicated that Tyrosol did not intercalate into a membrane but rather bound parallel on a membrane surface, in line with

previous assumptions [16,41]. The angle between the membrane bilayer normal and the orientation of Tyrosol was just about  $90^\circ$ , while all other compounds showed much larger angles (Figure 2F).

Thus, all 2-PEtOH derivatives intercalated into a lipid monolayer, except Tyrosol, where direct interactions with the lipid acyl chains were not expected.

As membrane integration and membrane activity of 2-PEtOH had been demonstrated in the past, we next determined the impact of 2-PEtOH derivatives on the structure of model membranes via laurdan fluorescence spectroscopy [1,2,8,9,14,17,20]. Laurdan is a fluorescent dye that incorporates in lipid bilayers. Changes in the laurdan fluorescence emission spectrum reflect changes in the dye's ultimate environment, e.g., caused by altered lipid packing. To quantify the impact of a molecule on the structure of a lipid bilayer, the generalized polarization (GP) value was calculated [42]. A high GP value ( $\approx + 0.4$ ) is characteristic for a rigid lipid bilayer with densely packed lipid molecules, i.e., the membrane gel state, whereas a low GP value ( $\approx - 0.2$ ) is characteristic for less densely packed lipid bilayers, i.e., the fluid membrane state. As these values are largely independent of the lipid head groups and acyl chains, changes in the GP value can provide information about changes in the lipid order upon the addition of substances [43].

To this end, unilamellar liposomes were prepared from *E. coli* lipids containing  $2 \mu\text{M}$  Laurdan as well as increasing concentrations of the substances analyzed here. Changes in lipid packing were determined via laurdan fluorescence spectroscopy and illustrated as changes in the GP values (Figure 3). For further details, see Materials and Methods.

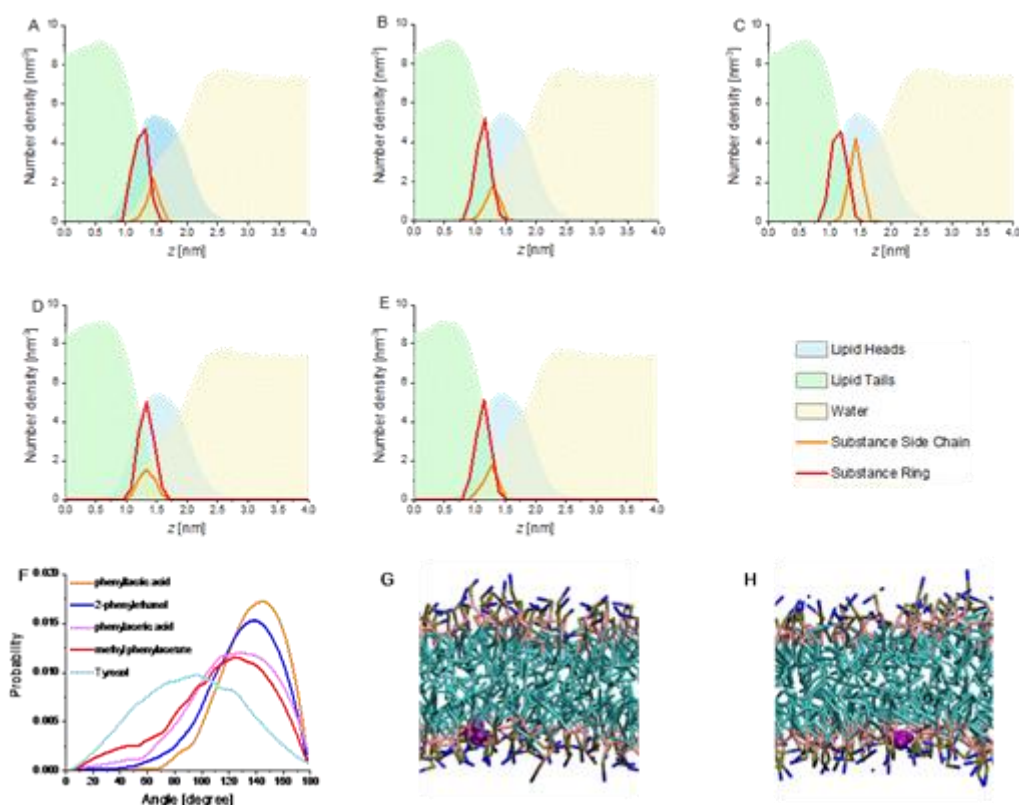


**Figure 2.** Number–density profiles, compound orientation relative to the membrane normal and simulation snapshots.

(A–E) The number–density profiles report the molar fraction of different chemical groups in the simulation box, perpendicular to the bilayer. (A) 2-PEtOH, (B) phenylacetic acid, (C) phenyllactic acid, (D) Tyrosol, and (E) methyl phenylacetate. All substances have shifts between the side chain and ring, except Tyrosol. Molar fractions of the solutes have been multiplied by 50 for clarity. All substances spontaneously insert close to the lipid head groups. (F) The angle between membrane normal and compound orientation (defined from side chain to aromatic ring) shows large values for methyl phenylacetate, phenylacetic acid, 2-PEtOH, and phenyllactic acid, indicative of their intercalation in the membrane. Smaller values are reported for Tyrosol, indicating its binding parallel to the membrane surface. (G,H) Representative simulation snapshots of 2-PEtOH and Tyrosol (purple) inserted in the headgroup region of the phospholipid membrane. Water is not shown for clarity.

2-PEtOH and 1-hexanol are well known to increase membrane fluidity [1,2,8]. In line with this, the GP values measured here with increasing 2-PEtOH and 1-hexanol concentrations, respectively, are constantly decreasing (Figure 3), indicating a membrane fluidizing effect of all substances. For the maximal tested concentrations of the two substances, 70 mM for 1-hexanol and 100 mM for 2-PEtOH, the GP value is around  $-0.2$ . This value is characteristic of a bilayer in the fluid (liquid crystalline) phase [42,43]. Here, 2-PEtOH acts like 1-hexanol, although the impact of 1-hexanol on the lipid acyl chain order was more pronounced already at lower concentrations.

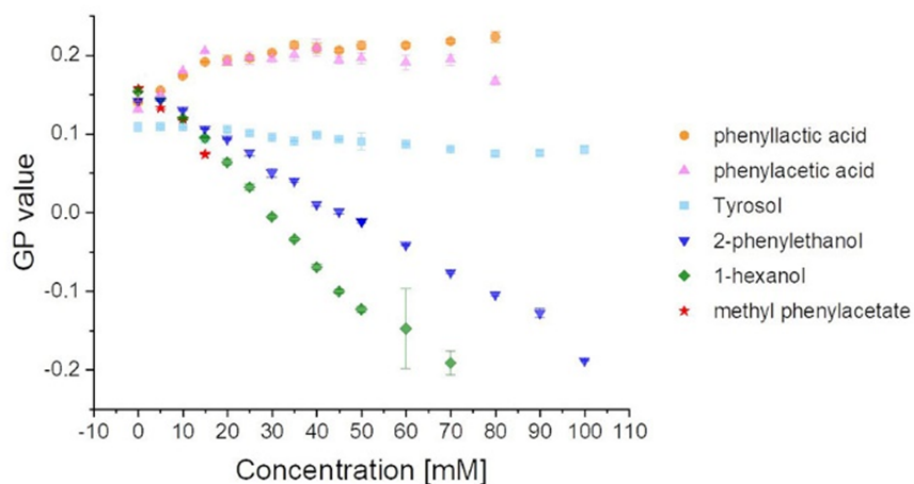


**Figure 3.** 2-PEtOH and derivatives affect the structure of the model membranes.

GP values determined at increasing substance concentrations are shown. The values indicate a fluidizing effect for the more hydrophobic substances 1-hexanol, 2-PEtOH, and methyl phenylacetate. Tyrosol seems to be largely ineffective, while phenyllactic acid and phenylacetic acid seem to have a slight ordering effect.

Yet, even though Tyrosol binds solely to membrane surfaces, an impact on the lipid order might be expected. However, we did not see any change of the GP values with increasing Tyrosol concentrations, and thus, apparently, surface adhesion of Tyrosol does not (significantly) affect the membrane structure.

Further, for phenylacetic acid and phenyllactic acid, it was suggested that they could incorporate into membranes [14,17,20,24], which is in line with the calculated logP values (Table 1). Yet, in contrast to 2-PEtOH, the addition of both phenyllactic acid as well as phenylacetic acid to *E. coli* lipid membranes did result in increasing GP values, which remained constant at concentrations larger than 15 mM. Thus, phenylacetic acid and phenyllactic acid both appeared to increase rather than decrease the membrane lipid order creating a more rigid membrane. Nevertheless, the membrane ordering effect was much lower than the disordering effect of 2-PEtOH or 1-hexanol.

To estimate whether the reverse impact of the two acids, compared to 2-PEtOH, might be caused by the negative charge, we additionally analyzed the impact of the methyl ester of phenylacetic acid, methyl phenylacetate, on the membrane structure. The addition of methyl phenylacetate to the model membranes resulted in decreasing GP values, as observed with 2-PEtOH or 1-hexanol. Consequently, membrane incorporation of methyl phenylacetate increased the membrane fluidity, and thus

masking the negative charge of phenylacetic acid seemed to have a significant impact on the membrane activity (as further discussed below).

### 3.2. 2-PEtOH and Derivatives Are Bacteriostatic

For all substances, except for Tyrosol, we showed that membrane binding had an impact on the membrane structure. Next, to test whether this membrane activity correlates with a potential bacteriostatic activity of the substances, the impact of 2-PEtOH, phenylacetic acid, phenyllactic acid, methyl phenylacetate, Tyrosol, and 1-hexanol on the growth of the bacterium *E. coli* was tested. For 2-PEtOH, it was already shown that it decreases bacterial growth starting at concentrations as low as 8 mM with explicit effects at 12–16 mM [7]. We followed bacterial growth in presence of increasing substance concentrations to calculate the (non-lethal) amount of substance that inhibits 50% bacterial growth (Figure 4).

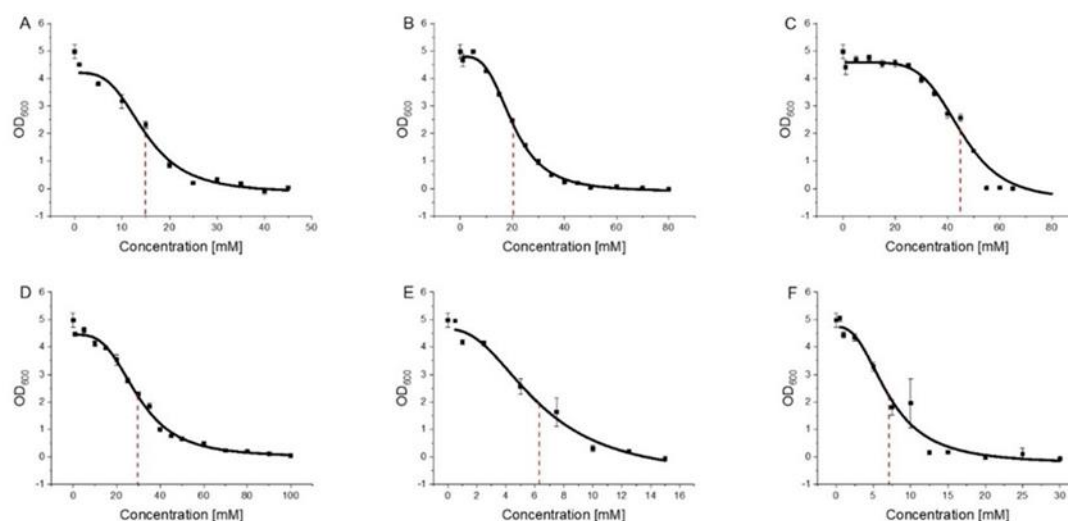


**Figure 4.** Determination of MIC<sub>50</sub> values.

The OD<sub>600</sub> was plotted against the substance concentration and a dose-response fit was performed for (A) 2-PEtOH, (B) phenylacetic acid, (C) phenyllactic acid, (D) Tyrosol, (E) methyl phenylacetate, and (F) 1-hexanol ( $n = 3$ ,  $\pm$ SD). The corresponding MIC<sub>50</sub> values are given in Table 1.

This minimal inhibitory (MIC<sub>50</sub>) value is a measure of the antimicrobial activity of compounds [44].

In excellent agreement with literature values, we here observed a clear effect of 2-PEtOH on *E. coli* growth with an MIC<sub>50</sub> value of  $\sim 15$  mM [5–9]. As for phenylacetic acid, we likewise observed a bacteriostatic effect with an MIC<sub>50</sub> value of  $\sim 20$  mM. However, when we masked the negative charge and analyzed the methyl phenylacetate

instead, the MIC<sub>50</sub> value was lowered to ~ 6.3 mM, a value lower than 2-PEtOH and in the same range as observed with 1-hexanol. This showed that masking the negative charge not only considerably affected the membrane activity of (methyl) phenylacetate (Figure 3) but also significantly enhanced its bacteriostatic efficiency. Surprisingly, while Tyrosol did not integrate into and affect the structure of biomembranes but rather lies flat on membrane surfaces (Figure 2H), it still affected the *E. coli* growth with an MIC<sub>50</sub> value of ~ 30 mM [16,40]. The naturally produced 2-PEtOH derivative phenyllactic acid was least active with an MIC<sub>50</sub> as high as ~ 45 mM. The determined MIC<sub>50</sub> values are summarized in Table 1 for each of the tested substances.

### *3.3. Hydrophobicity, Membrane Fluidity, and Bacterial Growth Correlate The*

The here-analyzed molecules with the highest logP values decreased the membrane order with increasing concentration, whereas phenylacetic acid and phenyllactic acid, which both have a low logP value, showed increasing GP values with increasing concentration. Thus, the higher the overall hydrophobicity of a molecule, the higher its fluidizing impact on a membrane. Nevertheless, as all molecules, except the control 1-hexanol as well as Tyrosol, had a methylene benzene group, the chemistry of the substituents was evidently important for the membrane activity of 2-PEtOH derivatives. In contrast to 2-PEtOH, phenylacetic acid and phenyllactic acid did not decrease but slightly increased the order of a lipid bilayer. Yet, when masking the negative charge via the formation of a methyl ester, methyl phenylacetate showed an even increased membrane fluidizing activity compared to 2-PEtOH. Thus, the incorporation of the hydrophobic methylene benzene group into the hydrophobic membrane core region, as well as (polar) interactions within the lipid head group region, likely together affect the membrane activity of 2-PEtOH derivatives (as well as of other substances). This appears to be nicely reflected by the calculated overall hydrophobicity, i.e., the calculated logP values.

Based on several subsequent studies, the bacteriostatic activity of 2-PEtOH was linked to biological membranes, albeit the exact mode of action is still unclear, and other target structures were also discussed [4,7–9]. Yet, the calculated logP values nicely correlated with the determined MIC<sub>50</sub> values (Figure 5), and with an increasing logP value, the MIC<sub>50</sub> decreased. In fact, when we plot the logarithm of the MIC<sub>50</sub> values determined for the 2-PEtOH derivatives against the calculated logP values, we



obtained a linear correlation with an  $r^2$  value of 0.987 (Figure 5). Thus, the hydrophobicity of the molecules, i.e., their calculated propensity to partition into biomembranes, correlated with the bacteriostatic activity, which indicated that the partition coefficient significantly determined the biological activity of the substances and links the bacterotoxic activity of the substances to biomembranes.

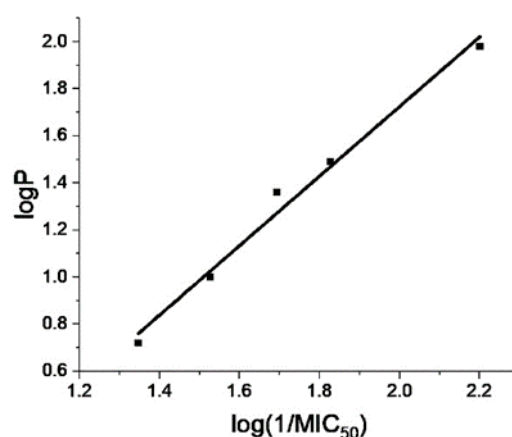


**Figure 5.** The  $\log P$  values of 2-PEtOH linearly correlate with the  $\log(1/MIC_{50})$  values.

The  $\log P$  values of 2-PEtOH and derivatives is plotted against the respective  $\log(1/MIC_{50})$  values. The correlation coefficient is  $r^2 = 0.987$ .

In most cases, a clear effect on membrane lipid order was already observed in the liposome-based assay at the  $MIC_{50}$  values, and, thus, changes in general membrane properties could well have an important impact on the bacteriostatic activity of the 2-PEtOH derivatives. Yet, there was no general correlation between the bacteriostaticity and the observed effect on the membrane structure: All substances clearly had an impact on bacterial growth, yet some substances increased the lipid order (phenylacetic acid, phenyllactic acid), Tyrosol did essentially not affect the membrane structure, whereas the remaining substances decreased the lipid order. Furthermore, it has to be noted that all molecules analyzed here might also have additional cellular targets.

In summary, our results indicate a correlation between the hydrophobicity of the 2-PEtOH derivatives analyzed here and their respective bacteriostatic activity, and our results link the biological activity of the molecules to cellular membranes.

**Author Contributions:** Conceptualization, N.H., E.T., T.B., and D.S.; methodology, I.S.K., S.P., A.C., and N.H.; software, A.C. and T.B.; validation, I.S.K., S.P., N.H., T.B., and D.S.; formal analysis, N.H., T.B., and D.S.; investigation, I.S.K., S.P., and A.C.; resources, T.B. and D.S.; writing—original draft preparation, I.S.K., T.B., and D.S.; writing—review and editing, N.H. and D.S.; visualization, I.S.K., T.B., and D.S.; supervision, T.B. and D.S.; project administration, T.B. and D.S.; funding acquisition, T.B. and D.S. All authors have read and agreed to the published version of the manuscript.

**Funding:** Isabel S. Kleinwächter, Nadja Hellmann, and Dirk Schneider were supported by DynaMem (state of Rhineland-Palatinate). Alessia Centi and Tristan Bereau acknowledge partial funding from the Emmy Noether Program of the Deutsche Forschungsgemeinschaft.

**Institutional Review Board Statement:** Not applicable.

**Informed Consent Statement:** Not applicable.

**Data Availability Statement:** All data is contained within this article.

**Acknowledgments:** We thank Hildegard Pearson for critically reading the manuscript.

**Conflicts of Interest:** The authors declare no conflict of interest.

## References

- [1] Ingram, L.O. Adaptation of membrane lipids to alcohols. *J. Bacteriol.* 1976, 125, 670–678, doi:10.1128/jb.125.2.670-678.1976.
- [2] Ingram, L.O.; Vreeland, N.S. Differential effects of ethanol and hexanol on the *Escherichia coli* cell envelope. *J. Bacteriol.* 1980, 144, 481–488, doi:10.1128/jb.144.2.481-488.1980.
- [3] Gutknecht, J.; Tosteson, D.C. Ionic permeability of thin lipid membranes: Effects of n-alkyl alcohols, polyvalent cations, and a secondary amine. *J. Gen. Physiol.* 1970, 55, 359–374, doi:10.1085/jgp.55.3.359.
- [4] Silver, S.; Wendt, L. Mechanism of action of phenethyl alcohol: Breakdown of the cellular permeability barrier. *J. Bacteriol.* 1967, 93, 560–566, doi:10.1128/jb.93.2.560-566.1967.

- [5] Zhu, Y.J.; Zhou, H.T.; Hu, Y.H.; Tang, J.Y.; Su, M.X.; Guo, Y.J.; Chen, Q.X.; Liu, B. Antityrosinase and antimicrobial activities of 2-phenylethanol, 2-phenylacetaldehyde and 2-phenylacetic acid. *Food Chem.* 2011, 124, 298–302, doi:10.1016/j.foodchem.2010.06.036.
- [6] Lilley, B.D.; Brewer, J.H. The selective antibacterial action of phenylethyl alcohol. *J. Am. Pharm. Assoc. Am. Pharm. Assoc.* 1953, 42, 6–8, doi:10.1002/jps.3030420103.
- [7] Anbazhagan, V.; Munz, C.; Tome, L.; Schneider, D. Fluidizing the Membrane by a Local Anesthetic: Phenylethanol Affects Membrane Protein Oligomerization. *J. Mol. Biol.* 2010, 404, 773–777, doi:10.1016/j.jmb.2010.10.026.
- [8] Stark, D.; Zala, D.; Münch, T.; Sonnleitner, B.; Marison, I.W.; Von Stockar, U. Inhibition aspects of the bioconversion of Lphenylalanine to 2-phenylethanol by *Saccharomyces cerevisiae*. *Enzyme Microb. Technol.* 2003, 32, 212–223, doi:10.1016/S0141-0229(02)00237-5.
- [9] Brossmer, R.; Bohn, B.; Schlicker, H. Influence of 2-Phenylethanol and 1,1'-Dimethylphenylethanol on metabolic activity and cell membrane function in ehrlich ascites tumor cells. *FEBS Lett.* 1973, 35, 191–194. ISSN 0014-5793
- [10] Prevost, C.; Moses, V. Action of Phenethyl Alcohol on the Sythesis of Macromolecules in *E. coli*. *J. Bacteriol.* 1966, 91, 1446–1452, doi:10.1128/jb.91.4.1446-1452.1966
- [11] Masker, W.E.; Eberle, H. Effect of phenethyl alcohol on deoxyribonucleic acid-membrane association in *Escherichia coli*. *J. Bacteriol.* 1972, 109, 1170–1174, doi:10.1128/jb.109.3.1170-1174.1972.
- [12] Lucchini, J.J.; Bonnavero, N.; Cremieux, A.; Le Goffic, F. Mechanism of bactericidal action of phenethyl alcohol in *Escherichia coli*. *Curr. Microbiol.* 1993, 27, 295–300, doi:10.1007/BF01575995.
- [13] Lovrien, R.; Hart, G.; Anderson, K.J. Quantitative aspects of phenyl substituted alcohol and ether bacteriostatic interaction with *Escherichia coli* B/5. *Microbios* 1977, 20, 153–172. PMID 84328
- [14] Dieuleveux, V.; Lemarinier, S.; Guéguen, M. Antimicrobial spectrum and target site of D-3-phenyllactic acid. *Int. J. Food Microbiol.* 1998, 40, 177–183, doi:10.1016/S0168-1605(98)00031-2.
- [15] Prema, P.; Smila, D.; Palavesam, A.; Immanuel, G. Production and characterization of an antifungal compound (3-phenyllactic acid) produced by *Lactobacillus plantarum* strain. *Food Bioprocess. Technol.* 2010, 3, 379–386, doi:10.1007/s11947-008-0127-1.

- [16] Lopez, S.; Bermudez, B.; Montserrat-De La Paz, S.; Jaramillo, S.; Varela, L.M.; Ortega-Gomez, A.; Abia, R.; Muriana, F.J.G. Membrane composition and dynamics: A target of bioactive virgin olive oil constituents. *Biochim. Biophys. Acta Biomembr.* 2014, 1838, 1638–1656, doi:10.1016/j.bbamem.2014.01.007.
- [17] Sandler, M.; Ruthven, C.R.J.; Goodwin, B.L.; Lees, A.; Stern, G.M. Phenylacetic acid in human body fluids: High correlation between plasma and cerebrospinal fluid concentration values. *J. Neurol. Neurosurg. Psychiatry* 1982, 45, 366–368, doi:10.1136/jnnp.45.4.366.
- [18] Sherwin, C.; Kennard, K.; Toxicity of phenylacetic acid. *J. Inherit. Metab. Dis.* 1919, 40, 259. ISSN 0141-8955
- [19] Hudgins, W.R.; Shack, S.; Myers, C.E.; Samid, D. Cytostatic activity of phenylacetate and derivatives against tumor cells. *Biochem. Pharmacol.* 1995, 50, 1273–1279, doi:10.1016/0006-2952(95)02013-3.
- [20] Mu, W.; Yu, S.; Zhu, L.; Zhang, T.; Jiang, B. Recent research on 3-phenyllactic acid, a broad-spectrum antimicrobial compound. *Appl. Microbiol. Biotechnol.* 2012, 95, 1155–1163, doi:10.1007/s00253-012-4269-8.
- [21] Dieuleveux, V.; Guéguen, M. Antimicrobial effects of D-3-phenyllactic acid on *Listeria monocytogenes* in TSB-YE medium, milk, and cheese. *J. Food Prot.* 1998, 61, 1281–1285, doi:10.4315/0362-028X-61.10.1281.
- [22] Mu, W.; Chen, C.; Li, X.; Zhang, T.; Jiang, B. Optimization of culture medium for the production of phenyllactic acid by *Lactobacillus* sp. SK007. *Bioresour. Technol.* 2009, 100, 1366–1370, doi:10.1016/j.biortech.2008.08.010.
- [23] Ning, Y.; Yan, A.; Yang, K.; Wang, Z.; Li, X.; Jia, Y. Antibacterial activity of phenyllactic acid against *Listeria monocytogenes* and *Escherichia coli* by dual mechanisms. *Food Chem.* 2017, 228, 533–540, doi:10.1016/j.foodchem.2017.01.112.
- [24] Hillenga, D.J.; Versantvoort, H.J.M.; Van der Molen, S.; Driessen, A.J.M.; Konings, W.N. *Penicillium chrysogenum* takes up the penicillin G precursor phenylacetic acid by passive diffusion. *Appl. Environ. Microbiol.* 1995, 61, 2589–2595, doi:10.1128/aem.61.7.2589-2595.1995.
- [25] Bittenbender, W.A.; Bittenbender, E.F.D. The effect of para-substituents on the bacteriostatic properties of phenylacetic acid. *J. Am. Pharm. Assoc. Am. Pharm. Assoc.* 1972, 28, 514–519. doi:10.1002/jps.3080280810

- [26] Giovannini, C.; Straface, E.; Modesti, D.; Coni, E.; Cantafora, A.; De Vincenzi, M.; Malorni, W.; Masella, R. Tyrosol, the Major Olive Oil Biophenol, Protects Against Oxidized-LDL-Induced Injury in Caco-2 Cells. *J. Nutr.* 1999, 129, 1269–1277, doi:10.1093/jn/129.7.1269.
- [27] Covas, M.; Miró-Casas, E.; Fitó, M.; Farré-Albadalejo, M.; Gimeno, E.; Marrugat, J.; De LA Torre, R. Bioavailability of tyrosol, an antioxidant phenolic compound present in wine and olive oil, in humans. *Drugs Exp. Clin. Res.* 2003, 29, 203–206. PMID: 15134375
- [28] Fujita, T.; Winkler, D.A. Understanding the Roles of the “two QSARs.” *J. Chem. Inf. Model.* 2016, 56, 269–274, doi:10.1021/acs.jcim.5b00229.
- [29] Parasassi, T.; De Stasio, G.; d’Ubaldo, A.; Gratton, E. Phase fluctuation in phospholipid membranes revealed by Laurdan fluorescence. *Biophys. J.* 1990, 57, 1179–1186, doi:10.1016/S0006-3495(90)82637-0.
- [30] Nweke, C.O.; Ogbonna, C.J. Statistical models for biphasic dose-response relationships (hormesis) in toxicological studies. *Ecotoxicol. Environ. Contam.* 2017, 12, 39–55, doi:10.5132/eec.2017.01.06.
- [31] Sezonov, G.; Joseleau-Petit, D.; D’Ari, R. Escherichia coli physiology in Luria-Bertani broth. *J. Bacteriol.* 2007, 189, 8746–8749, doi:10.1128/JB.01368-07.
- [32] Gray, W.T.; Govers, S.K.; Xiang, Y.; Parry, B.R.; Campos, M.; Kim, S.; Jacobswagner, C. Nucleoid size scaling and intracellular organization of translation across bacteria. *Cell* 2019, 177, 1632–1648, doi:10.1016/j.cell.2019.05.017.Nucleoid.
- [33] Petrache, H.I.; Dodd, S.W.; Brown, M.F. Area per lipid and acyl length distributions in fluid phosphatidylcholines determined by <sup>2</sup>H NMR spectroscopy. *Biophys. J.* 2000, 79, 3172–3192, doi:10.1016/S0006-3495(00)76551-9.
- [34] Centi, A.; Dutta, A.; Parekh, S.H.; Bereau, T. Inserting Small Molecules across Membrane Mixtures: Insight from the Potential of Mean Force. *Biophys. J.* 2020, 118, 1321–1332, doi:10.1016/j.bpj.2020.01.039.
- [35] Hoffmann, C.; Centi, A.; Menichetti, R.; Bereau, T. Molecular dynamics trajectories for 630 coarse-grained drug-membrane permeations. *Sci. Data* 2020, 7, 1–7, doi:10.1038/s41597-020-0391-0.
- [36] Hess, B.; Kutzner, C.; Van Der Spoel, D.; Lindahl, E. GRGMACS 4: Algorithms for highly efficient, load-balanced, and scalable molecular simulation. *J. Chem. Theory Comput.* 2008, 4, 435–447, doi:10.1021/ct700301q.

- [37] De Jong, D.H.; Singh, G.; Bennett, W.F.D.; Arnarez, C.; Wassenaar, T.A.; Schäfer, L.V.; Periole, X.; Tieleman, D.P.; Marrink, S.J. Improved parameters for the martini coarse-grained protein force field. *J. Chem. Theory Comput.* 2013, 9, 687–697, doi:10.1021/ct300646g.
- [38] Berau, T.; Kremer, K. Automated Parametrization of the Coarse-Grained Martini Force Field for Small Organic Molecules. *J. Chem. Theory Comput.* 2015, 11, 2783–2791, doi:10.1021/acs.jctc.5b00056.
- [39] Sardesai, Y.; Bhosle, S. Tolerance of bacteria to organic solvents. *Res. Microbiol.* 2002, 153, 263–268, doi:10.1016/S0923-2508(02)01319-0.
- [40] Bhal, S.; Log, P. Making Sense of the Value. *Adv. Chem. Dev Inc. (ACD/Labs)*. Available online: [https://www.google.com/url?sa=t&rct=j&q=&esrc=s&source=web&cd=&cad=rja&uact=8&ved=2ahUKEwjwpJ2cotfvAhXzh\\_oHHahMA6AQFjABegQIBhAD&url=https%3A%2F%2Fwww.acdlabs.com%2Fdownload%2Fapp%2Fphyschem%2Fmaking\\_sense.pdf&usg=AOvVaw3rpY\\_xb\\_4mMyKpgWCWb3bm](https://www.google.com/url?sa=t&rct=j&q=&esrc=s&source=web&cd=&cad=rja&uact=8&ved=2ahUKEwjwpJ2cotfvAhXzh_oHHahMA6AQFjABegQIBhAD&url=https%3A%2F%2Fwww.acdlabs.com%2Fdownload%2Fapp%2Fphyschem%2Fmaking_sense.pdf&usg=AOvVaw3rpY_xb_4mMyKpgWCWb3bm) (accessed on 21.07.2018).
- [41] Paiva-Martins, F.; Gordon, M.H.; Gameiro, P. Activity and location of olive oil phenolic antioxidants in liposomes. *Chem. Phys. Lipids* 2003, 124, 23–36, doi:10.1016/S0009-3084(03)00032-X.
- [42] Parasassi, T.; De Stasio, G.; Ravagnan, G.; Rusch, R.M.; Gratton, E. Quantitation of lipid phases in phospholipid vesicles by the generalized polarization of Laurdan fluorescence. *Biophys. J.* 1991, 60, 179–189, doi:10.1016/S0006-3495(91)82041-0.
- [43] Parasassi, T.; Di Stefano, M.; Loiero, M.; Ravagnan, G.; Gratton, E. Influence of cholesterol on phospholipid bilayers phase domains as detected by Laurdan fluorescence. *Biophys. J.* 1994, 66, 120–132, doi:10.1016/S0006-3495(94)80763-5.
- [44] Levison, M.E.; Levison, J.H. Pharmacokinetics and Pharmacodynamics of antibacterial agents. *Infect. Dis Clin. North. Am.* 2009, 23, doi:10.1016/j.idc.2009.06.008.















